TECHNICAL REPORT CR-RD-SS-97-49

PREDICTION OF HINGE MOMENT
COEFFICIENTS FOR NOSE-MOUNTED CANARD
CONTROLS AT SUPERSONIC SPEEDS

Michael G. Landers
Dynetics, Inc.
1000 Explorer Boulevard
Huntsville, AL 35806

U.S. ARMY AVIATION AND MISSILE COMMAND
Redstone Arsenal, Alabama   35898-5000

19971121 051

DESTRUCTION NOTICE

DISCLAIMER

TRADE NAMES

REPORT DOCUMENTATION PAGE	*Form Approved* *OMB No. 074-0188*

1. AGENCY USE ONLY	2. REPORT DATE August 1997	3. REPORT TYPE AND DATES COVERED Final Aug 96 – Aug 97

4. TITLE AND SUBTITLE

Prediction of Hinge Moment Coefficient for Nose-Mounted Canard Controls at Supersonic Speeds

5. FUNDING NUMBERS

DAAH01-96-C-R194

6. AUTHOR(S)

Michael G. Landers

7. PERFORMING ORGANIZATION NAME(S) AND ADDRESS(ES)

Dynetics, Inc.
1000 Explorer Boulevard
Huntsville, Alabama 35806

8. PERFORMING ORGANIZATION REPORT NUMBER

9. SPONSORING / MONITORING AGENCY NAME(S) AND ADDRESS(ES)

Commander, U. S. Army Aviation and Missile Command
Missile Research, Development, and Engineering Center
ATTN: AMSAM-RD-SS
Redstone Arsenal, AL 35898-5000

10. SPONSORING / MONITORING AGENCY REPORT NUMBER

TR-CR-RD-SS-97-49

11. SUPPLEMENTARY NOTES

12a. DISTRIBUTION / AVAILABILITY STATEMENT

Approved for public release; distribution is unlimited.

12b. DISTRIBUTION CODE

A

13. ABSTRACT *(Maximum 200 Words)*
The prediction of nose-mounted canard hinge moments in supersonic flow poses a unique problem for which the semi-empirical methods utilized in engineering-level aerodynamic prediction codes may not provide sufficient accuracy for preliminary design of the control actuation system. While providing accurate predictions of canard normal force, such codes generally cannot adequately predict canard hinge moments due to both their empirical nature and inability to address the local flowfield conditions on the rocket nose. It has been shown in this report that the local flowfield properties must be characterized to accurately determine the longitudinal center-of-pressure of the canards. A theoretical approach has been developed to predict normal force coefficient, longitudinal center-of-pressure, and subsequent hinge moment coefficient for nose-mounted canards. The method is based on shock-expansion theory and airfoil strip theory, and accounts for local flowfield properties, tip pressure losses, and body carryover effects. In contrast to aerodynamic code predictions, the theoretical method consistently estimates canard longitudinal center-of-pressure with a higher degree of accuracy, resulting in good agreement with experimental data for nose-mounted canard hinge moments at Mach 1.25 to 2.00.

14. SUBJECT TERMS
Nose-mounted Canards, Canard Control, Prediction, Hinge Moments

15. NUMBER OF PAGES
119

16. PRICE CODE

17. SECURITY CLASSIFICATION OF REPORT UNCLASSIFIED	18. SECURITY CLASSIFICATION OF THIS PAGE UNCLASSIFIED	19. SECURITY CLASSIFICATION OF ABSTRACT UNCLASSIFIED	20. LIMITATION OF ABSTRACT UL

TABLE OF CONTENTS

LIST OF FIGURES

LIST OF TABLES

LIST OF SYMBOLS

Symbol	Definition
A	Canard aspect ratio
A_{cs}	Canard cross-sectional area
b	Canard span (two panels excluding body)
c	Canard airfoil section local chord
C_{hm}	Canard airfoil section hinge moment coefficient
C_{HM}	Canard hinge moment coefficient corrected for tip effects and body carryover interference
C_N	Canard airfoil section normal force coefficient
C_{Nc}	Canard-alone normal force coefficient
C'_{Nc}	Canard normal force coefficient corrected for tip effects
CN	Canard normal force coefficient corrected for tip effects and body carryover interference, $CN_{w(B)}$
$C_{P_{Ln}}$	Pressure coefficient of lower surface region n
$C_{P_{Un}}$	Pressure coefficient of upper surface region n
C_r	Canard root chord
C_{TIP}	Canard tip chord
d	Reference length, diameter of model
dy	Incremental change along canard semispan
HM	Canard hinge moment
J	Number of airfoil strips
j	Airfoil strip variable
$k_{w(B)}$	Wing in presence of body interference factor with control deflection
$K_{w(B)}$	Wing in presence of body interference factor with angle of attack
M, M_L	Local Mach number
M_n	Normal component of freestream Mach number
M_{Ln}	Mach number of lower surface region n
M_{Un}	Mach number of upper surface region n

Symbol	Definition
M_∞	Freestream Mach number
NF	Canard normal force
P_{Ln}	Static pressure on lower surface on region n
P_∞	Freestream static pressure
P_t	Tunnel total pressure
$P_{t\infty}$	Freestream total pressure
P_{tLn}	Total pressure on lower surface of region n
P_{tUn}	Total pressure on upper surface of region n
q_∞	Freestream dynamic pressure
R	Canard leading-edge radius, degrees
r	Experimental result
S	Reference area
s	Canard semispan including body radius
U_{CHM}	Uncertainty in canard hinge moment coefficient
U_{CN}	Uncertainty in canard normal force coefficient
U_D	Total Uncertainty in experimental data
U_d	Uncertainty in model reference diameter
U_{HM}	Uncertainty in canard hinge moment
U_{NF}	Uncertainty in canard normal force
U_{Pt}	Uncertainty in tunnel total pressure
U_{q_∞}	Uncertainty in freestream dynamic pressure
U_r	Uncertainty in experimental result
U_s	Uncertainty in model reference area
U_{XCP}	Uncertainty in canard longitudinal center-of-pressure location
U_{XJ}	Uncertainty in independent measured variable
U_α	Uncertainty in model angle of attack
U_δ	Uncertainty in canard deflection angle
X_{CP}	Canard longitudinal center-of-pressure

Symbol	Definition
X_{HL}	Canard hingeline location measured from leading edge
X_J	Independent measured variable
X_{LE}	Distance to canard leading edge measured from y-axis along canard strip
α	Angle of attack, degrees
β	$\sqrt{M^2 - 1}$
δ	Compression angle of freestream flow, degrees
δ_c, δ_w	Canard (wing) deflection angle, degrees
$\dfrac{\partial r}{\partial X_J}$	Absolute sensitivity of experimental result with independent variable
ϕ	Rocket body roll angle, degrees
γ	Ratio of specific heats, (1.4 for air)
Λ_{LE}	Canard leading-edge sweep angle, degrees
μ	Mach angle, degrees
ν_L	Local Prandtl-Meyer expansion angle
ν_{Ln}	Prandtl-Meyer expansion angle of lower surface region n
ν_{Un}	Prandtl-Meyer expansion angle of upper surface region n
τ	Canard semispan to body radius ratio
θ	Local body slope along rocket nose, degrees
θ_N	Canard semivertex angle of region n, degrees
θ_s	Canard shock wave angle, degrees

Chapter 1

INTRODUCTION

Current U.S. free-flight (unguided) rockets may not provide sufficient range or accuracy to counter the threat of long-range rocket and cannon systems of potential adversaries [1]. In recent years, much interest has been given to increasing the range and accuracy of existing tube-launched, supersonic free-flight rockets by the integration of a low-cost inertial guidance and control package [1, 2]. Such a control package could be developed to utilize canard controls (aerodynamic control surfaces located forward of the rocket center-of-gravity) to provide the advantages of a simple control design with a large control force-to-control package weight ratio.

Incorporation of non-deployable, all-movable canards into an existing free-flight rocket would not only require adequate clearance between the canards and the launch tube but also sufficient packaging volume for the control actuation system (CAS) within the rocket. Such requirements may dictate that the canards be positioned along the rocket nose, conformal with the varying radius segments of the nose. Since most supersonic guided rockets are designed with canard controls located on the cylindrical body section aft of the missile nose, the nose-mounted canard control configuration which is span-constrained for launch considerations is considered unique.

Figure 1.1 illustrates the flowfield characteristics which may be encountered for canards located both fore and aft of the rocket nose. With the canards located some distance aft of the rocket nose, it is convenient to assume the flow has expanded about the nose to a nominal freestream value with properties which are uniform along the canard span. In addition, interference between the nose bow shock and the canards is not an issue. However, canards mounted forward on the rocket nose are inclined to the freestream flow due to the conformity of the canard with the varying radius of the nose shape. Thus the canards are subject to the local flowfield conditions in the expanding flow region behind the nose shock. For extreme cases, large gradients in flow properties along the canard span may exist. Additionally, the canards

1

$$M_L = M_\infty \cos(\alpha)$$

$$M_\infty$$

α

Nose Shock

$\Theta_{C.G.}$
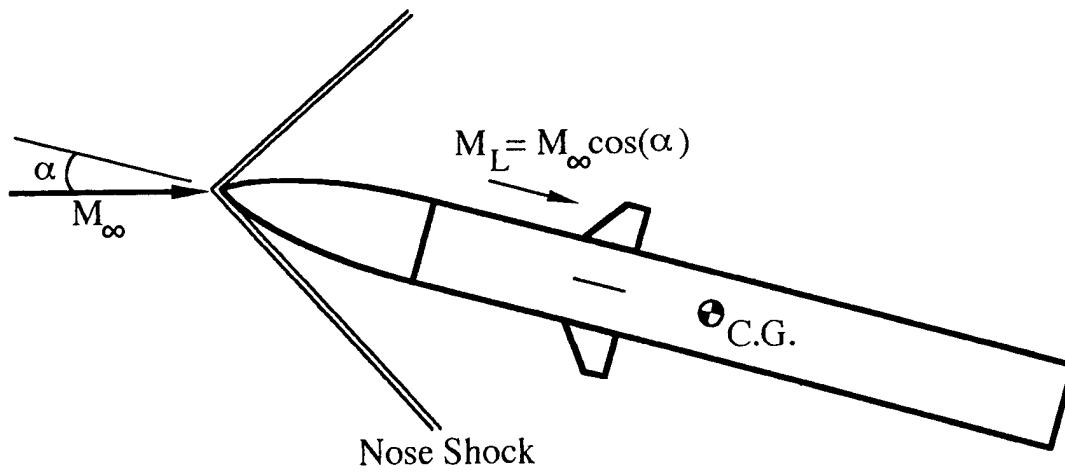
(a) Canards Mounted on Cylindrical Section Aft of Rocket Nose

$$M_L \neq M_\infty \cos(\alpha)$$

$$M_\infty$$

α

Nose Shock

$\Theta_{C.G.}$
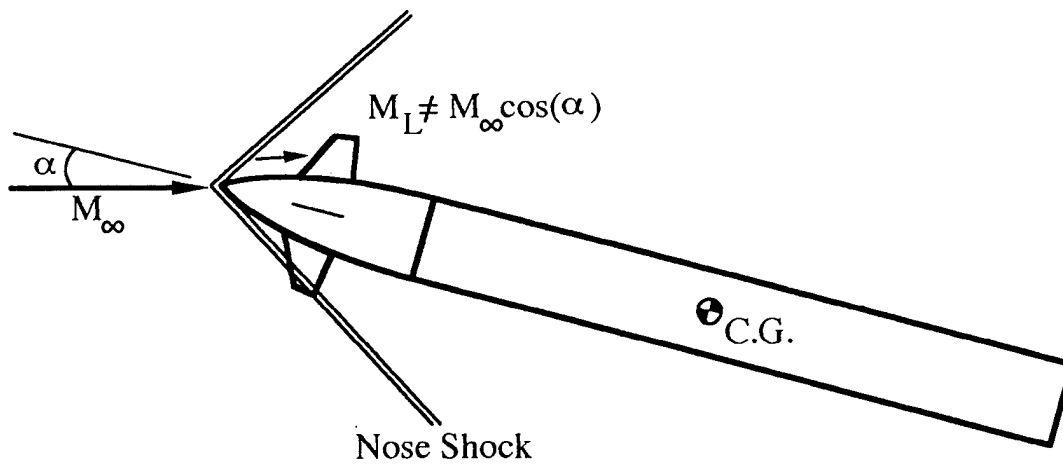
(b) Canards Mounted on Rocket Nose in Proximity of Nose Shock

Figure 1.1 Variations in Canard Flowfield Characteristics with Location on Rocket

may be subject to interaction with the nose bow shock wave, depending upon the freestream flow conditions, physical geometry of the canards, and the location of the canards along the rocket nose. This could also result in significant flow property gradients over different areas of the canard. Therefore, it is postulated that accurate predictions of nose-mounted canard aerodynamics are dependent upon characterizing the local flowfield conditions.

The aerodynamic characteristics of interest in canard design include the canard normal force coefficient (CN), the canard longitudinal center-of-pressure (Xcp), and the canard hinge moment coefficient (CHM). The canard hinge moment is determined from both the normal force and the center-of-pressure location of the normal force relative to the hinge line. In the design of all-movable canard controls, the control effectiveness and maximum canard torques must be accurately assessed to determine the weight and size of the control actuator. It is desired that a canard develop maximum control effectiveness with minimum hinge moment, since increasing hinge moment requires a more powerful control actuator and thereby incurs a weight penalty. For nose-mounted canards, the size, weight, and power requirements of the CAS must be minimized due to the limited packaging volume available.

The prediction of nose-mounted canard aerodynamics in supersonic flow poses a unique problem for which engineering-level, aerodynamic prediction codes may not provide sufficient accuracy for preliminary or advanced design. Such state-of-the-art, rapid prediction tools are based on semi-empirical methods and empirical databases [3, 4] to predict canard-alone aerodynamics. The slender-body theory developed in NACA 1307 [5] is utilized to account for interference, or carryover, effects associated with the canard in the presence of a rocket body of infinite length and uniform diameter. Experiences with codes such as the U.S. Air Force Missile DATCOM 6/93 [6] have shown them to be inadequate in providing accurate predictions (within approximately 10%) and general trends of nose-mounted canard aerodynamics. These codes are typically constrained to configurations with canards mounted aft of the rocket nose on a cylinder of uniform diameter as shown in Figure 1.1(a). In general, the accuracy in aerodynamic predictions of these codes tends to lessen due to the extrapolation of data beyond the realm of the experimental database, the violation of underlying assumptions in the methodologies, and their inability to account for the local flowfield conditions [7].

While the canard normal force can be determined to a high degree of accuracy with semi-empirical methods, the longitudinal center-of-pressure is generally difficult to ascertain due to its sensitivity to Mach number and nonlinearities associated with canard angle of attack and deflection angle. Since the canard hinge moment is dependent upon both the normal force and the center-of-pressure position of the normal force relative to the hinge line, accurate determination of hinge moment is often difficult. Nielsen and Goodwin [8] have concluded that "for accurate hinge moment prediction, it has been found that accurate knowledge is required of the fin axial center-of-pressure positions- within about two percent of the root chord. Based on the present state-of-the-art, if the error [in canard Xcp between theory and experiment] represents less than about two percent of the root chord, it is considered that good agreement is obtained." Accurate determination of canard hinge moment is complicated by the fact that any external factors influencing canard normal force and center-of-pressure location will have a direct affect on canard hinge moment. Factors which can influence nose-mounted canard aerodynamics include: canard-body interference (with/without body vortices), canard-nose shock wave interaction, canard-canard interference, canard choking, gap effects, and nonlinearities in canard-alone normal force and longitudinal center-of-pressure with angle of attack and canard deflection angle.

One approach to providing accurate predictions of nose-mounted canard aerodynamics is to assemble a systematic database of wind tunnel test data for various canard planforms and locations and to interpolate in the database. This empirical approach would require an extensive amount of data to cover a wide range of nose shapes, canard geometries, and canard locations along the nose. Another approach would be to develop a validated, theoretical method which is applicable to a wide range of configurations and may provide more accurate predictions of the aerodynamics of nose-mounted canards than current semi-empirical codes. To this end an analytical method based on shock-expansion theory and airfoil strip theory has been developed to determine canard-alone normal force and longitudinal center-of-pressure. Corrections are made for canard-body interference and tip effects on normal force and center-of-pressure and the subsequent hinge moments for nose-mounted canards are calculated. Emphasis is placed on

providing a theoretical approach to estimate canard longitudinal center-of-pressure within two percent of the root chord.

To maintain the scope of this research, the problem has been limited to predicting normal force coefficient, longitudinal center-of-pressure, and hinge moment coefficient for a single canard located in the horizontal plane of the rocket at three positions along a pointed ogive nose for supersonic Mach numbers. Comparisons with experimental data and DATCOM predictions were made to show the validity of the theoretical technique. The theoretical approach provides a more accurate characterization of the nose-mounted canard hinge moments than DATCOM for the cases studied. In addition, the theoretical approach has been coded in a subroutine that could easily be incorporated to enhance DATCOM predictions.

The new method presented in this thesis could provide more accurate predictions of nose-mounted canard aerodynamics than current semi-empirical prediction codes. In particular, such an approach could be utilized in developing and sizing the CAS to meet packaging requirements for preliminary design purposes.

Chapter 2

BACKGROUND

Prior to developing a theoretical-based approach to predicting canard aerodynamics, an extensive literature search was performed at the U.S. Army Redstone Scientific Information Center to obtain information and experimental test data on nose-mounted canard aerodynamics. Numerous searches revealed a vast array of general information on canards but only a few specific references to nose-mounted canards. Classic textbooks [9-12] and NACA reports [5, 13-15], which provide theoretical approaches for determining the aerodynamic characteristics of wings and control surfaces, generally do not address nose-mounted canard controls. The uniqueness of nose-mounted canards became apparent when less than a dozen documents were identified which address the issue in both theory and experiment.

Of primary interest was a series of wind tunnel tests conducted with the Army Generalized Missile model in the early 1970's by the U.S. Army Missile Command (MICOM), the U.S. Naval Weapons Center, and Nielsen Engineering and Research, Inc. [16-20]. The tests were performed to determine the aerodynamics of nose-mounted canards and to provide a database for future Army missile designs. Extensive data were obtained for canards mounted at various longitudinal positions along an ogive rocket nose at Mach numbers of 0.6 to 4.5. The experimental data was included in the *CANARD* database [21] which resides on the U.S. Army Missile Command Aerodynamic Analyzer System.

A theoretical approach for predicting canard hinge moments detailed by Nielsen and Goodwin [8, 22-23] was also identified. In this approach, semi-empirical methods are first utilized to predict canard-alone normal force coefficient and center-of-pressure for a lifting surface. The center-of-pressure is then corrected for airfoil thickness by a factor based on theoretical aspects of shock-expansion theory and airfoil strip theory. However, the accuracy in canard hinge moment predictions is highly dependent upon the initial, semi-empirical estimate of the center-of-pressure. Depending on the location of the initial estimate relative to the control hingeline, the forward shift in center-of-pressure due to the thickness correction may, in some

6

cases, actually worsen hinge moment predictions. Therefore, the theoretical aspects advanced in the thickness correction have been expanded to derive a new method to estimate nose-mounted canard aerodynamic characteristics based solely on first principles, eliminating the empirical basis in the Nielsen approach.

Chapter 3

DESCRIPTION OF EXPERIMENTAL DATA

Experimental data for nose-mounted canards were researched and obtained to validate a theoretical approach for predicting canard normal force coefficient, longitudinal center-of-pressure, and hinge moment coefficient. A description of the experimental data, the wind tunnel tests, and model geometry is presented here. In addition, proper consideration is given to experimental uncertainties for the data presented. Observations of the test data are presented which provide some simplifications in developing the theoretical approach.

3.1   *CANARD* Database

Three wind tunnel tests performed in the early 1970's by the U.S. Army Missile Command, the U.S. Naval Weapons Center, and Nielsen Engineering and Research, Inc. [16-20] obtained experimental data for canard controls located at various longitudinal positions along a rocket nose. These tests were conducted at the CALSPAN 8-foot transonic wind tunnel in April 1973, the NASA Ames 6- by 6-foot Supersonic Wind Tunnel in June 1974, and the Arnold Engineering Development Center (AEDC) Tunnel A in October 1975. Devised to investigate the effectiveness of small, nose-mounted canards in providing control for a maneuvering rocket, these tests examined the effects of canard geometry and canard longitudinal position for a Mach number range of 0.6 to 4.5. To provide a database for future Army missile designs, the data were compiled into the *CANARD* database [21] which currently resides on the U.S. Army Missile Command Aerodynamic Analyzer System.

3.2   Wind Tunnel Model and Instrumentation

The wind tunnel model consisted of a sting-mounted body of revolution, 5 inches in diameter and 52 inches in length. Five nose shapes were tested, one of which was a pointed 3-caliber tangent ogive. The model allowed for a set of four canards to be mounted at three distinct longitudinal positions along the model nose. As shown in Figure 3.1, these positions are defined

8

at model station 6.704, 9.127, and 15.000 for canard position 1, 2, and 3 respectively. Tail fins were also mounted on the model but they have no effect on canard aerodynamics in supersonic flow. The model was instrumented with a total of nine strain gage balances to measure aerodynamic forces and moments: four canard balances, four tail fin balances, and a single main balance.

Of the four canard geometries tested only two canard configurations were tested at all three mounting positions along the nose. These two canards maintained the same aspect ratio with one canard having twice the planform area. In considering a non-deployable, nose-mounted canard constrained to fit within a launch tube, the canard with the smaller semispan was chosen for analysis. The canard was defined by a straight-tapered, clipped-delta planform with a modified double-wedge cross-section and aspect ratio of 1.154 (canard-panel alone). The geometric characteristics of the canard are detailed in Figure 3.2.

Three individual sets of canards were used, one set for each position along the model nose, such that the canards were mounted flush to the ogive nose at each position. As shown in Figures 3.1 and 3.2, although the planform shape remained constant, the leading and trailing edge sweep angles of the canards (relative to the freestream flow) varied depending upon the local body slope at the given mounting position. The balance attachment point for the canards remained perpendicular to the model body centerline at each mounting position such that canard hinge moments were resolved about the hingeline defined as the centerline of each attachment point. The canard hingeline was located 1.17 inches aft of the canard leading edge measured along the root chord. The canard balances supplied by MICOM were three-component balances which measured canard normal force, hinge moment, and root bending moment. Each canard balance was mounted parallel with the model centerline. Remote-controlled electric motors were installed internal to the model to provide independent canard deflections (δ_c) from -5 to +15 degrees. Sign conventions for the canard normal force and hinge moment are shown in Figure 3.3 where a positive canard deflection produces a positive normal force.
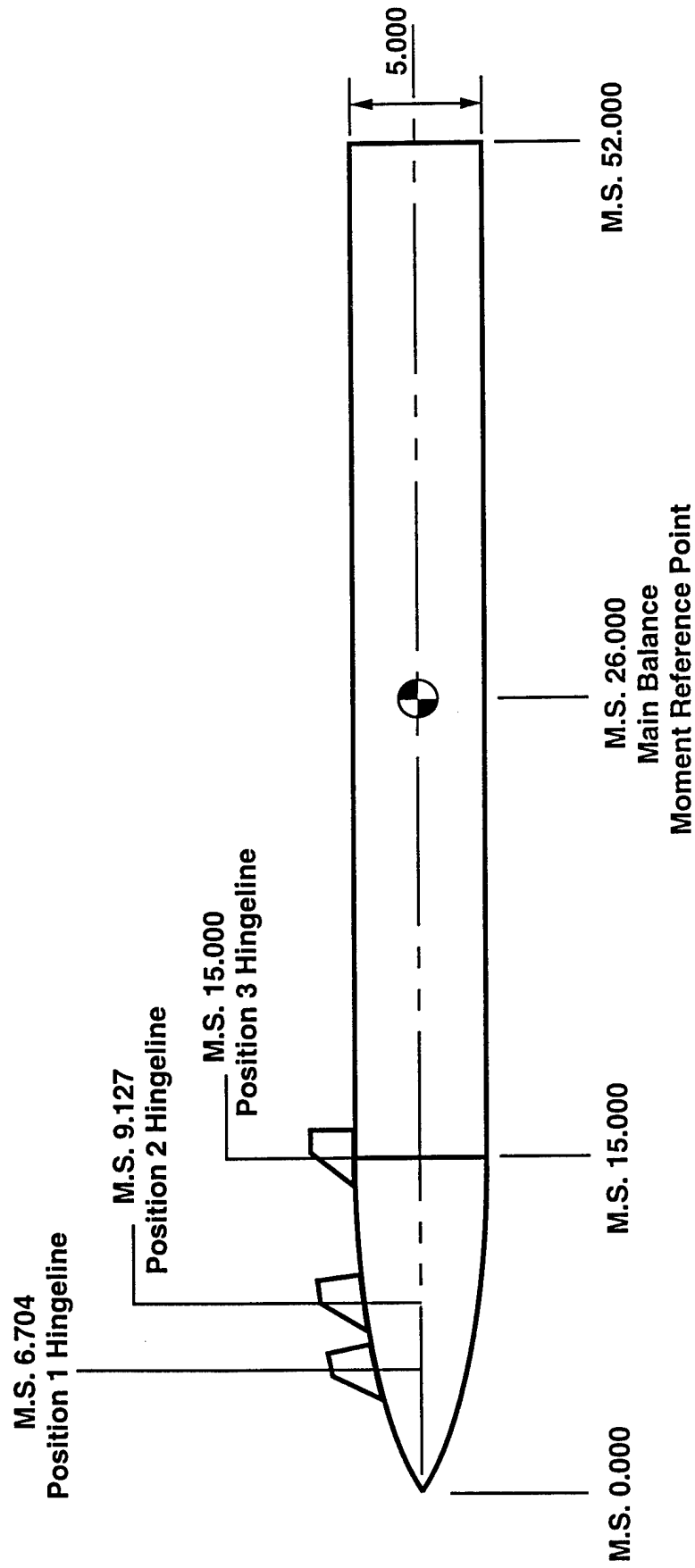
Figure 3.1 Dimensioned Drawing of Wind Tunnel Test Model

11

R=0.015

0.030

0.600

$\Lambda_{LE} = 43.025°$

Hingeline

1.170

2.000

1.500

0.666

0.100

0.666

0.666

0.666

R=0.015

Position 3

$\Lambda_{TE} = -7.237°$

$\theta = 7.237°$

$\Lambda_{LE} = 35.788°$

Hingeline

1.170

Position 2

$\Lambda_{TE} = -10.169°$

$\theta = 10.169°$

$\Lambda_{LE} = 32.856°$

Hingeline

1.170
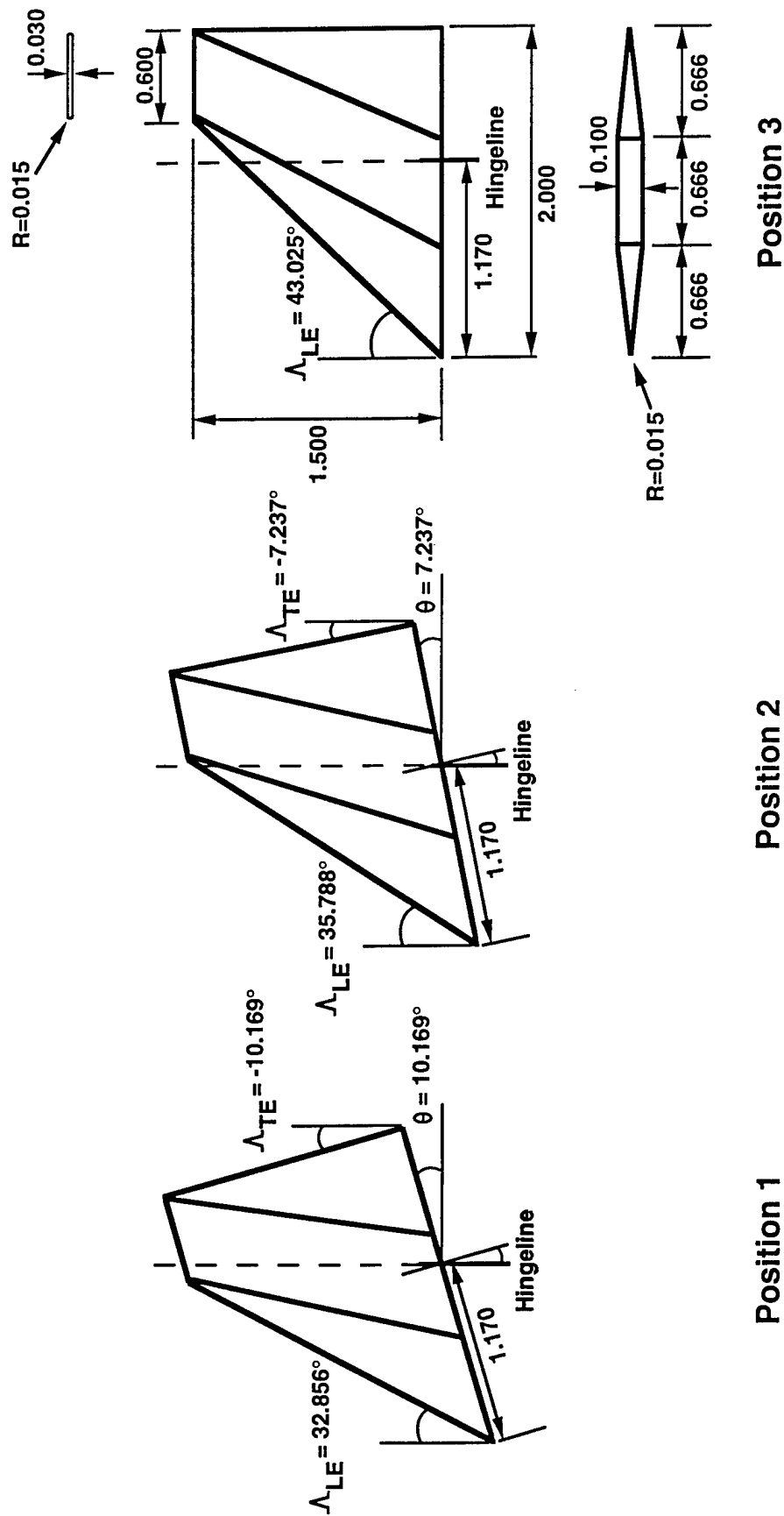
Position 1

Figure 3.2 Dimensioned Drawing of Canard at Three Positions Along Rocket Nose
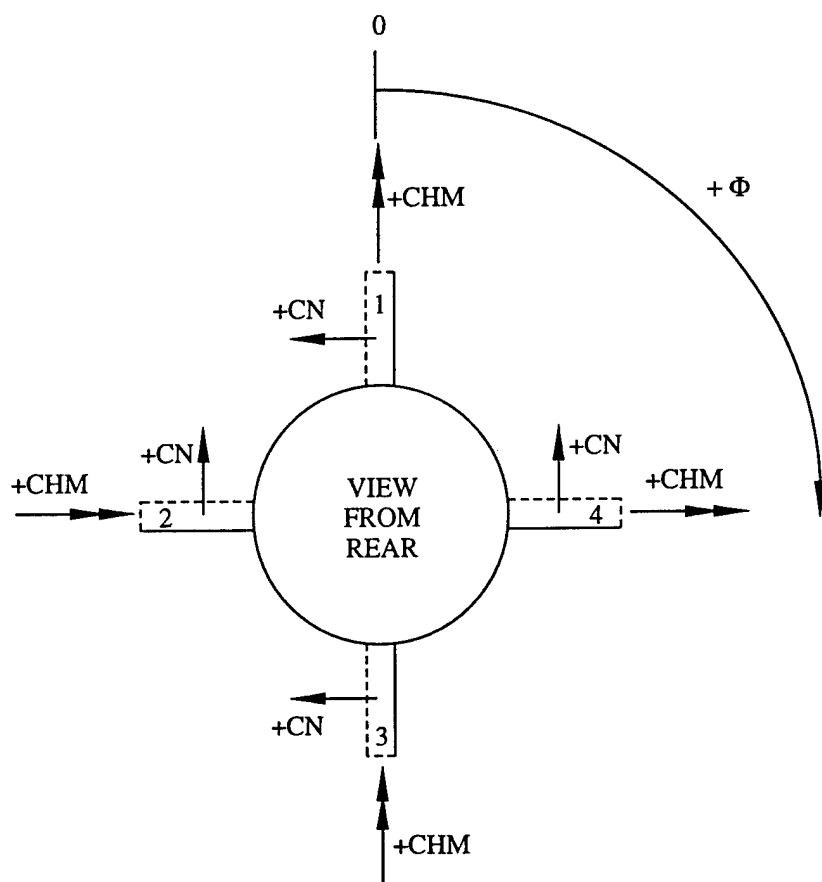
Figure 3.3 Canard Force and Moment Sign Conventions

3.3   Wind Tunnel Test Description

The model configuration of interest was tested in three separate wind tunnel facilities to obtain aerodynamic data from Mach 0.6 to 4.5. The Calspan 8-foot Transonic Wind Tunnel was used to obtain test data at Mach 0.6 to 1.25, the NASA Ames 6- by 6-foot Supersonic Wind Tunnel was used to obtain test data at Mach 1.5 and 2.0, while Mach 1.5 to 4.5 data were obtained in Tunnel A at AEDC. The three-component canard balances supplied by MICOM to measure canard aerodynamics were statically calibrated by each tunnel facility prior to testing.

Data were obtained for model angles of attack from -3 to 12 degrees with canard deflections from -3 to 15 degrees. Both total angle of attack sweeps at discrete body roll angles and body roll angle sweeps at discrete total angles of attack were performed. For total angle of attack sweeps, roll angles of 0 and 45 degrees were tested. The canards were individually deflected by a remote-control actuation system. Aerodynamic coefficients were calculated using the maximum model diameter of 5.00 inches and corresponding reference area of 19.63 square inches.

3.4   Experimental Data Analysis

The experimental data contained in the *CANARD* database were analyzed to evaluate the quality of the data, to observe data trends, and to obtain a consistent set of data for validation of the theoretical approach. Since the theoretical approach is limited to canards mounted in the horizontal plane, only canard 2 (ϕ_c=270) and canard 4 (ϕ_c=90) at a model roll angle of zero degrees were considered. Plots of canard normal force coefficient and hinge moment coefficient variations with angle of attack and canard deflection showed that data for canard 4 were often corrupted due to a reported balance problem. For this reason, the data for canard 4 were neglected. In addition hinge moment coefficient data for both horizontal canards at zero body roll angle obtained during the AEDC test were corrupted which precluded use of this data.

A consistent set of pitch-sweep data were obtained from the Calspan and NASA Ames tests for canard 2 located at three longitudinal positions along the nose at Mach 1.25, 1.50, and 2.00. The test conditions for these continuous-flow tunnels were reported as dynamic pressures of 550 psf at Mach 1.25 and 500 psf for Mach 1.50 and 2.00 with freestream total pressures of

approximately 0.5 atmospheres. The data set consisted of data for canard 2 at zero body roll angle, 0 to 12 degrees angle of attack, and 0, 3, and 9 degrees canard deflection. For this data both canard 2 and canard 4 were mutually deflected in the same direction while canard 1 and canard 3 remained undeflected. No data were available to determine the mutual interference from adjoining undeflected canards or the interference for mutually deflected canards located 180 degrees apart.

Plots of canard normal force coefficient, longitudinal center-of-pressure, and hinge moment coefficient variations with angle of attack are shown in Figures 3.4-3.12 for the experimental data of interest. The data are presented for Mach 1.25, 1.50, and 2.00 at the three canard positions along the ogive nose with zero canard deflection.

In Figures 3.4, 3.5, and 3.6, canard normal force coefficient is shown to be essentially linear with angle of attack to approximately ten degrees for all three Mach numbers. At each Mach number the normal force coefficient tends to decrease with canard location along the nose, from position 1 to position 3. It is also observed that canard normal force coefficient decreases with increasing Mach number at each canard position.
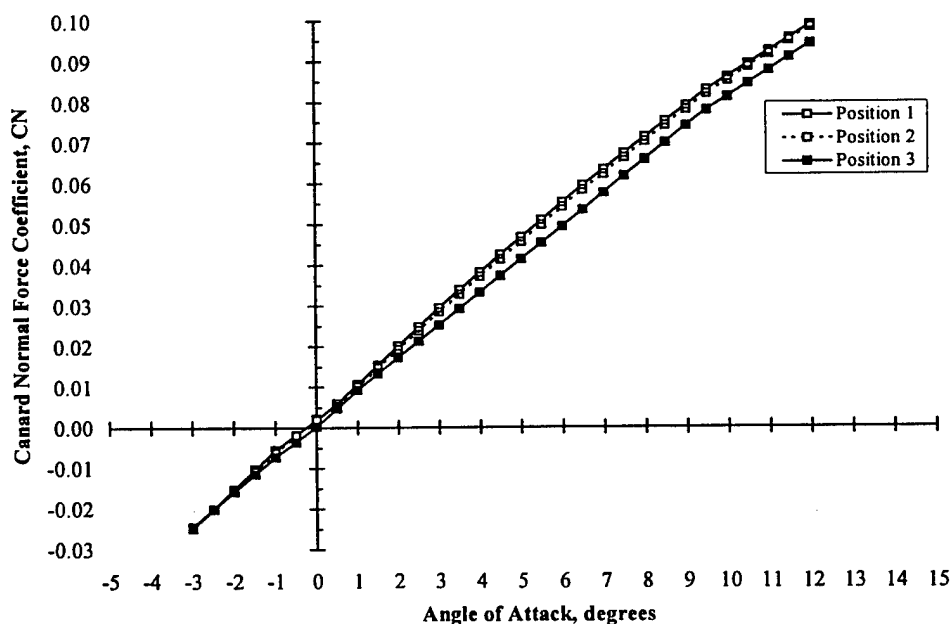
Figure 3.4 Canard Normal Force Coefficient Variation with Angle of Attack
(Mach 1.25, δ=0°)
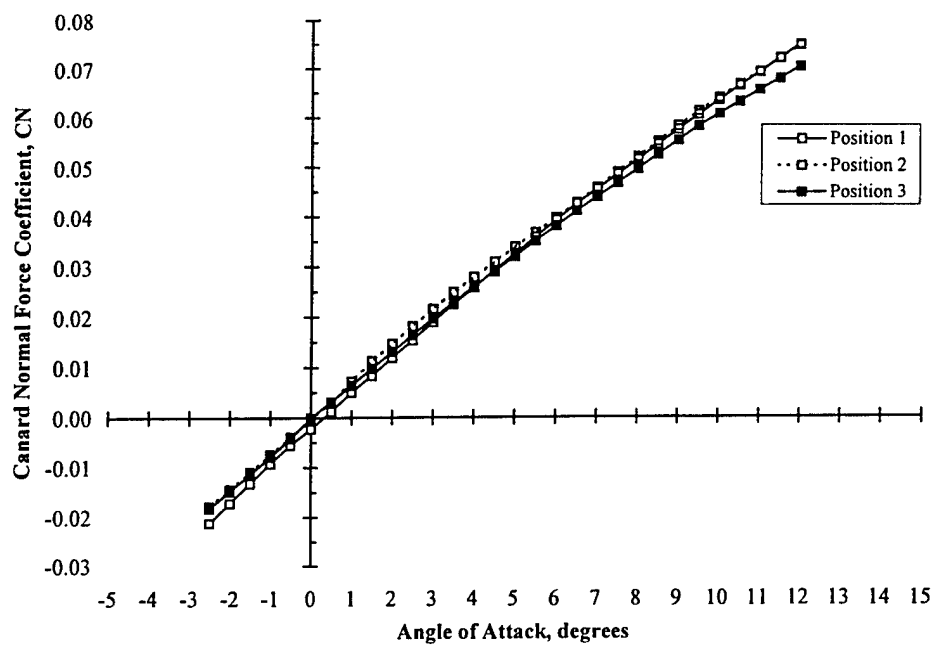
Figure 3.5 Canard Normal Force Coefficient Variation with Angle of Attack
(Mach 1.50, δ=0°)
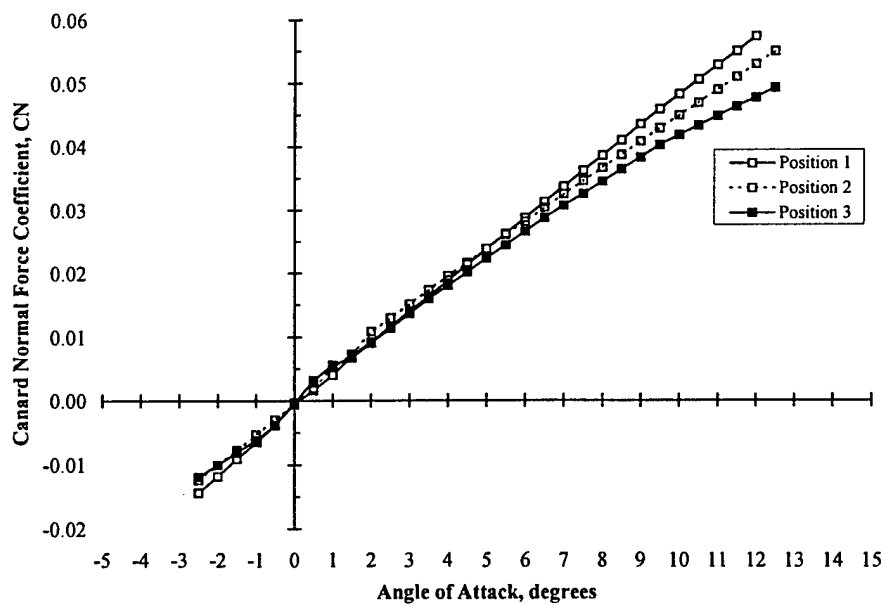
Figure 3.6 Canard Normal Force Coefficient Variation with Angle of Attack
(Mach 2.00, δ=0°)

Figures 3.7, 3.8, and 3.9 show the variations in canard longitudinal center-of-pressure with angle of attack at zero canard deflection. The canard center-of-pressure is invariant with angle of attack but experiences a noticeable shift with canard position along the nose. For Mach 1.25, the canard longitudinal center-of-pressure shifts rearward from position 1 to position 3. At Mach 1.50 and 2.00, the canard longitudinal center-of-pressure shifts forward from position 1 to position 3 but remains aft of the canard hingeline. Such shifts in canard center-of-pressure may be attributed to variations in canard leading-edge Mach number and sweep angle conditions which alter the canard pressure distribution at each position along the nose.
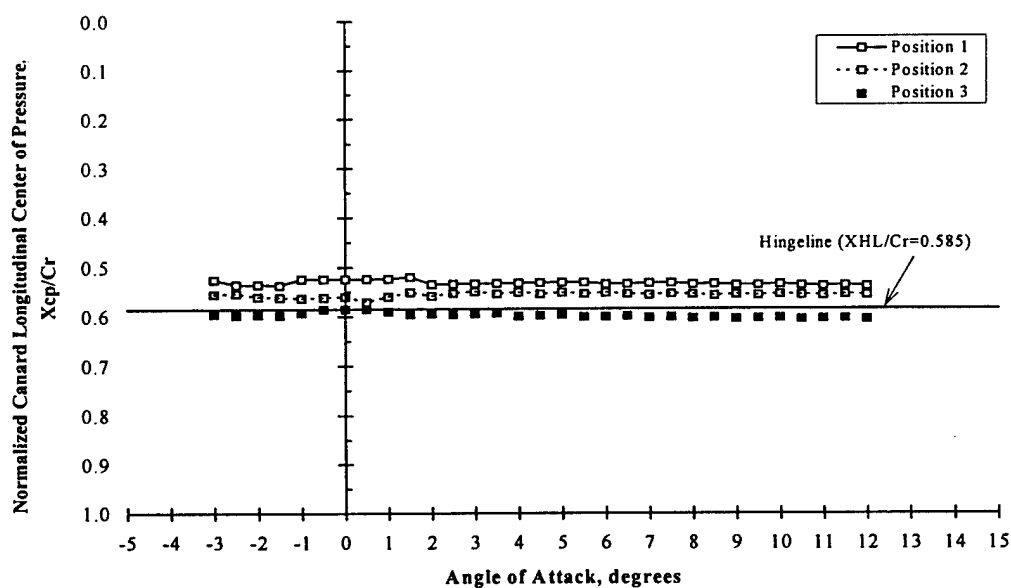
Figure 3.7 Canard Center-of-Pressure Variation with Angle of Attack
(Mach 1.25, δ=0°)
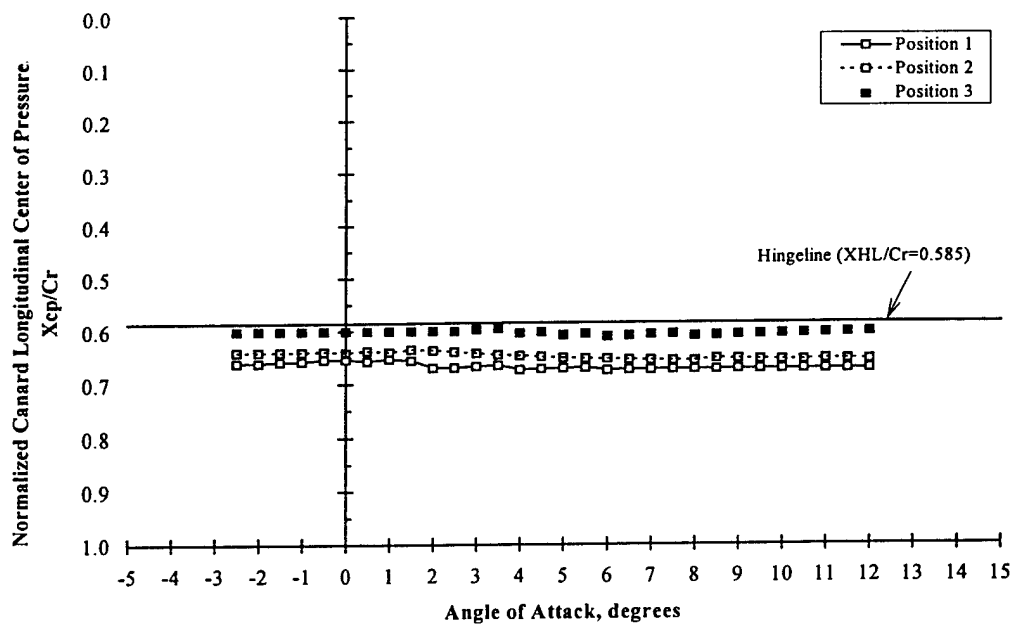
Figure 3.8 Canard Center-of-Pressure Variation with Angle of Attack
(Mach 1.50, δ=0°)
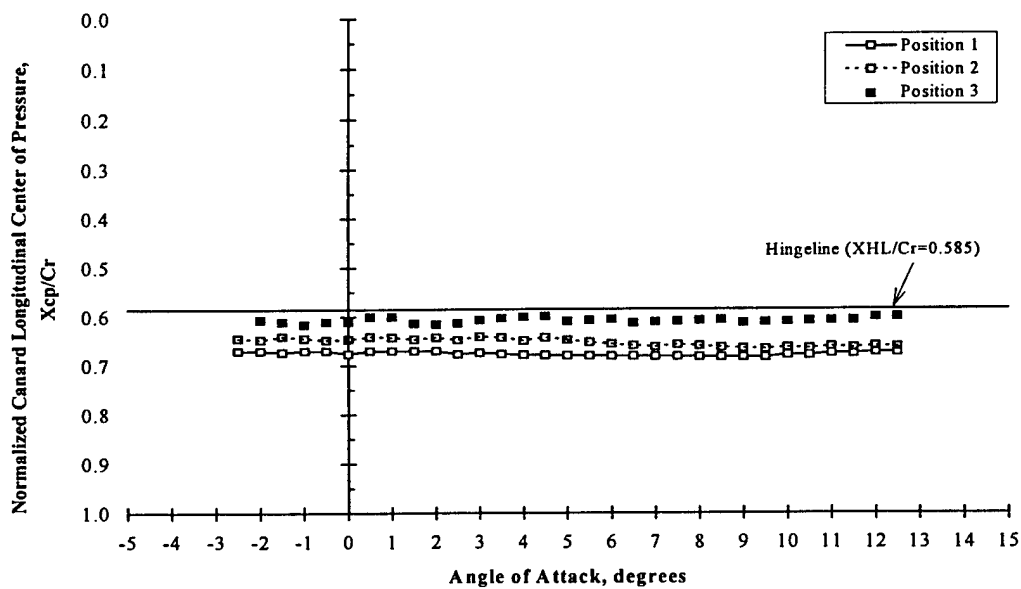
Figure 3.9 Canard Center-of-Pressure Variation with Angle of Attack
(Mach 2.00, δ=0°)

Variations in canard hinge moment coefficient with angle of attack and canard position are shown in Figures 3.10, 3.11, and 3.12. Indicative of the canard center-of-pressure location relative to the hingeline, the hinge moment is shown to vary significantly with canard position at each Mach number. For a given canard position, the hinge moment tends to decrease with increasing Mach number for a supersonic leading-edge condition. It will be shown that a subsonic leading-edge condition exists for positions 1 and 2 at Mach 1.25 and such trends do not apply. Similar trends were observed for canard deflections greater than zero.
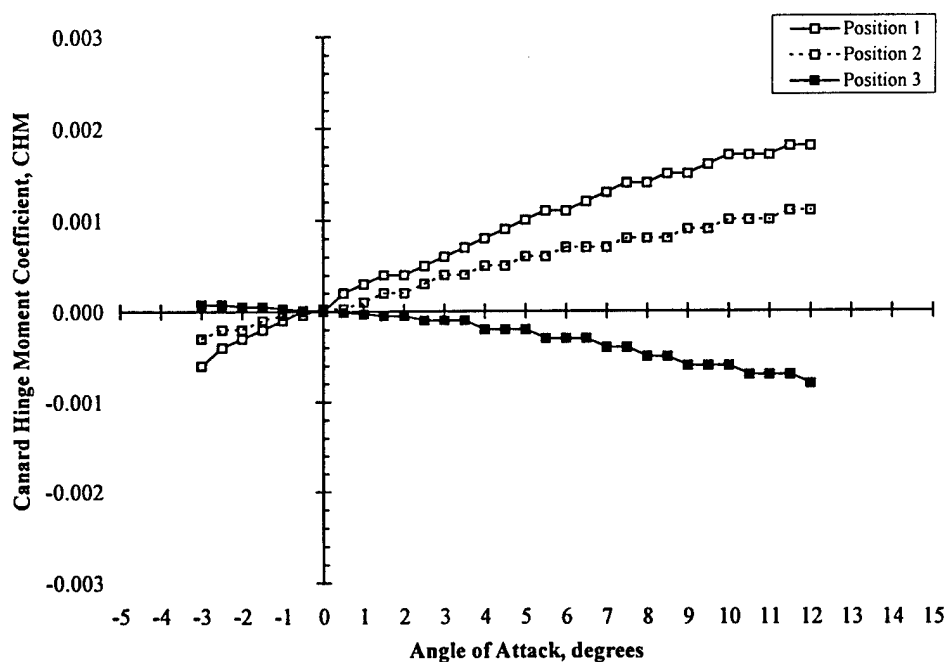
Figure 3.10 Canard Hinge Moment Coefficient Variation with Angle of Attack
(Mach 1.25, δ=0°)
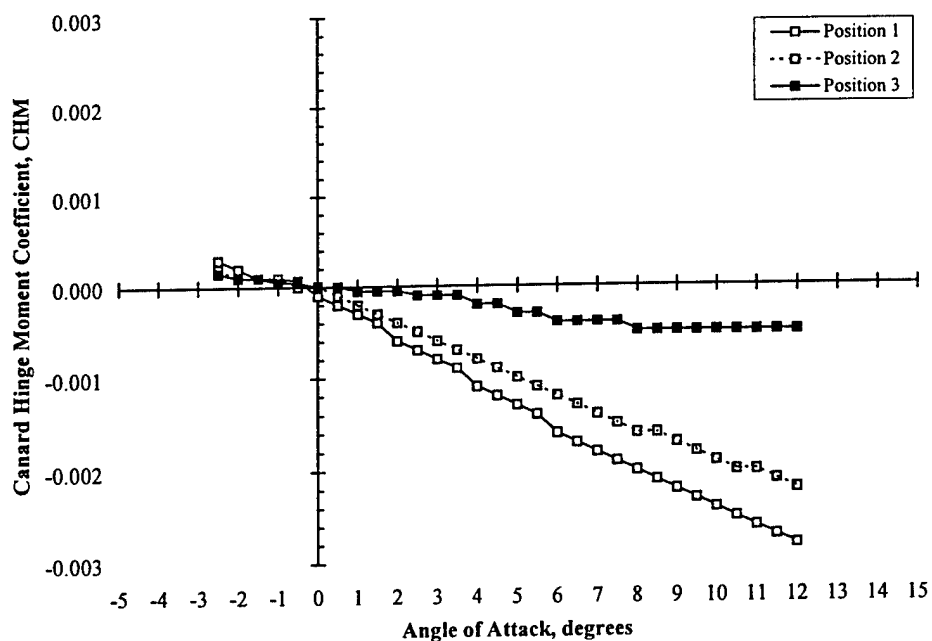
Figure 3.11 Canard Hinge Moment Coefficient Variation with Angle of Attack
(Mach 1.50, δ=0°)
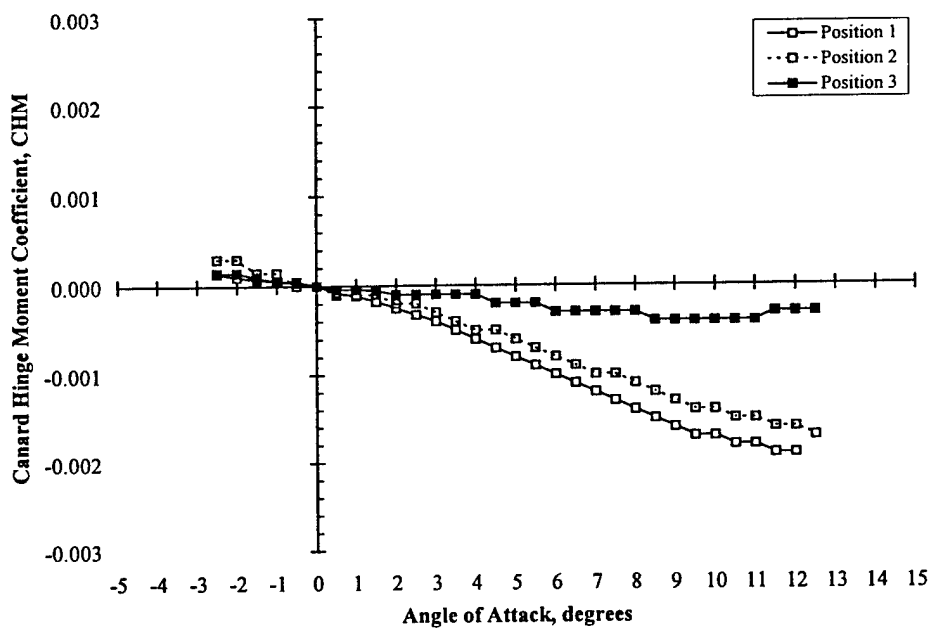
Figure 3.12 Canard Hinge Moment Coefficient Variation with Angle of Attack
(Mach 2.00, δ=0°)

Figures 3.13, 3.14, and 3.15 show the variation in canard longitudinal center-of-pressure with angle of attack and nose location for canard deflections of 0, 3, and 9 degrees at Mach 2.00. For a given canard position along the nose, the center-of-pressure is seen to be invariant with canard deflection. Similar trends were observed for Mach 1.25 and 1.50.

The previous figures illustrate some characteristics and peculiarities of nose-mounted canard aerodynamics. Examining the trends exhibited generalizations and limitations which aided in developing the theoretical approach.
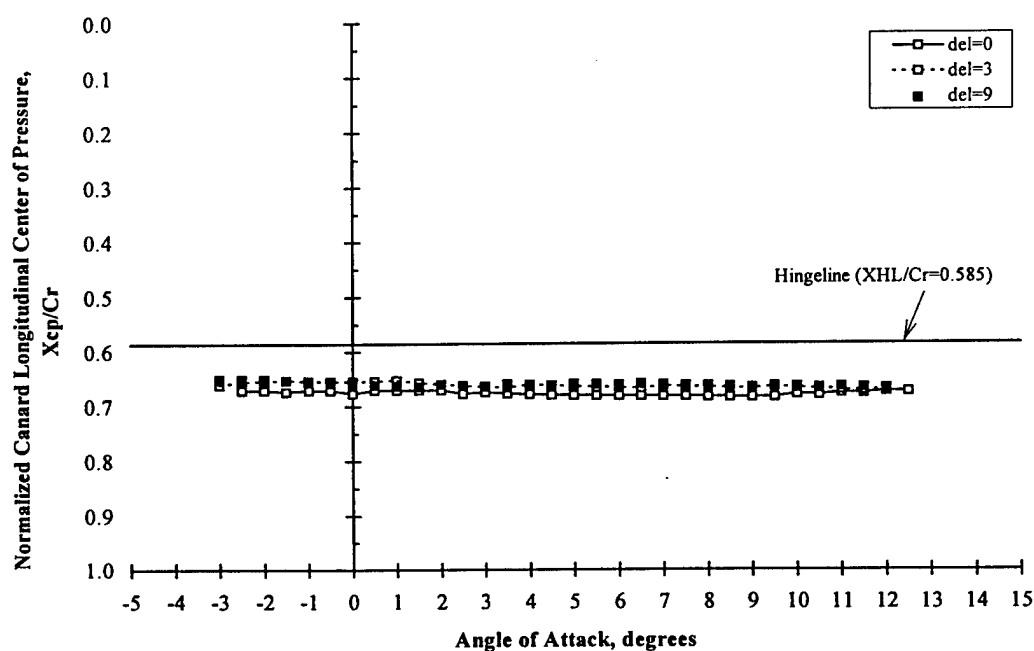
Figure 3.13 Canard Center-of-Pressure Variation with Angle of Attack
(Position 1, Mach 2.00)
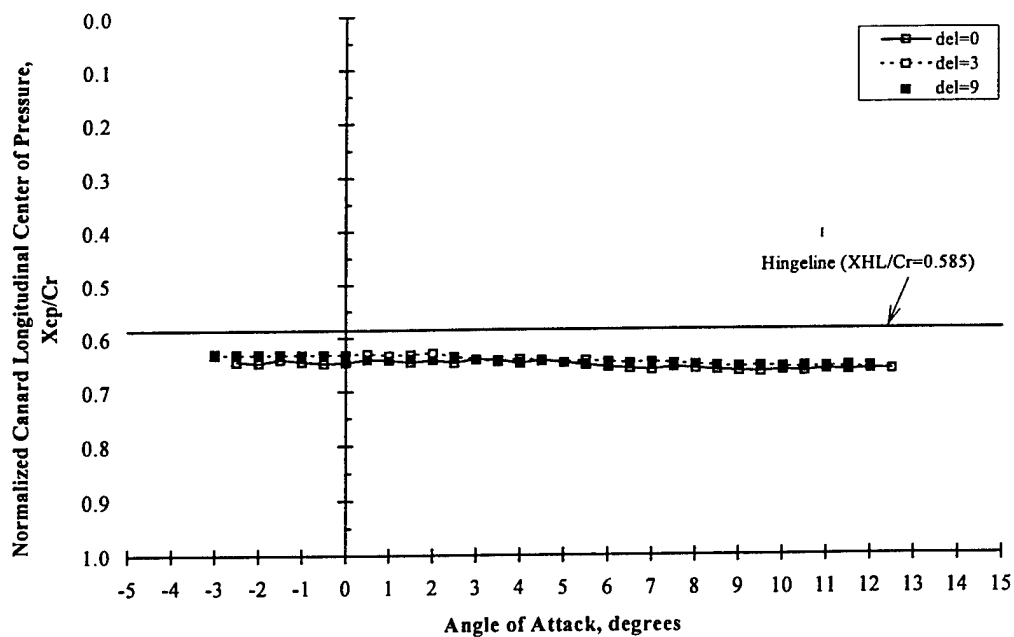
Figure 3.14 Canard Center-of-Pressure Variation with Angle of Attack
(Position 2, Mach 2.00)
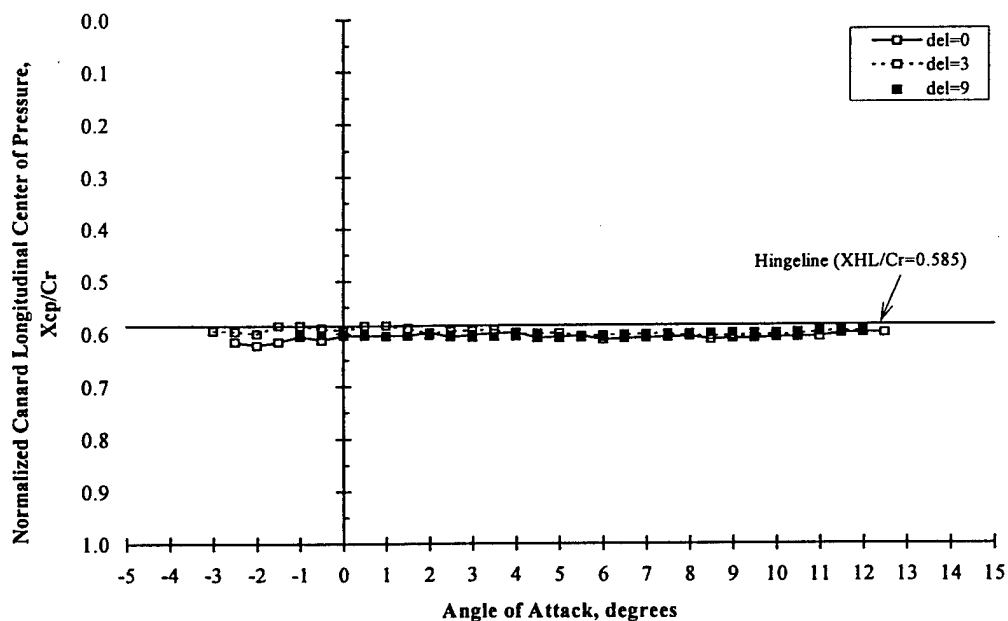
Figure 3.15 Canard Center of-Pressure Variation with Angle of Attack
(Position 3, Mach 2.00)

3.4.1 Nose-Shock/Canard Interaction

One concern with nose-mounted canards is the potential for strong nose-shock/canard interactions which could be difficult to theoretically model. Observations made from Figures 3.4-3.15 did not reveal a distinct interaction of the nose bow shock wave with the horizontal canard at angles of attack or canard deflections. To support this assumption the Zonal Euler Solver (ZEUS) code [24, 25] was utilized to characterize the nose shock shape and to compute the local flowfield properties at the three canard positions along the nose. The ZEUS code solves the Euler equations in finite-volume form by a computational method based on a second-order Godunov scheme. Application of the code is limited to steady, supersonic flow. The code is well validated for the prediction of body-alone aerodynamics and flowfield properties for missiles of traditional shapes [12].

The body-alone (ogive/cylinder) configuration of this study was modeled in ZEUS using a single zone defined by a 72 x 36 uniform mesh. Considering pitch-plane symmetry, the rocket was modeled as axisymmetric to reduce computational time. The starting cross-flow plane for the ZEUS space-marching scheme was taken at 0.05 inches from the model nose tip. For the sharp-nose model this initial flowfield data plane was constructed from an approximate solution about a circular cone from the model nose to 0.05 inches aft of the model nose. The shock-fitting option was used to locate the nose bow shock wave in relation to the canards for Mach 1.25, 1.50, 2.00, and 3.00 freestream conditions at zero and ten degrees angle of attack. Computed nose bow shock shapes are shown in Figure 3.16 for Mach numbers of 1.50, 2.00, and 3.00 at zero degrees angle of attack viewed from the top with the canards in the horizontal plane. The cases for Mach 1.25 could not be computed due to subsonic flow regions in the starting solution. The cases for ten degrees angle of attack showed no appreciable change in shock location in the horizontal plane. It is readily apparent that the nose bow shock will not intersect the canards located at any position along the nose for Mach numbers less than and equal to 2.00.
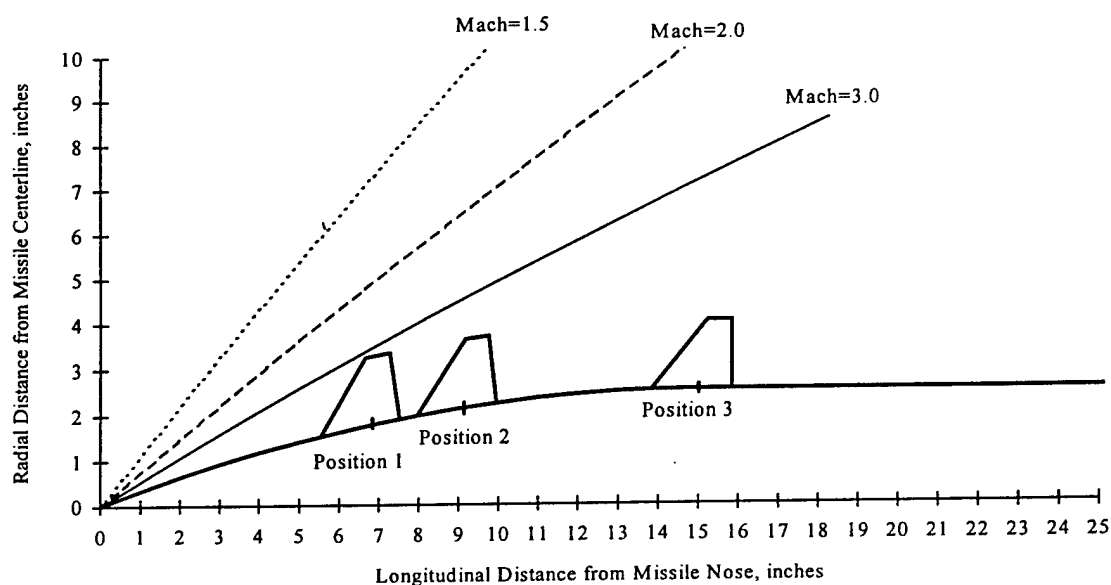
Figure 3.16 Nose Bow-Shock Wave Shapes Developed from ZEUS Calculations
(View From Top with Canards in Horizontal Plane)

3.4.2 Determination of Local Mach Number

For canards mounted on the nose of a rocket, in the vicinity of the nose bow shock and a region characterized by expanding flow, the local Mach number of the flow just ahead of the canards may be significantly different from the freestream Mach number. Numerous methods exist to determine the local Mach number, including shock-expansion theory and numerical solutions to the Euler equations, which have been coded in industry-standard prediction codes such as DATCOM and ZEUS, respectively. Such codes allow the rapid determination of local Mach number at any longitudinal position along the rocket surface. Computational fluid dynamics codes, such as the ZEUS code, also provide the local Mach number gradient from the rocket surface to the edge of the nose bow shock wave. This allows the leading-edge Mach number to be determined at any spanwise location along the canard.

The body-alone configuration was modeled in both DATCOM and ZEUS at the freestream Mach numbers of 1.25, 1.50, and 2.00 and angles of attack from zero to ten degrees.

The calculated local Mach numbers at each longitudinal canard position along the nose surface are shown in Table 3.1.

Table 3.1 Local Mach Numbers at Canard Longitudinal Positions Along Rocket Nose

	M=1.25		M=1.50		M=2.00	
	DATCOM	ZEUS*	DATCOM	ZEUS	DATCOM	ZEUS
Position 1	1.14	N/A	1.38	1.36	1.82	1.80
Position 2	1.22	N/A	1.45	1.41	1.91	1.87
Position 3	1.36	N/A	1.58	1.54	2.08	2.05

* Existence of subsonic flow precludes solution

The DATCOM and ZEUS estimates differ by less than three percent. At positions 1 and 2, the flow about the rocket nose is expanding behind the nose shock wave. At position 3, the local Mach number exceeds the freestream value due to expansion about the nose/cylinder juncture. The ZEUS-predicted, spanwise variation of the local Mach number along the canard leading edge was less than three percent at positions 1 and 2. Due to the expanding flow about the nose/cylinder juncture, position 3 exhibited a five percent spanwise variation in local Mach number along the canard leading edge. With such small variations, the flow along the canard leading edge at each position was considered uniform.

For each canard location, the velocity components in the plane of the canard were obtained from ZEUS predictions and the slope of the local flow was calculated. The local slope of the flow coincided with the local body tangent at each position. The local flow was also shown to be uniform in the plane of the canard for angles of attack from zero to ten degrees. Since significant differences between the local and freestream Mach number for supersonic flow about the ogive nose can occur, it is postulated that the local Mach number relative to the canard

must be determined and incorporated into the theory to accurately predict nose-mounted canard aerodynamic characteristics.

3.4.3 Determination of Canard Leading-Edge Condition

In analyzing the experimental data, the canard leading-edge condition (supersonic or subsonic) may be defined by the local Mach number. The Mach angle (μ) given by $\mu = \dfrac{1}{M_L}$, defines the angle between the local velocity and the component of local velocity normal to the canard leading edge. From the ZEUS predictions, it was determined that the local flow at each canard position was nearly uniform along the canard semispan and inclined to the same degree as the canard inclination angle (i.e. the local flow is uniformly parallel with the local body tangent). Therefore the local Mach number for which the supersonic leading-edge condition exists can be determined from the complement of the canard geometric leading-edge sweep angle, θ, shown in Figure 3.17, as

$$M_L = \frac{1}{\sin\theta} = \frac{1}{\sin(90.0 - 43.025)} = 1.36 \ . \tag{3.1}$$

Thus for local Mach numbers greater than and equal to approximately 1.36, the canard will be characterized by a supersonic leading edge ($\theta > \mu$), where the velocity component normal to the leading edge is supersonic. In this case the leading edge is ahead of the Mach wave as shown in Figure 3.17. Likewise, local Mach numbers less than 1.36 result in a subsonic leading edge where the leading edge is behind the Mach angle ($\theta < \mu$). For this case the normal Mach number will be subsonic and no shock wave will be created at the leading edge. Based on the predicted local Mach numbers given in Table 3.1, Table 3.2 summarizes the canard leading-edge conditions for each freestream Mach number and canard position.
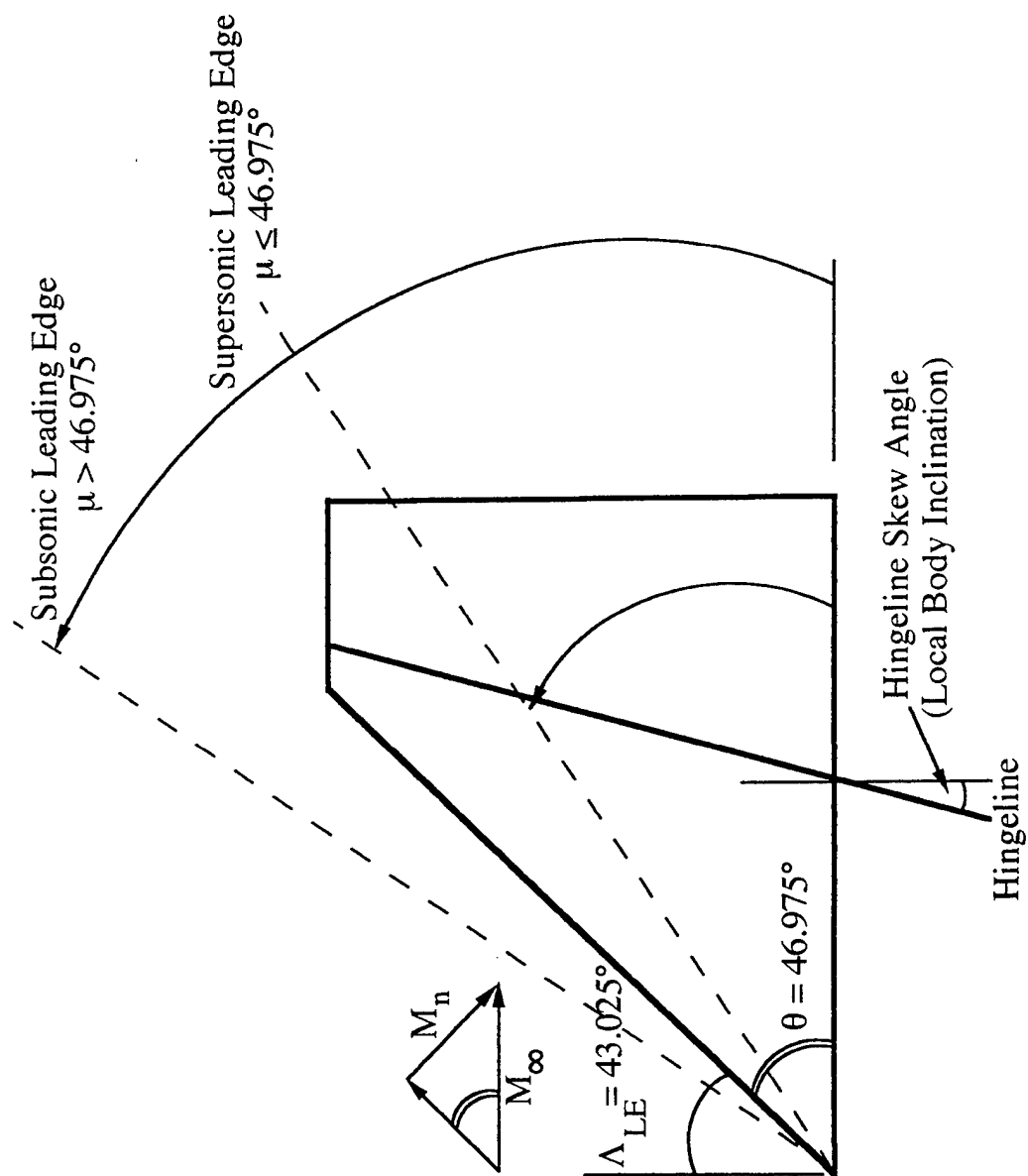
Figure 3.17 Definition of Canard Leading-Edge Conditions

Table 3.2 Leading-Edge Conditions for Canard Longitudinal Positions Along Rocket Nose

	M=1.25	M=1.50	M=2.00
Position 1	Subsonic	Supersonic	Supersonic
Position 2	Subsonic	Supersonic	Supersonic
Position 3	Supersonic	Supersonic	Supersonic

Theoretical methods, such as shock-expansion theory, which are limited to supersonic flow can only provide aerodynamic predictions for canard configurations characterized by a supersonic leading edge.

3.5   Uncertainty in Experimental Data

In an attempt to validate a theoretical approach with experimental data it becomes imperative to quantify uncertainties in the experimental data. Assessing the quality of wind tunnel test data requires a knowledge of the uncertainties associated with the experimental measurements obtained during the test, including model balance data and tunnel operating condition measurements. Coleman and Stern [26] have stated that uncertainty "defines the $\pm U$ interval about that quantity within which we expect the true (but unknown) value of that quantity to lie 95 times out of 100." With renewed emphasis on assessing data quality and developing standards for wind tunnel testing, the analysis techniques for estimating measurement uncertainty have been well documented. [26-30]

An uncertainty analysis was performed on the experimental data obtained from the *CANARD* database. In particular uncertainties associated with canard normal force coefficient, canard hinge moment coefficient, and canard longitudinal center-of-pressure were considered. The uncertainties associated with the independent measurements of systems utilized during the wind tunnel tests are presented in Table 3.3.

Table 3.3 Estimated Uncertainties in System Measurements

Canard Balance		Wind Tunnel Model			Wind Tunnel Facility*		
Normal Force (lbf)	Hinge Moment (in-lbf)	Model Geometry (in.)	δcanard (degrees)	Canard Hingeline Location (in.)	M	P$_T$ (in. of Hg)	α (degrees)
± 0.40	± 0.25	± 0.005	± 0.20	± 0.01	± 1.0%	± 0.004	± 0.10

* Calspan tunnel uncertainties were assumed to be comparable to quoted NASA Ames 6-by-6 foot wind tunnel

Since uncertainties in model geometric parameters and canard balance force and moment measurements were incompletely documented in post-test reports, expert sources [31-33] familiar with these types of three-component panel balances (the MICOM balances in particular) and the wind tunnel model were consulted to confirm the estimated uncertainties shown in Table 3.3. However, uncertainties in tunnel operating conditions and flow quality were not reported for the Calspan and NASA Ames tests. Therefore, estimated uncertainties in wind tunnel operating conditions were also obtained from an expert source [33].

As described in Appendix A, an error propagation technique based on a Taylor series approach was used to estimate the uncertainties in canard normal force coefficient, canard hinge moment, and the calculated longitudinal center-of-pressure. These results are summarized in Table 3.4. Since the uncertainties vary with angle of attack and canard deflection angle, Table 3.4 presents uncertainties obtained for the experimental data at maximum balance loads with ten degrees angle of attack and 9 degrees canard deflection. Detailed uncertainty bands are shown on the following plots of experimental data.

Table 3.4 Estimated Uncertainties in Experimental Data

Mach	U_{CN}/CN	U_{CHM}/CHM	$U_{Xcp}/Croot$		
			Position 1	Position 2	Position 3
1.25	± 5.01%	± 5.01%	± 0.0061	± 0.0054	± 0.0052
1.50	± 5.01%	± 5.01%	± 0.0080	± 0.0071	± 0.0053
2.00	± 5.01%	± 5.01%	± 0.0081	± 0.0075	± 0.0054

The raw wind tunnel test data were considered quality data, with very small flow angularity biases observed at zero angle of attack. Model asymmetry biases could not be addressed due to the lack of test data for the model configuration inverted at ϕ=180 degrees. Although post-test documentation stated excellent instrument repeatability in balance measurements for the repeat runs performed, no repeat runs were performed for the configuration of interest. Therefore, raw wind tunnel data are presented herein and no smoothing or bias removal has occurred.

It was noted that the raw wind tunnel test data of the *CANARD* database were stored to four decimal places with only two significant digits. Due to low tunnel dynamic pressure coupled with a large model reference area, low canard balance loading was developed which resulted in small canard moments and required a minimum of five decimal places with two significant digits. Due to the lack of sufficient decimal places and significant digits, some of the canard hinge moment data plots exhibit a stairstep effect with variation in angle of attack. The uncertainties associated with this data-reduction round-off were not addressed.

Chapter 4

THEORETICAL APPROACH

The calculation of canard hinge moment involves determining the canard normal force and the longitudinal center-of-pressure position. Accurate prediction of the canard longitudinal center-of-pressure location relative to the control hingeline can greatly affect the hinge moment acting on the canard, thus providing requirements for defining the control actuation system.

A hinge moment prediction method incorporating shock-expansion theory and strip theory has been advanced by Nielsen and Goodwin [8] to predict the shift in center-of-pressure due to airfoil thickness for all-movable canard controls at supersonic speeds. With an initial, semi-empirical estimate of the center-of-pressure, the Nielsen approach determines the shift in center-of-pressure based on a theoretical correction for airfoil thickness. Depending on the accuracy of the initial center-of-pressure estimate, the thickness correction may, in some cases, actually worsen hinge moment predictions. Therefore, the theoretical aspects advanced in this thickness correction have been expanded to derive a new method to estimate nose-mounted canard aerodynamic characteristics based solely on first principles, eliminating any empirical aspects. Numerous aerodynamic theories exist which predict wing-alone aerodynamic characteristics [9, 13-15]. The approach chosen for this study utilizes two-dimensional shock-expansion theory to determine canard normal force, longitudinal center-of-pressure, and resulting moment about the relative hingeline for a given airfoil section. This method has been expanded herein to provide canard-alone normal force coefficient and longitudinal center-of-pressure. Calculations of the canard normal force and hinge moment for each section strip are integrated along the canard semispan from root to tip using the two-dimensional strip theory technique. Thus, the three-dimensional canard shape is characterized using two-dimensional flow relations.

Theoretical corrections to canard-alone center-of-pressure and normal force coefficient are included which are based on linear theory and slender-body theory. These corrections account for three-dimensional effects which are not represented in shock-expansion theory such as the canard tip pressure loss and canard-body interference. Lastly, the position of the hingeline

relative to the normal force acting at the center-of-pressure determines the hinge moment for the canard on the rocket nose.

4.1 Limitations and Generalizations

In the application of the theoretical methods the following limiting assumptions are made: (1) supersonic, inviscid, compressible flow, (2) an attached shock on the canard leading edge (sharp leading edge), (3) supersonic leading-edge condition, and (4) relatively low angles of attack and canard deflections sufficient for linear aerodynamics ($\alpha, \delta \leq 10°$).

Observations from the experimental data analyses have provided generalizations about nose-mounted canard aerodynamics which may offer simplifications in the theoretical approach. The theoretical approach is restricted in application to a single canard mounted in the horizontal plane of the rocket nose. First, it is assumed that the nose shock wave does not intersect the canard and the canard is located ahead of the influence of body vortices. The flow about the canard is considered isentropic such that shock-expansion relations for compressible flow may be considered. The effects of mutual canards are not considered.

ZEUS calculations indicated that the local flow ahead of a canard is uniform across the semispan and inclined at the same angle as the local body tangent. Therefore the canard inclined on the body at any location along the nose can be modeled as the canard-alone having zero trailing edge sweep with the flow parallel to the canard as shown in Figure 3.17. Thus the hingeline, which is perpendicular to the body centerline for the canard inclined on the nose, becomes skewed by the local inclination angle for the canard-alone model.

The canard may be described by a spanwise series of two-dimensional, symmetric airfoil sections, each of which is comprised of a series of straight line segments. Each straight line segment represents a compression or expansion region for the flow. It is assumed that the local flowfields in the different regions of an airfoil section are independent of each other such that no shock reflections/interactions occur and the flow through each region is uniform.

Such limiting assumptions and generalizations for nose-mounted canards has provided a means to develop a theoretical approach which does not involve large amounts of computational time or storage and could be easily incorporated as a subroutine into such rapid aerodynamic

prediction codes as Missile DATCOM. The details of this technique are outlined in the following sections.

4.2   Shock-Expansion and Airfoil Strip Theory

Shock-expansion theory allows the exact calculation of the aerodynamic forces on a two-dimensional airfoil section (strip) in compressible, supersonic flow by the stepwise application of isentropic oblique shock wave and Prandtl-Meyer expansion relations. Such theoretical relations, which have been obtained from the application of the physical principles of mass, momentum, and energy conservation to fluid flows, are well documented in NACA Report 1135 [34] as well as numerous texts [35-37].

Nielsen and Goodwin [8] have described the method for calculating the pressure distribution on a symmetric airfoil section using shock-expansion theory as follows. Consider a symmetric airfoil section which is described by a series of straight line segments (N) for an upper and lower surface relative to the freestream flow as shown in Figure 4.1. Each segment on the upper and lower surface provides a compression or expansion region for which oblique shock theory and Prandtl-Meyer expansion theory may be applied to characterize the local Mach number, local compression/expansion angle, and the local surface pressure coefficient. The variation in pressure coefficient between the upper and lower surface regions determines the normal force coefficient and hinge moment coefficient.

For an airfoil section at positive angle of attack, region 1 of the lower surface provides a compression of the freestream flow through an angle

$$\delta = \alpha + \theta_1 .$$

(4.1)
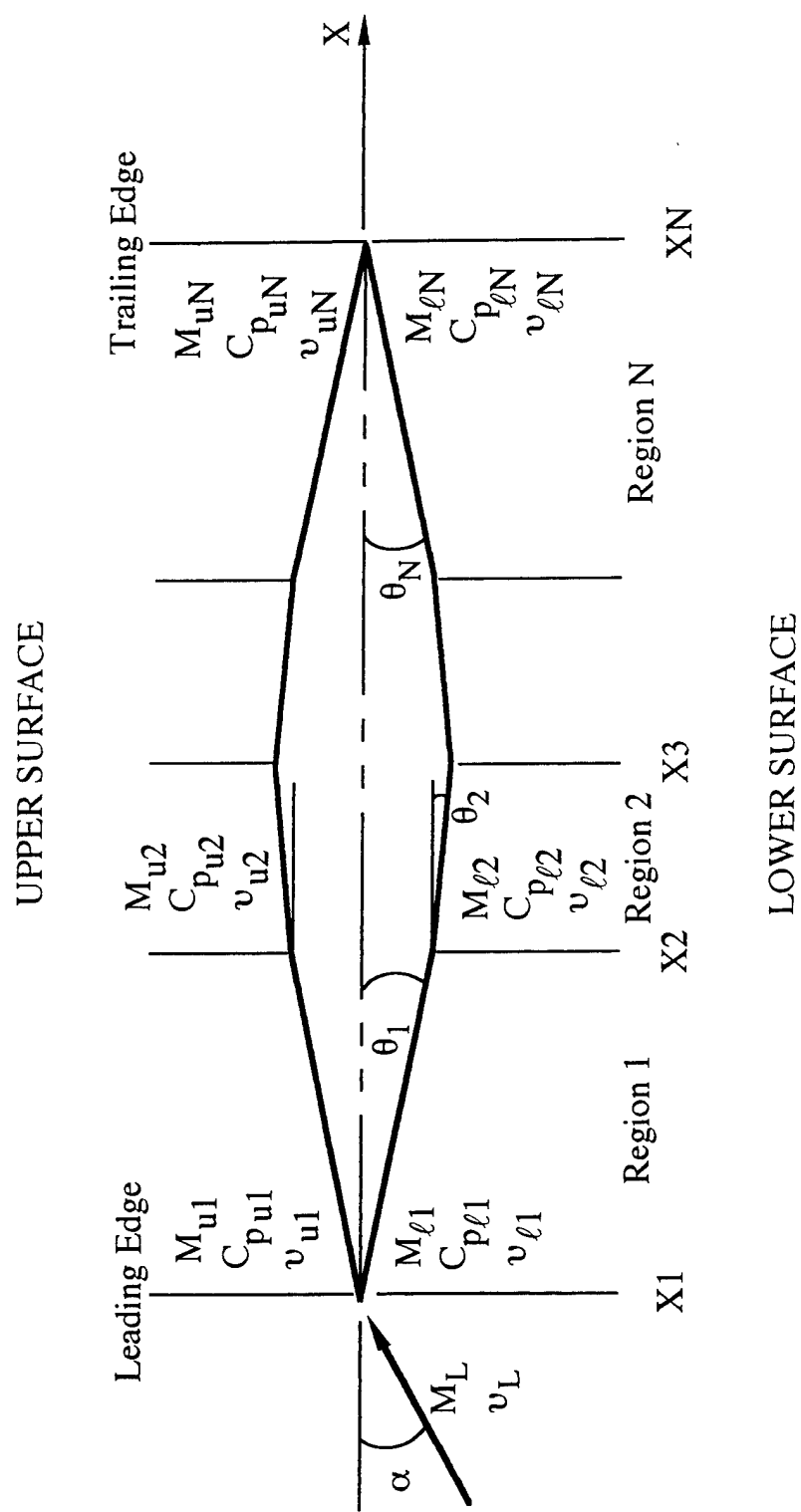
Figure 4.1 Symmetric Airfoil Section Defining Regions for Shock-Expansion Theory

The shock wave angle, θ_S, is determined by an iterative solution of the equation

$$\cot \delta = \tan \theta_s \left[\frac{(\gamma + 1)M_\infty^2}{2\left(M_\infty^2 \sin^2 \theta_s - 1\right)} - 1 \right] .$$ (4.2)

The maximum shock wave angle for an attached shock is given by

$$\sin \theta_{S\text{max}} = \left[\frac{-\left[4 - (\gamma + 1)M_\infty^2\right] + \sqrt{(\gamma + 1)^2 M_\infty^4 + 8(\gamma + 1)(\gamma - 1)M_\infty^2 + 16(\gamma + 1)}}{4\gamma M_\infty^2} \right]^{1/2}$$ (4.3)

Solving Equation 4.2 with $\theta_{S\text{max}}$ will determine the maximum value of δ for an attached shock, δ_{max}, at the local Mach number. If $\delta < \delta_{\text{max}}$ then Equation 4.2 can be solved for the value of θ_S which is less than $\theta_{S\text{max}}$ for an attached shock. The local Mach number, Prandtl-Meyer angle, and ratio of total pressure to freestream total pressure for region 1 of the lower airfoil surface are determined by

$$M_{L_1} = \left\{ \frac{(\gamma + 1)^2 M_\infty^4 \sin^2 \theta_s - 4\left(M_\infty^2 \sin^2 \theta_s - 1\right)\left(\gamma M_\infty^2 \sin^2 \theta_s + 1\right)}{\left[2\gamma M_\infty^2 \sin^2 \theta_s - (\gamma - 1)\right]\left[(\gamma - 1)M_\infty^2 \sin^2 \theta_s + 2\right]} \right\}^{1/2}$$ (4.4)

$$v_{L_1} = \sqrt{\frac{\gamma + 1}{\gamma - 1}} \tan^{-1} \sqrt{\frac{\gamma - 1}{\gamma + 1}\left(M_{L_1}^2 - 1\right)} - \tan^{-1} \sqrt{\left(M_{L_1}^2 - 1\right)}$$ (4.5)

$$\frac{P_{t_{L_1}}}{P_{t_\infty}} = \left[\frac{(\gamma + 1)M_\infty^2 \sin^2 \theta_s}{(\gamma - 1)M_\infty^2 \sin^2 \theta_s + 2} \right]^{\frac{\gamma}{\gamma - 1}} \left[\frac{\gamma + 1}{2\gamma M_\infty^2 \sin^2 \theta_s - (\gamma - 1)} \right]^{\frac{1}{\gamma - 1}} .$$ (4.6)

The pressure coefficient for region 1 of the lower surface is given by

$$C_{P_{L_1}} = \frac{P_{L_1} - P_\infty}{q_\infty} = \frac{4\left(M_\infty^2 \sin^2 \theta_s - 1\right)}{(\gamma + 1)M_\infty^2} \quad . \tag{4.7}$$

The remaining regions, n=2, 3, ...N, on the lower surface of the airfoil are all characterized by expansions in the flow; therefore, the equations for the local flow quantities and pressure coefficient are identical. For these regions the flow expands through the angle (θ_{n-1} - θ_n). Therefore the Prandtl-Meyer angle for region n is

$$v_{L_n} = v_{L_{n-1}} + \left(\theta_{n-1} - \theta_n\right) \tag{4.8}$$

and the local Mach is given by the empirical relation [38]

$$M_{L_n} = \frac{1 + 1.3604\bar{v} + 0.0962\bar{v}^2 - 0.5127\bar{v}^3}{1 - 0.6722\bar{v} - 0.3278\bar{v}^2} \tag{4.9}$$

where

$$\bar{v} = \left(\frac{v_{L_n}}{v_{max}}\right)^{2/3} \quad ; \qquad v_{max} = \frac{\pi}{2}\left(\sqrt{\frac{\gamma + 1}{\gamma - 1}} - 1\right) \quad . \tag{4.10}$$

The ratio of static pressure to total pressure in region n is calculated by

$$\frac{P_{L_n}}{P_{t_{L_n}}} = \left(1 + \frac{\gamma - 1}{2} M_{L_n}^2\right)^{\frac{-\gamma}{\gamma - 1}} \quad . \tag{4.11}$$

Since the expansion is isentropic, $P_{t_{L_n}} = P_{t_{L_1}}$, and the equation for pressure coefficient is

$$C_{P_{L_n}} = \frac{\left(\dfrac{P_{L_n}}{P_{t_{L_n}}}\right)\left(\dfrac{P_{t_{L_1}}}{P_{t_\infty}}\right) - \dfrac{P_\infty}{P_{t_\infty}}}{\dfrac{q_\infty}{P_{t_\infty}}} \qquad (4.12)$$

where $\left(\dfrac{P_{t_{L_1}}}{P_{t_\infty}}\right)$ is defined by Equation 4.6 and the freestream relations are

$$\frac{P_\infty}{P_{t_\infty}} = \left(1 + \frac{\gamma - 1}{2} M_\infty^2\right)^{\frac{-\gamma}{\gamma - 1}} \qquad (4.13)$$

and

$$\frac{q_\infty}{P_{t_\infty}} = \frac{\gamma}{2} M_\infty^2 \left(\frac{P_\infty}{P_{t_\infty}}\right) \qquad (4.14)$$

Evaluating Equations 4.8 through 4.14 for the regions n=2, 3, ...N, provides the pressure distribution on the lower surface of the airfoil section.

The pressure distribution on the upper surface is determined in like manner. In calculating the pressure coefficient for region 1 of the upper airfoil surface at positive angles of attack, one must first determine if the flow compresses or expands. For the case $\alpha \leq \theta_1$, the freestream flow is compressed and a shock wave is developed on the upper surface leading edge. The procedure described for region 1 of the lower surface is applicable where the freestream flow is now deflected through the angle

$$\delta = -(\alpha - \theta_1) \quad . \qquad (4.15)$$

The shock wave angle, θ_S, for the upper surface is then determined from Equation 4.2. Likewise the local flow quantities may be determined from Equations 4.4 through 4.6. The pressure coefficient for compressing flow in region 1 of the upper surface is defined by Equation 4.7.

For the case of $\alpha > \theta_1$, the freestream flow is expanded through and angle $(\alpha - \theta_1)$ in region 1 of the upper surface. Therefore the Prandtl-Meyer angle for region 1 is

$$v_{U_1} = v_\infty + (\alpha - \theta_1) \tag{4.16}$$

where

$$v_\infty = \sqrt{\frac{\gamma+1}{\gamma-1}} \tan^{-1} \sqrt{\frac{\gamma-1}{\gamma+1}(M_\infty^2 - 1)} - \tan^{-1} \sqrt{(M_\infty^2 - 1)} \ . \tag{4.17}$$

The local Mach number is given by Equations 4.9 and 4.10. The static to total pressure ratio and pressure coefficient in region 1 of the upper surface are calculated by Equations 4.11 and 4.12, respectively. If region 1 on the upper surface is defined by an expansion of the freestream flow, no shock wave exists, and

$$\frac{P_{t_{U_1}}}{P_{t_\infty}} = 1.0 \ . \tag{4.18}$$

The remaining regions, n=2, 3, ...N, on the upper surface of the airfoil are all characterized by flow expansions. Hence the procedure for obtaining the pressure coefficients for region n on the upper surface are identical to that described for the same region on the lower surface in Equations 4.8 through 4.12.

With the pressure distribution calculated for each region of the airfoil section, the increment in normal force coefficient for region n may be determined from the difference in

upper and lower surface pressure coefficient as

$$(C_N)_n = \frac{\left(C_{P_{L_n}} - C_{P_{U_n}}\right)\left(x_n - x_{n-1}\right)}{L_{ref}} .$$ (4.19)

Likewise, the increment in hinge moment for region n about the local hingeline, measured from the leading edge along the local chord, is given as

$$(C_{hm})_n = \left[(C_N)_n\right]\left[\left(\frac{X_{HL}}{c}\right)_{LE} - \left(\frac{x_n + x_{n-1}}{2c}\right)\right]$$ (4.20)

where c is the local airfoil-strip chord. The local hingeline measured from the leading edge for each strip may be determined from simple geometric relations with the hingeline skew angle given by the local inclination angle of the canard on the nose.

Since the pressure in each region is considered uniform, the center-of-pressure of each region in a strip is located at the centroid of the surface constituting the region. Summing the aerodynamic coefficients from Equation 4.19 and 4.20 for N regions provides the strip normal force and hinge moment coefficients, respectively. The moment arm between the hingeline and longitudinal center-of-pressure location for each airfoil strip is obtained from the strip normal force coefficient and strip hinge moment coefficient by

$$\frac{\left(X_{HL} - X_{CP}\right)_{LE}}{c} = \frac{\sum_{n=1}^{N}(C_{hm})_n}{\sum_{n=1}^{N}(C_N)_n} .$$ (4.21)

Now, consider the canard shown in Figure 4.2. The application of strip theory allows calculation of canard aerodynamic characteristics from the integration of the aerodynamic characteristics of each airfoil strip, j. The canard planform can be divided into any number of longitudinal two-dimensional strips, J, with the canard root chord defined as j=1 and the tip
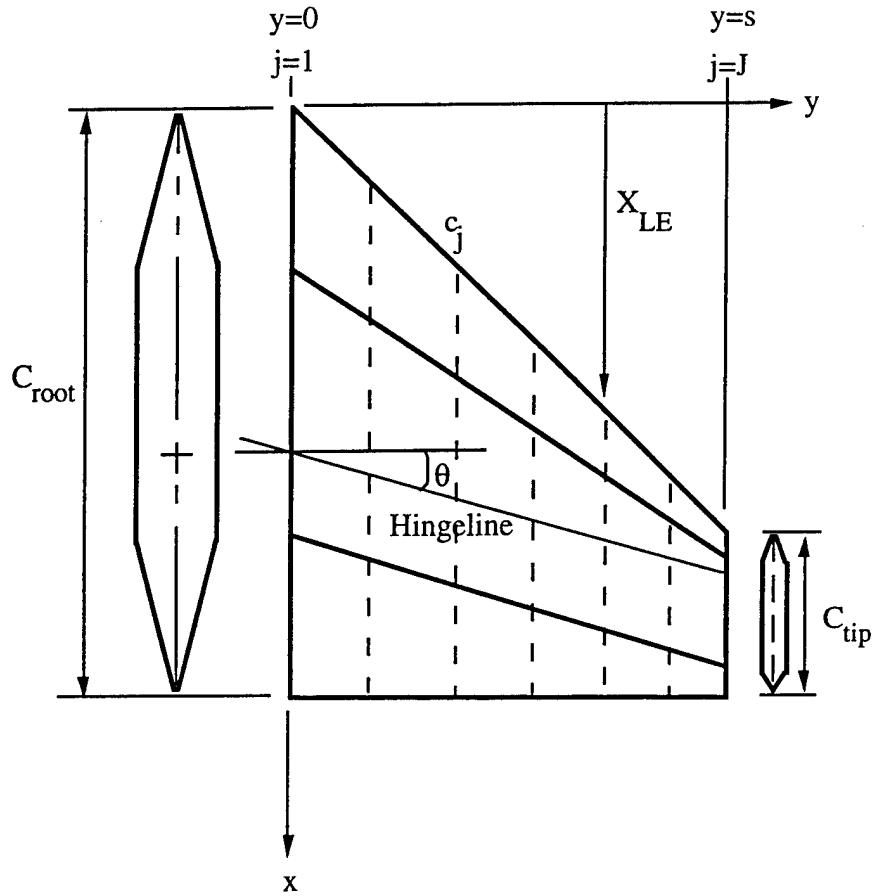
Figure 4.2 Canard Planform Defining Regions for Airfoil Strip Theory

chord as j=J. Each airfoil strip is defined by N upper and lower surface regions as presented in Figure 4.1. Utilizing strip theory to sum over all the strips of a canard, the moment arm for the entire canard in terms of the root chord may be calculated by

$$\left(\frac{(X_{HL}-X_{CP})_{LE}}{C_r}\right) = \frac{\int_0^{b/2} \frac{c^2}{C_r} C_N \left[\left(\frac{X_{HL}}{c}-\frac{X_{CP}}{c}\right)_{LE}\right]dy}{\int_0^{b/2}(cC_N)dy} \quad . \tag{4.22}$$

The numerator defines the hinge moment coefficient and the denominator defines the normal force coefficient for the canard alone. For the known value of canard hingeline location relative to the leading edge at the root chord $\left(\dfrac{X_{HL}}{C_r}\right)_{LE}$ the longitudinal center-of-pressure position $\left(\dfrac{X_{CP}}{C_r}\right)_{LE}$ for the canard alone may also be determined from Equation 4.22.

Thus far canard-alone aerodynamic characteristics have been evaluated for two-dimensional airfoils of infinite span or aspect ratio. In reality, airfoils are characterized by finite aspect ratio and thereby experience three-dimensional effects associated with the local flow as well as external influences. Corrections may be applied to the two-dimensional, canard-alone normal force and center-of-pressure to account for three-dimensional effects. Such corrections are addressed in the following sections.

4.3   Canard Tip Effects

For a canard of finite aspect ratio, a pressure loss occurs in the region of the tip as a result of the pressure differential between the upper and lower surfaces of the canard. The air on the lower surface is at a higher pressure than the surrounding air and tends to flow outward toward the tip. The low pressure air on the upper surface tends to draw the lower surface air in over the tip, decreasing the value of the upper pressure. For the canard in supersonic flow, such pressure losses are limited to the region of influence within the tip Mach cone defined by the local Mach number.

For a two-dimensional airfoil of finite thickness, Bonney [11] has shown that the normal force for the canard of finite aspect ratio can be corrected for tip losses by

$$C'_{N_c} = C_{N_c}\left[\left(1-\frac{1}{2\beta A}\right)\left(1-2\left\{\frac{0.6M^4-M^2+1}{\left(M^2-1\right)^{3/2}}\right\}\left\{\frac{A_{cs}}{c^2}\right\}\right)\right] . \qquad (4.23)$$

The correction in brackets is comprised of two parts. The factor in the first set of parentheses represents the aspect-ratio correction to two-dimensional lift due to lift of a flat plate of zero

thickness. The factor in the second set of parentheses accounts for a particular combination of Mach number and airfoil thickness ratio. This term is generally neglected since it becomes very small for practical values of airfoil thickness ratio applicable at supersonic speeds. Equation 4.23 is applicable for high aspect ratio fins and can be applied down to the limiting aspect ratio given by $1/\beta$.

The loss of pressure within the tip Mach cone also results in a forward shift in the canard longitudinal center-of-pressure. For the Mach numbers of interest to this study, the tip Mach cone angles were determined in Section 3.4.3. The area influenced by each Mach cone was calculated and the centroid of the area determined. The canard-alone pitching moment about the leading edge was determined from the normal force acting at the center-of-pressure, neglecting tip effects. Next, the pitching moment about the leading edge due to tip effect was determined for the normal force increment acting at the area centroid of the Mach cone. The incremental change in pitching moment and normal force resulted in an estimated two percent forward shift in the canard longitudinal center-of-pressure due to tip effects. Therefore the center-of-pressure for the canard-alone is multiplied by 0.98 to adjust for tip effects.

4.4   Corrections for Freestream Mach Number

It has been previously concluded that the local Mach number of the flow in the nose region is significantly different from the freestream Mach number ahead of the nose bow shock wave. Classical theories, such as the shock-expansion theory, use "freestream" flow conditions, M_∞, P_∞, $P_{t\infty}$, and q_∞ just ahead of the canard leading-edge shock. For the case of nose-mounted canards, such "freestream" conditions are replaced by flow properties in the nose region ahead of the canard leading-edge shock. Therefore the local Mach number for nose-mounted canards must be determined and applied as the "freestream" value in shock-expansion theory to accurately predict the aerodynamic characteristics of the canards.

For consistent comparison with classical aerodynamic prediction techniques and wind tunnel data, the theoretical canard aerodynamic characteristics determined for such local flow conditions on the nose are referenced to the actual freestream flow conditions ahead of the nose bow shock wave. In this case, canard-alone normal force coefficient may be referenced to actual

rocket freestream conditions by Equation 4.24.

$$\left(C_{N_c}^{'}\right)_{FS} = \left(C_{N_c}^{'}\right)\left(\frac{M_L^2}{M_\infty^2}\right)$$ (4.24)

4.5   Canard-Body Interference Effects

To this point only canard-alone aerodynamic characteristics have been considered. However, the canard aerodynamics are also influenced by the rocket body. Interference effects for the canard in the presence of the body have been estimated by Pitts, Nielsen, and Kaattari [5] using slender-body theory. Slender-body theory is mainly applicable to sharp-nosed, slender bodies with canards mounted on a cylindrical section (uniform diameter) sufficiently aft of the expanding nose section. The theory is also restricted to small angles of attack and canard deflection.

For the rocket body at angle of attack and zero canard deflection, the normal force coefficient for the canard (wing) in the presence of the body is given by

$$C_{N_{W(B)}} = K_{W(B)}\left(C_{N_\alpha}\right)_W \alpha_W \quad ; \quad \delta_W = 0 \ .$$ (4.25)

Here, C_{N_W} is defined as the normal force coefficient for the canard-alone adjusted for tip effects and freestream reference conditions, $\left(C_{N_c}^{'}\right)_{FS}$ of Equation 4.24. The value of the canard-body interference factor with angle of attack, $K_{W(B)}$, is given by slender-body theory as

$$K_{W(B)} = \frac{2}{\pi} \frac{\left\{\left(1+\frac{r^4}{s^4}\right)\left[\frac{1}{2}\tan^{-1}\frac{1}{2}\left(\frac{s}{r}-\frac{r}{s}\right)+\frac{\pi}{4}\right]-\frac{r^2}{s^2}\left[\left(\frac{s}{r}-\frac{r}{s}\right)+2\tan^{-1}\frac{r}{s}\right]\right\}}{\left(1-\frac{r}{s}\right)^2}$$ (4.26)

which is only a function of the body radius, r, and the maximum semispan of the canard in combination with the body, s. This term characterizes the body upwash effect on the canard.

Likewise for the rocket body at zero angle of attack and canard (wing) deflected through the angle δ_W, the normal force coefficient for the canard in the presence of the body is given by

$$C_{N_{W(B)}} = k_{W(B)} \left(C_{N_\alpha} \right)_W \delta_W \quad ; \quad \alpha = 0 \quad . \tag{4.27}$$

The value of the canard-body interference factor with canard deflection, $k_{W(B)}$, is given by slender-body theory as

$$k_{W(B)} = \frac{1}{\pi^2} \left[\frac{\pi^2}{4} \frac{(\tau+1)^2}{\tau^2} + \frac{\pi(\tau^2+1)^2}{\tau^2(\tau-1)^2} \sin^{-1} \frac{\tau^2-1}{\tau^2+1} - \frac{2\pi(\tau+1)}{\tau(\tau-1)} + \right. $$

$$\left. \frac{(\tau^2+1)^2}{\tau^2(\tau-1)^2} \left(\sin^{-2} \frac{\tau^2-1}{\tau^2+1} \right)^2 - \frac{4(\tau+1)}{\tau(\tau-1)} \sin^{-1} \frac{\tau^2-1}{\tau^2+1} + \frac{8}{(\tau-1)^2} \log \frac{\tau^2+1}{2\tau} \right] \tag{4.28}$$

where τ is the semispan-radius ratio, s/r.

With the interference terms defined and assuming $\left(C_{N_\delta} \right)_W = \left(C_{N_\alpha} \right)_W$, the normal force coefficient for the canard in the presence of the nose is given by

$$C_{N_{W(B)}} = \left(C_{N_\alpha} \right)_W \left(K_{W(B)} \alpha + k_{W(B)} \delta_W \right) \quad . \tag{4.29}$$

The applicability of the interference terms defined in Equation 4.29 is questionable since the terms are restricted to slender wing-body combinations with the wing leading edge located downstream of the influence of the nose on a cylindrical section (s/r is constant). The nose-mounted canards are mounted on an expanding section of the nose where the semispan-radius ratio is not constant and the assumption of an infinite cylindrical body does not hold. Therefore the validity of slender-body theory estimations of body upwash is not known. As the body angle of attack increases, the magnitude of the velocity component normal to the body increases. This

results in an effective increased angle of attack on the canards mounted on the body, known as the body carryover interference.

It was not known how well slender-body theory results would characterize the body carryover interference for canards mounted on the rocket nose or if the carryover interference would be significant. To characterize body carryover interference, the ZEUS code was again used to determine the local velocity components in the vicinity of the canards at Mach 1.25, 1.50, and 2.00 and angles of attack of zero to ten degrees. The flowfield characteristics were obtained for the midspan station at each canard position. The local effective angle of attack was calculated by the geometric relation of the two velocity components. Dividing this local angle of attack by the actual body angle of attack provided the effective body upwash, $K_{W(B)}$. It was observed that the canard-body interference factor was constant with angle of attack and Mach number for a given canard position along the nose. The r/s ratio at each hingeline position along the nose was calculated as 0.542, 0.588, and 0.625 for position 1, 2, and 3 respectively. These values of r/s ratio were used to calculate the carryover interference factor given by slender-body theory in Equation 4.26. The values of $K_{W(B)}$ estimated from ZEUS are compared with slender-body theory in Table 4.1. Note that a significant difference appears between the interference factor calculated by slender-body theory and ZEUS.

Additionally, DATCOM estimations of carryover interference were analyzed. Based on slender-body theory, DATCOM methods are corrected for angle of attack with empirical data and agree to within five percent of the ZEUS predictions. Due to this good agreement between ZEUS and DATCOM predictions of carryover interference, the DATCOM values were utilized in subsequent calculations for canards mounted on the rocket nose.

Table 4.1 Comparison of Canard-Body Interference Factor , $K_{W(B)}$

	$K_{W(B)}$	
	Slender-Body Theory (Eq. 4.26)	ZEUS
Position 1	1.49	1.30
Position 2	1.54	1.30
Position 3	1.58	1.32

Another effect of the body influence on the canard is a shift in the longitudinal center-of-pressure. From slender-body theory, the center-of-pressure for a canard in the presence of an infinite cylinder at angle of attack and zero canard deflection is given by

$$\left(\frac{X_{CP}}{C_r}\right)_{W(B)\alpha} = \frac{1}{\left(1-\dfrac{r}{s}\right)} \times$$

$$\frac{2\left(\dfrac{1}{3}+\dfrac{r^4}{s^4}\right)\tan^{-1}\left(\dfrac{s}{r}\right)+\dfrac{2}{3}\dfrac{r^3}{s^3}\ln\left[\left(\dfrac{s^2+r^2}{2s^2}\right)^2\dfrac{s}{r}\right]-\dfrac{1}{3}\dfrac{r^3}{s^3}\left(2\pi-1+\dfrac{s^2}{r^2}\right)}{\left(1+\dfrac{r^2}{s^2}\right)^2\tan^{-1}\left(\dfrac{s}{r}\right)-\dfrac{r^2}{s^2}\left[\pi+\left(\dfrac{s}{r}-\dfrac{r}{x}\right)\right]}-\dfrac{\dfrac{r}{s}}{\left(1-\dfrac{r}{s}\right)}$$

$$(4.30)$$

Nielsen [9] has concluded that the center-of-pressure of a canard in the presence of the body with canard deflection and zero body incidence may be approximated by the canard-alone center-of-pressure as

$$\left(\frac{X_{CP}}{C_r}\right)_{W(B)\delta} = \left(\frac{X_{CP}}{C_r}\right)_{W}$$

$$(4.31)$$

The canard center-of-pressure in the presence of the body may now be determined by

$$\left(\frac{X_{CP}}{C_r}\right)_\alpha = \left(\frac{X_{CP}}{C_r}\right)_W - \left[\left(\frac{X_{CP}}{C_r}\right)_{W(B)\,r/s=0} - \left(\frac{X_{CP}}{C_r}\right)_{W(B)\,r/s}\right] \qquad (4.32)$$

where the corrections due to canard-body interference for the r/s ratio are applied.

Finally, the hinge moment for the canard in the presence of the body may be determined from the normal force coefficient defined by Equation 4.29 and the longitudinal center-of-pressure given in Equations 4.31 and 4.32 as

$$C_{HM} = \frac{C_r}{d}\left\{\left(C_{N\alpha}\right)_W K_{W(B)}\alpha\left(\frac{X_{HL} - \left(X_{CP}\right)_\alpha}{C_r}\right) + \left(C_{N\alpha}\right)_W k_{W(B)}\delta_W\left(\frac{X_{HL} - \left(X_{CP}\right)_\delta}{C_r}\right)\right\} . \qquad (4.33)$$

Through the application of this fundamental theoretical approach it is concluded that the hinge moments for canards mounted on the rocket nose may be estimated with better accuracy than current aerodynamic predictions codes such as Missile DATCOM. Due to the complexity and repetitiveness of the theoretical methods, a computer subroutine has been coded to perform the calculations and provide estimates of canard normal force coefficient, center-of-pressure, and hinge moment coefficient.

4.6   Description of *FINCHM* Code

A FORTRAN subroutine, *FINCHM*, has been developed which incorporates the theoretical methods previously described to determine normal force coefficient, longitudinal center-of-pressure, and hinge moment coefficient for the canard mounted along the rocket nose. For versatility, the code was developed to maximize the use of the input variables common to Missile DATCOM. Thus the subroutine could be easily incorporated into DATCOM to provide a more accurate approach for estimating the aerodynamic characteristics of nose-mounted canards. A listing of the *FINCHM* subroutine and the main program appears in Appendix B.

Due to the scope of this research, additional limitations were imposed on the code regarding applicable airfoil shapes and canard planforms. The code is limited to symmetric airfoil shapes which can be modeled in DATCOM, particularly double-wedge and modified double-wedge airfoils. Canard planform is limited to a straight-tapered delta/clipped-delta shape with no trailing-edge sweep. Only one canard panel is modeled in the horizontal plane with positive angle of attack and canard deflection. However, the robustness of the code will allow easy modifications to include other airfoil sections and canard planforms.

The following sequence of calculations are performed in *FINCHM*. First, the required rocket and canard-alone geometric parameters are defined along with the local Mach number, freestream Mach number, and canard deflection angles for a given canard position along the nose. The significance of characterizing the local flow along the nose dictates that an external method be used in estimating the local Mach number. Such methods discussed in Section 3.4.2 include ZEUS and DATCOM. The local Mach number calculated by DATCOM could be easily passed to the *FINCHM* subroutine. Another key input is the canard hingeline skew angle. For a canard inclined on the nose, this is defined as the angle between a line normal to the local flow and the hingeline as shown in Figure 3.17. For the case where the canard hingeline is perpendicular to the rocket centerline axis, such as for the experimental data presented in this thesis, the hingeline skew angle for the canard-alone is defined as the local inclination angle of the canard on the body. The number of airfoil strips to be used in the strip theory are also input at this point.

Next, the canard-body carryover interference terms are calculated for angle of attack and canard deflections from slender-body theory and passed to the subroutine. The canard-body interference factors with angle of attack, $\left(K_{W(B)}\right)_\alpha$, determined from the ZEUS results discussed in Section 4.5 were hardwired in the code to obtain the theoretical results shown in this thesis. However, if the subroutine was incorporated into DATCOM, the interference terms calculated by DATCOM would suffice and could be easily passed into the *FINCHM* subroutine.

A check for an attached shock along the canard leading edge is performed for the root chord and tip chord at the local Mach number. If the leading edge angle exceeds that required for shock attachment, a modified leading-edge angle is defined as the maximum for an attached

shock wave angle determined at an angle of attack of ten degrees. The canard geometry is then modified accordingly.

The canard planform geometry is next dissected into a number of airfoil strips and shock-expansion theory is progressively applied through the compression/expansion regions of each strip at angle of attack and zero canard deflection. Simpson's Rule of Integration is employed to integrate the canard-alone normal force and pitching moment about the leading edge for each strip along the canard semispan and to determine the longitudinal center-of-pressure for the canard-alone. Canard tip effects are then applied to the canard-alone normal force coefficient and center-of-pressure. Finally, the normal force coefficient and center-of-pressure are corrected for canard-body interference effects and the hinge moment coefficient is calculated.

Based on an assumption of linear aerodynamics, the variation in canard-alone normal force coefficient with angle of attack is determined at a one degree angle of attack. This slope is used to determine the canard-alone normal force coefficient for angles of attack greater than one degree. Starting with the application of canard-body interference, the procedure to determine hinge moment coefficient is repeated for angles of attack to ten degrees.

For canard deflections greater than zero, the canard deflection angle is summed with the angle of attack to give an "effective" angle of attack. This "effective" angle of attack is multiplied by the slope of the canard-alone normal force coefficient to estimate the canard-alone normal force coefficient for canard deflections at angle of attack. The procedure is then repeated to account for canard-body interference effects and canard hinge moment coefficients are calculated. Aerodynamic coefficients are referenced to the freestream Mach number ahead of the rocket nose shock for comparison to experimental data and DATCOM predictions.

Chapter 5

COMPARISON OF EXPERIMENTAL DATA WITH PREDICTIONS

The *FINCHM* code was utilized to estimate the canard normal force coefficient, longitudinal center-of-pressure, and hinge moment coefficient for the canard configurations shown in Figures 3.1 and 3.2. The *FINCHM* output for the theoretical data presented in the plots of this section appears in Appendix C. The results were compared with experimental data to validate the theoretical approach. In addition Missile DATCOM 6/93 predictions were obtained to assess the accuracy of the theoretical approach in relation to semi-empirical methods.

The geometric characteristics of the canard were modeled and the hingeline skew angle at each of the three longitudinal positions along the rocket nose was determined as the local tangent to the nose at the hingeline location. DATCOM estimates of local Mach number at each canard position, given in Table 3.1, were input to the *FINCHM* code along with the corresponding freestream Mach numbers of 1.25, 1.50, or 2.00. Based on a strip resolution study performed to ascertain prediction convergence, the canard planform was divided into 101 equally-spaced airfoil strips for the theoretical computations. Theoretical estimations of the canard aerodynamic characteristics were determined for the local Mach number conditions along the ogive nose.

For the DATCOM predictions the body-canard configuration geometry was modeled exactly as that of the experimental data with four canards, two horizontal canards mutually deflected in pitch and two vertical canards at zero deflection. Again, DATCOM predicts canard aerodynamics based on the input freestream Mach number ahead of the nose bow shock. Depending upon the difference between the local Mach number and the freestream Mach number, inaccurate predictions may be realized for nose-mounted canards. Also, DATCOM utilizes a semi-empirical method to obtain the canard center-of-pressure as a function of freestream Mach number, canard aspect ratio, and canard leading-edge sweep angle for a thin wing.

Figures 5.1-5.24 present comparisons of *FINCHM* calculations and DATCOM predictions with the *CANARD* experimental data. Data are presented for a canard mounted in the horizontal plane for Mach 1.25, 1.50, and 2.00 at angles of attack from -3 to 12 degrees and canard deflections of 0, 3, and 9 degrees. The data correspond to the aerodynamic characteristics of the canard in the presence of the rocket nose. The *FINCHM* coefficients are referenced to freestream Mach number for direct comparison with experimental data and DATCOM predictions. Due to the subsonic nature of the local flow, theoretical results were not obtained for canard position 1 and 2 at Mach 1.25. Estimated experimental uncertainty bands, which were determined in Appendix A, are included in the analysis plots.

Figures 5.1-5.3 show the aerodynamic characteristics for the canard at Mach 1.25 and position 3. *FINCHM* and DATCOM predictions of canard normal force coefficient are shown in Figure 5.1 to generally overpredict the experimental data. The linearity of the normal force coefficient is obvious in the *FINCHM* results while DATCOM accounts for nonlinearities with angle of attack and canard deflection.

Figure 5.2 shows the variations in canard longitudinal center-of-pressure with angle of attack for zero canard deflection. Recalling from the experimental data analysis that center-of-pressure did not vary significantly with canard deflection (see Figures 3.13-3.15), the data for canard deflections of three degrees and nine degrees were not included in the plots. DATCOM predicts the center-of-pressure at a location slightly aft of the canard hingeline. Compared with DATCOM predictions, the *FINCHM* approach offers excellent agreement with experimental data for canard longitudinal center-of-pressure.

The resultant canard hinge moment predictions, calculated from the normal force and the moment arm (defined by the difference in center-of-pressure and hingeline locations), are shown in Figure 5.3. Due to the inability of DATCOM to predict canard center-of-pressure to sufficient accuracy for this case, experimental canard hinge moment predictions are grossly underpredicted. The resolution of the experimental data is observed by the stairstep effect. *FINCHM* predictions agree well with experimental data for zero and three degrees canard deflection but tend to overestimate hinge moment at nine degrees deflection, although data trends are correct. The sensitivity of the canard hinge moment to center-of-pressure location is obvious.
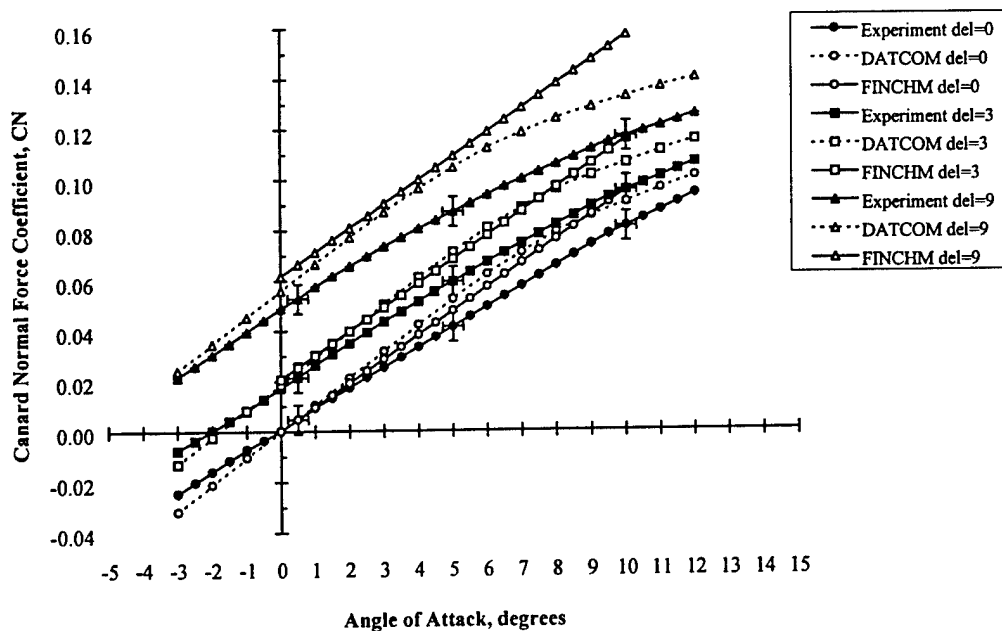
Figure 5.1 Canard Normal Force Coefficient Variation with Angle of Attack
(Position 3, Mach 1.25)
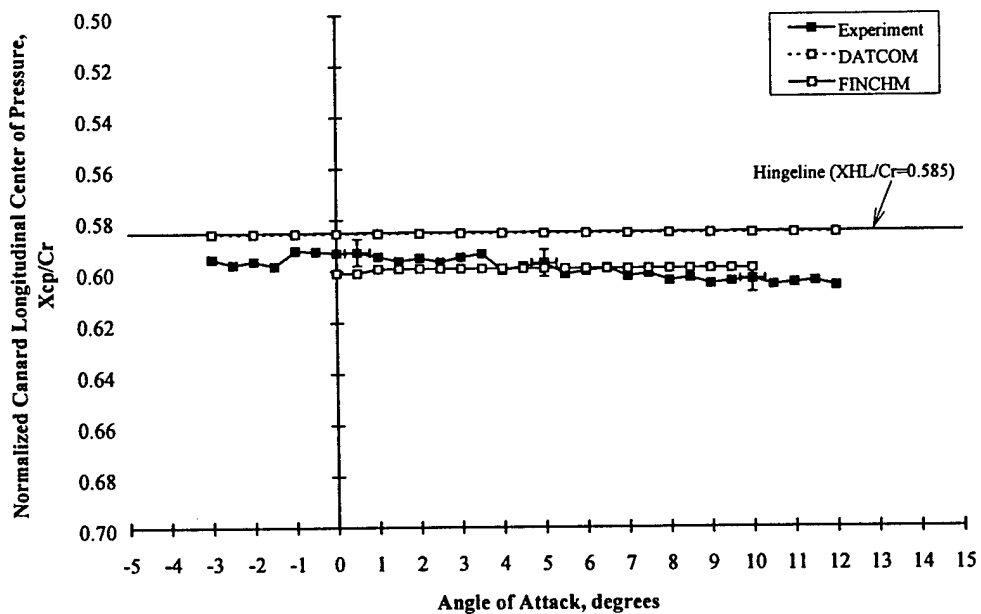
Figure 5.2 Canard Center-of-Pressure Variation with Angle of Attack
(Position 3, Mach 1.25)
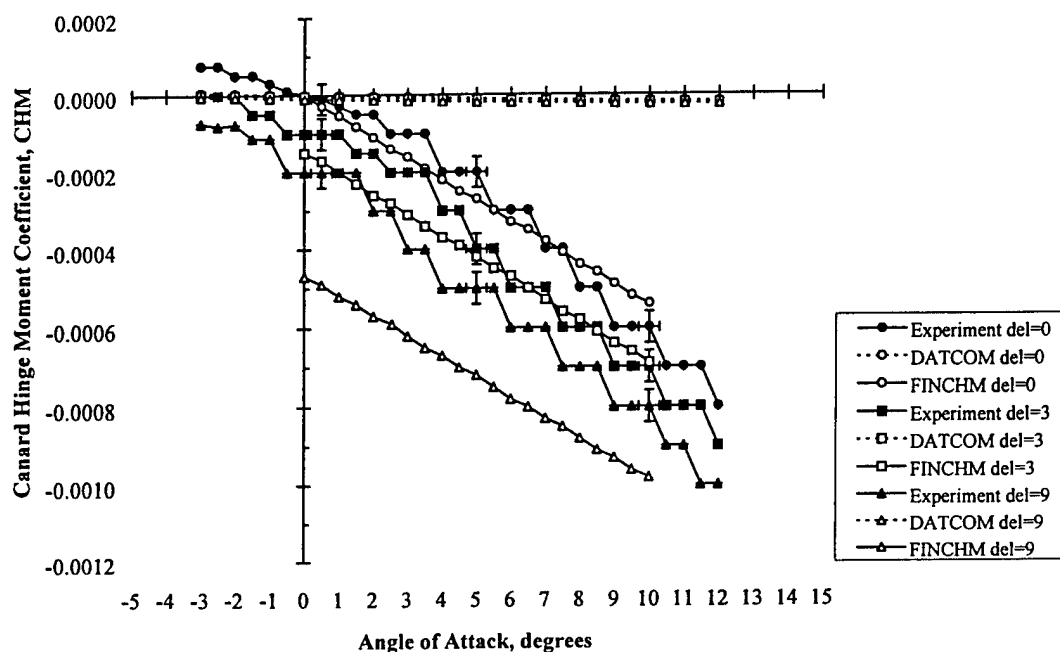
Figure 5.3 Canard Hinge Moment Coefficient Variation with Angle of Attack
(Position 3, Mach 1.25)

Figures 5.4-5.12 present a complete set of canard aerodynamic data for Mach 1.50 at the three canard positions along the rocket nose. Comparing Figures 5.4, 5.5, and 5.6 it can be seen that DATCOM predictions of canard normal force coefficient are invariant with canard position. However, such predictions show excellent agreement with experimental data for all canard deflections at position 1 and 2 while generally overpredicting normal force at position 3. *FINCHM* predictions show fair agreement with experiment for position 1 and 2 up to five degrees angle of attack but significantly overpredict normal force for angles of attack greater than five degrees and canard deflection of nine degrees.

Comparisons of canard center-of-pressure estimates at zero deflection in Figures 5.7, 5.8, and 5.9 show that *FINCHM* results consistently match experimental data for the three canard positions. The DATCOM predictions of canard center-of-pressure are invariant with canard position along the nose. DATCOM underpredicts center-of-pressure at position 1 and 2 but shows good agreement at canard position 3.
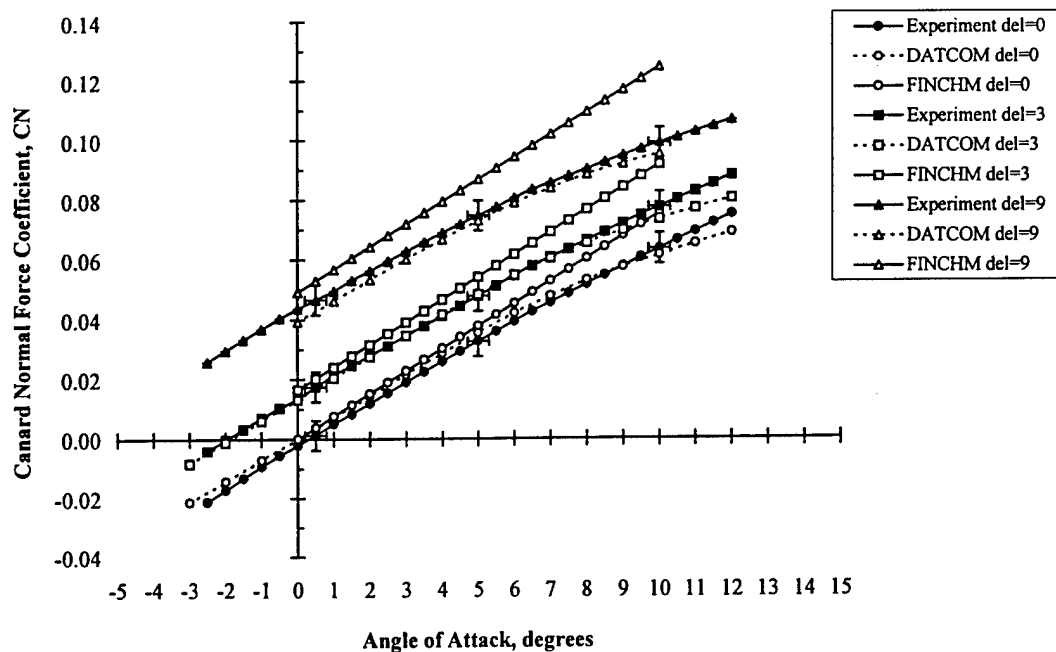
Figure 5.4 Canard Normal Force Coefficient Variation with Angle of Attack
(Position 1, Mach 1.50)
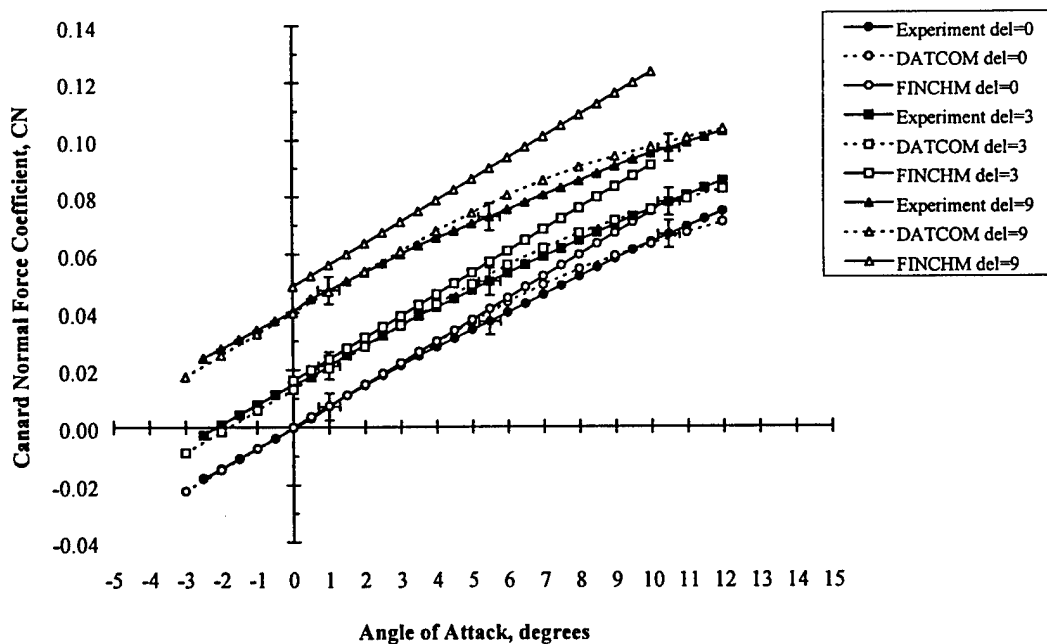
Figure 5.5 Canard Normal Force Coefficient Variation with Angle of Attack
(Position 2, Mach 1.50)
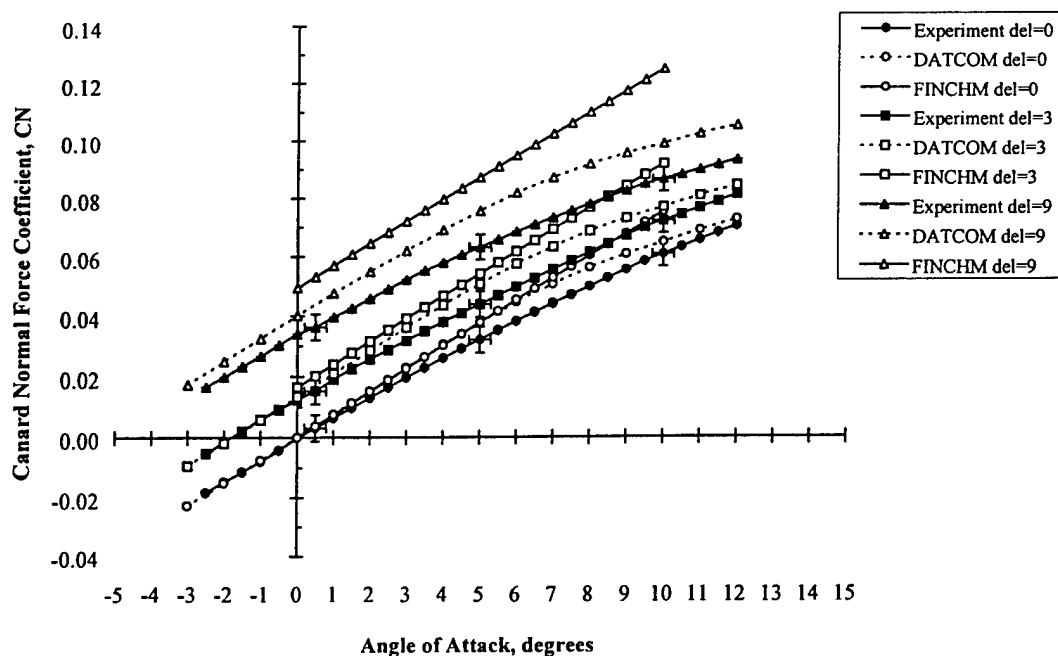
Figure 5.6 Canard Normal Force Coefficient Variation with Angle of Attack
(Position 3, Mach 1.50)
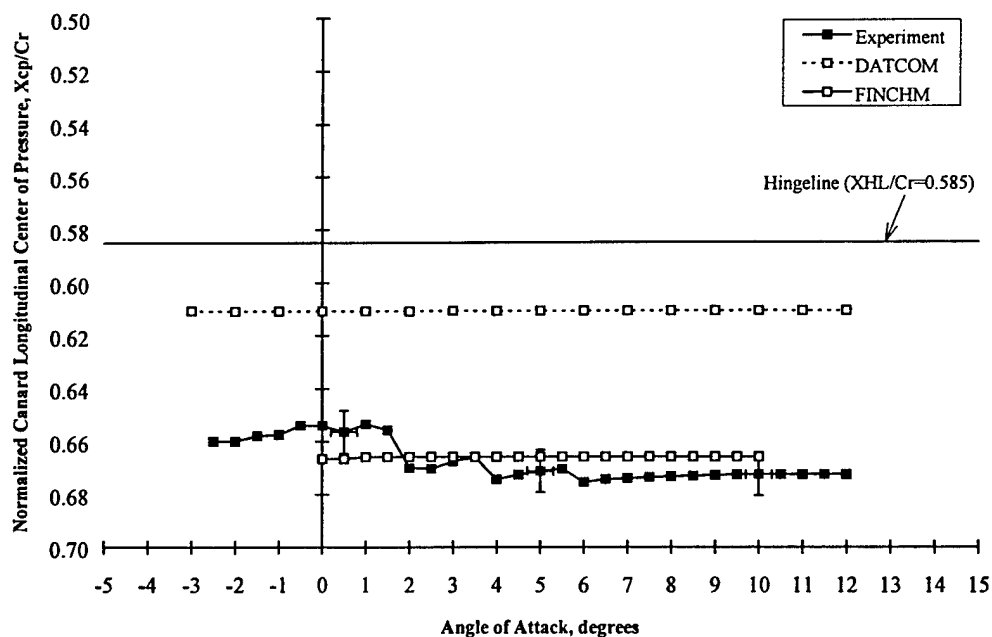
Figure 5.7 Canard Center-of-Pressure Variation with Angle of Attack
(Position 1, Mach 1.50)
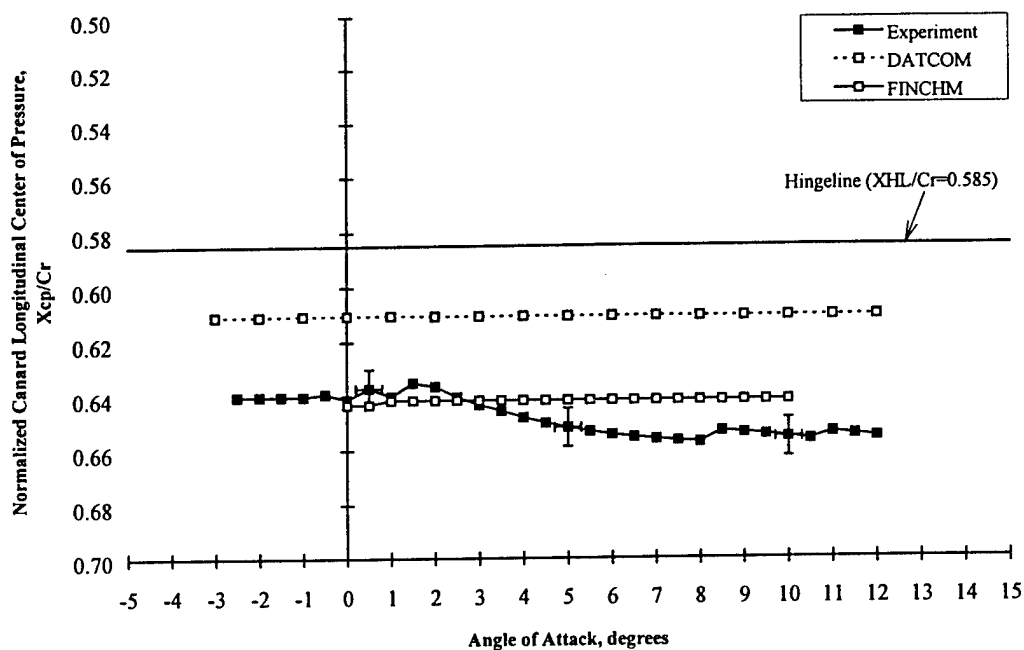
Figure 5.8 Canard Center-of-Pressure Variation with Angle of Attack
(Position 2, Mach 1.50)
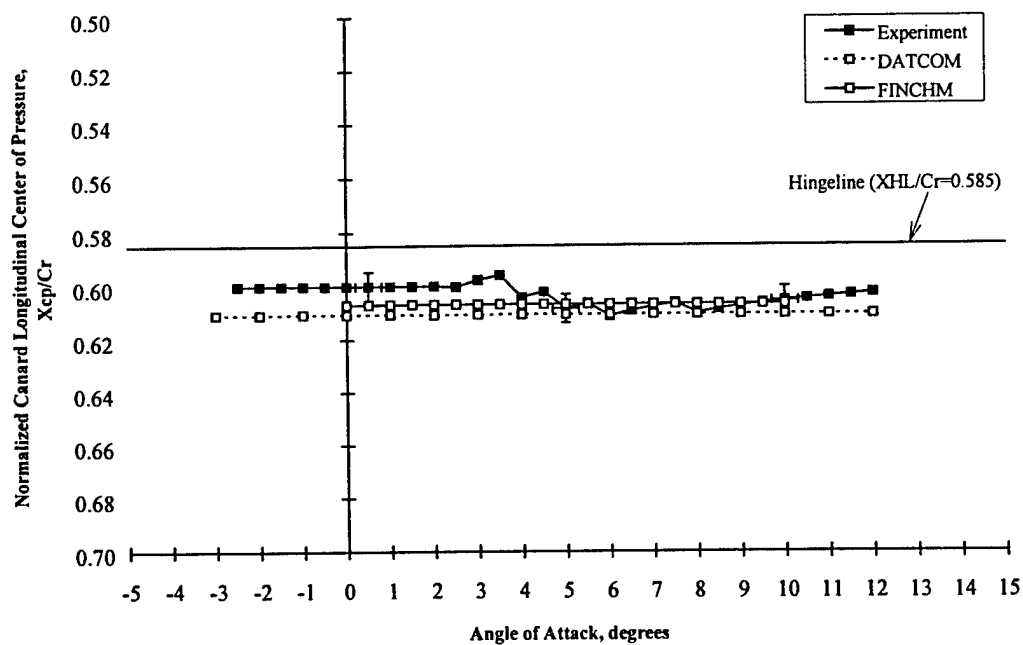
Figure 5.9 Canard Center-of-Pressure Variation with Angle of Attack
(Position 3, Mach 1.50)

Although *FINCHM* overpredicts normal force to some degree, the accurate prediction of center-of-pressure results in generally excellent agreement in hinge moment for all canard positions and deflections as shown in Figures 5.10-5.12. In contrast, DATCOM offers excellent predictions of normal force but poor predictions of center-of-pressure at position 1 and 2 which result in poor estimations of hinge moment. For position 3 where DATCOM center-of-pressure predictions generally match experimental data, excellent agreement is obtained for hinge moment. Therefore the canard hinge moment is shown to be more sensitive to relatively small shifts in longitudinal center-of-pressure location than relatively large changes in canard normal force.

Comparison of theoretical and DATCOM estimations of canard aerodynamic characteristics with experimental data for Mach 2.00 is shown in Figures 5.13-5.21. Figures 5.13, 5.14, and 5.15 show that both *FINCHM* and DATCOM estimations of canard normal force coefficient generally agree for all three canard locations. Again, DATCOM predictions are invariant with canard position. In comparison to experimental data, the theoretical predictions yield excellent agreement at position 1 but tend to overpredict normal force at position 2 and 3 for angles of attack greater than five degrees and canard deflection of nine degrees. However, the *FINCHM* predictions show better agreement overall.

FINCHM predictions are in excellent agreement with experimental canard center-of-pressure data at each of the three canard locations as shown in Figures 5.16-5.18. In contrast, DATCOM predictions of center-of-pressure show no variation with canard position and generally do not agree with experimental data.

Estimates of canard hinge moment at each position for a Mach number of 2.00 are shown in Figures 5.19-5.21. Due to the excellent prediction of center-of-pressure, *FINCHM* estimates of canard hinge moment coefficient generally agree with experimental data except at position 1 and a canard deflection of nine degrees. While DATCOM predictions of hinge moment agree favorably for position 2 at low angles of attack, general experimental trends are not matched. This is attributable to the fact that DATCOM predictions of normal force coefficient and center-of-pressure are invariant with canard position along the nose due to the inability to account for the local Mach number.
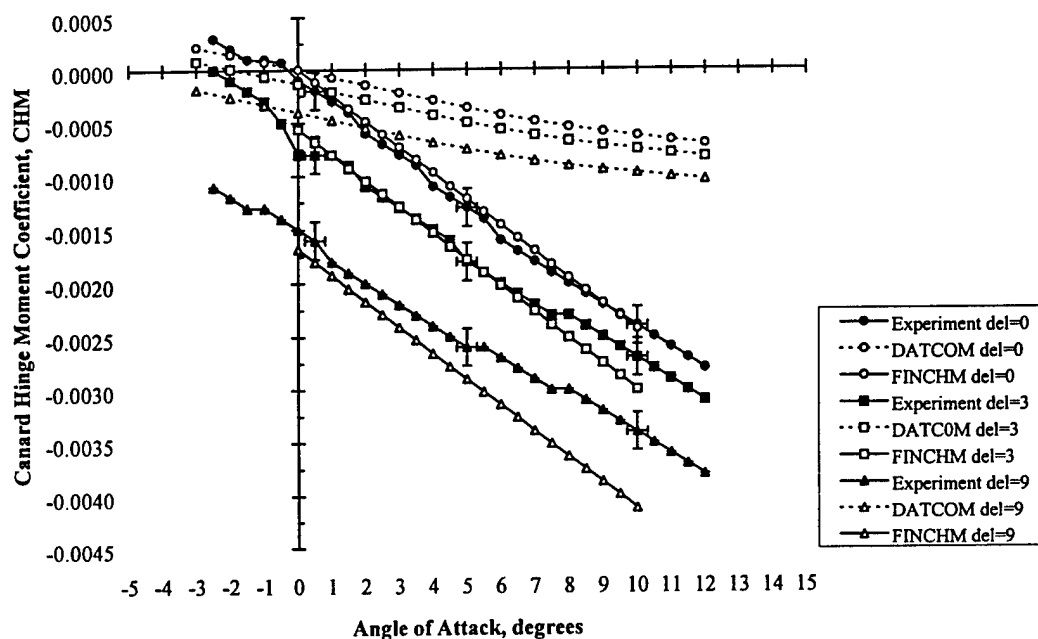
Figure 5.10 Canard Hinge Moment Coefficient Variation with Angle of Attack
(Position 1,Mach 1.50)
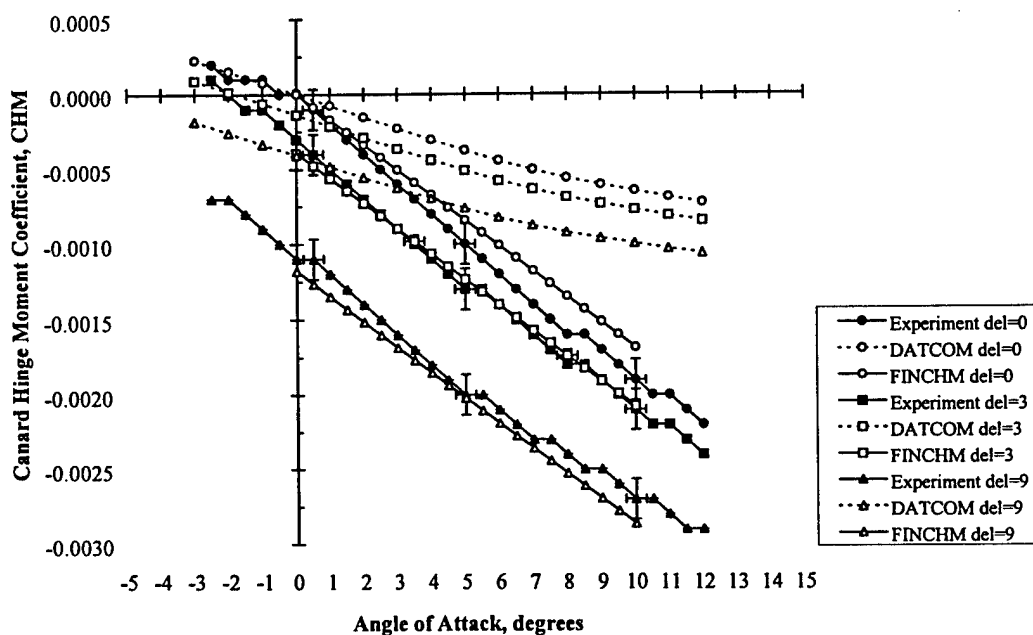
Figure 5.11 Canard Hinge Moment Coefficient Variation with Angle of Attack
(Position 2, Mach 1.50)
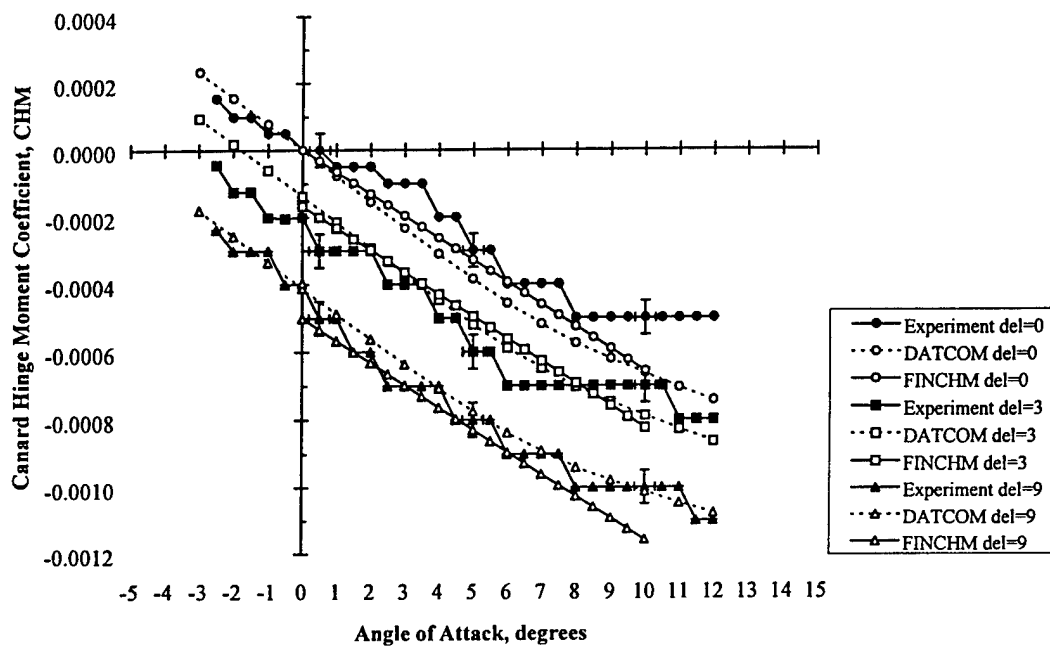
Figure 5.12 Canard Hinge Moment Coefficient Variation with Angle of Attack
(Position 3, Mach 1.50)
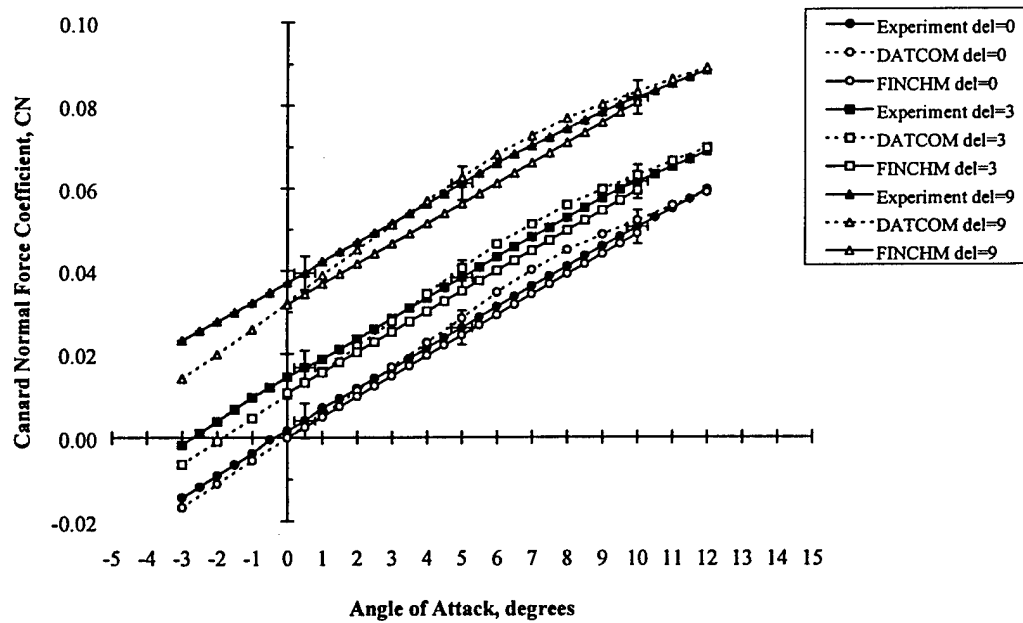
Figure 5.13 Canard Normal Force Coefficient Variation with Angle of Attack
(Position 1, Mach 2.00)
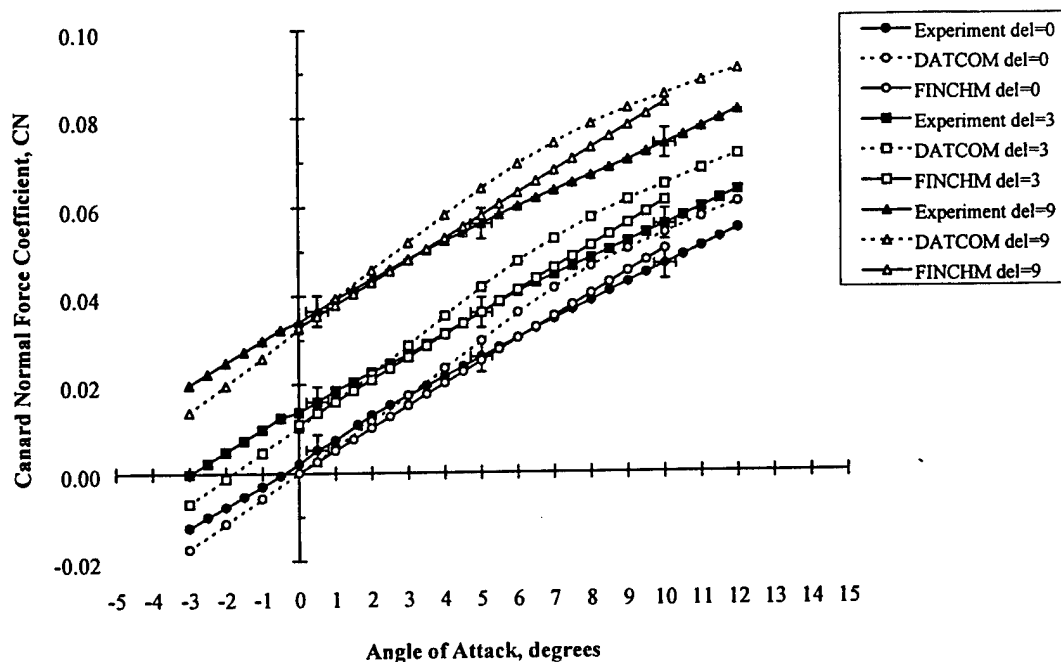
Figure 5.14 Canard Normal Force Coefficient Variation with Angle of Attack
(Position 2, Mach 2.00)
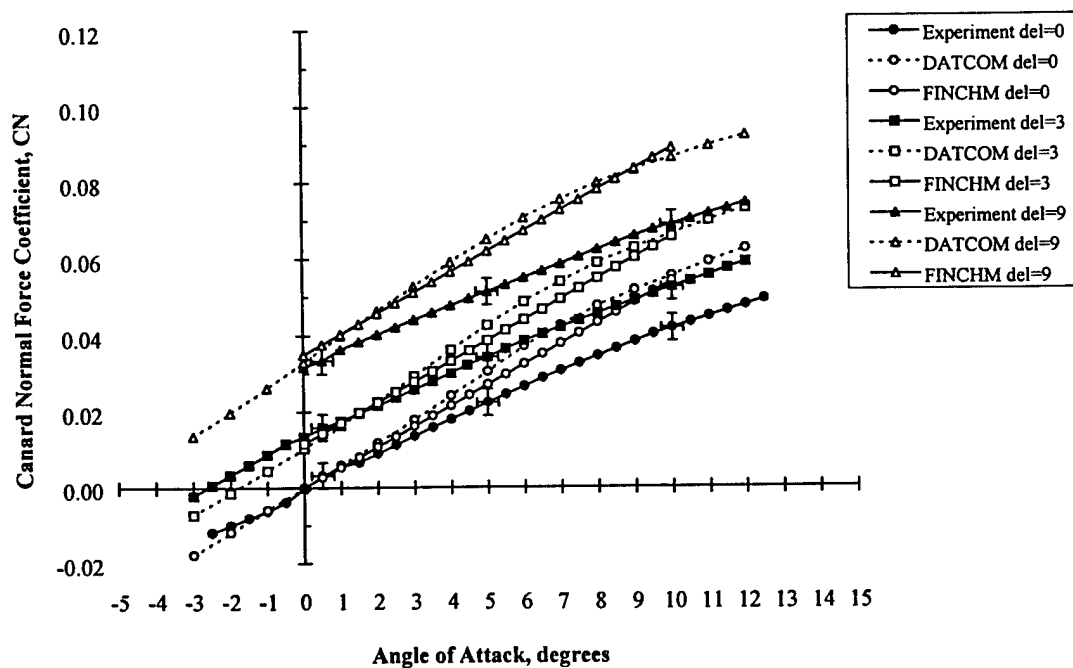
Figure 5.15 Canard Normal Force Coefficient Variation with Angle of Attack
(Position 3, Mach 2.00)
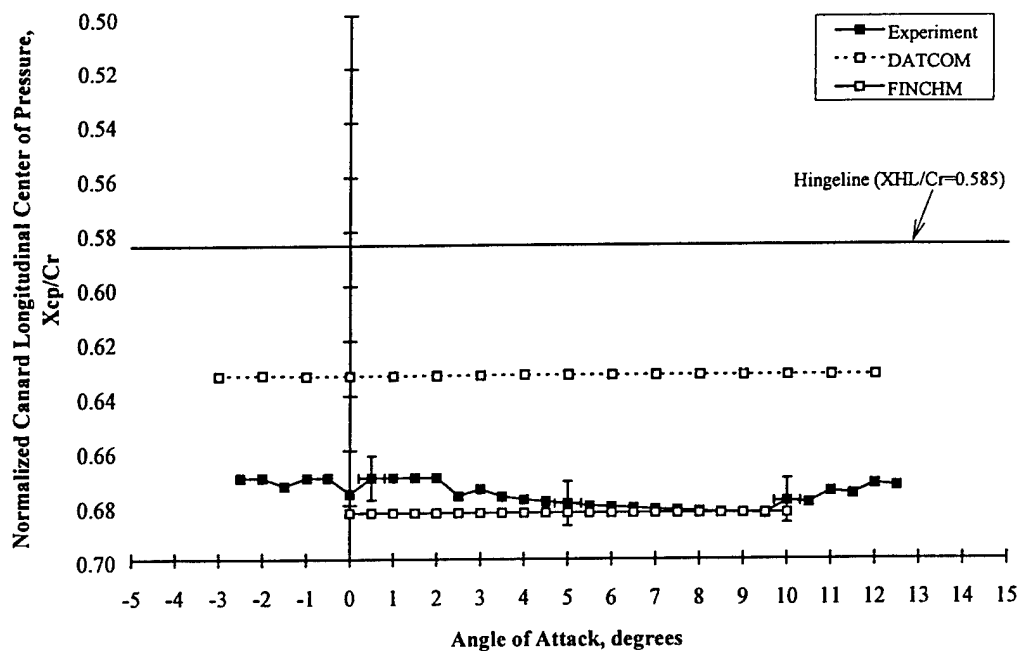
Figure 5.16 Canard Center-of-Pressure Variation with Angle of Attack
(Position 1, Mach 2.00)
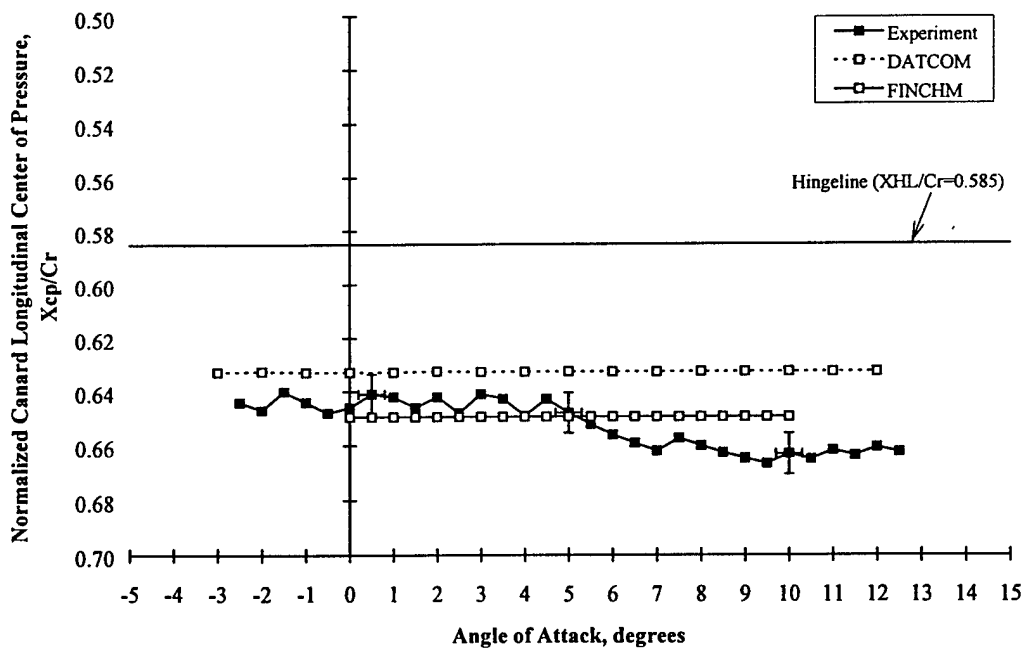
Figure 5.17 Canard Center-of-Pressure Variation with Angle of Attack
(Position 2, Mach 2.00)
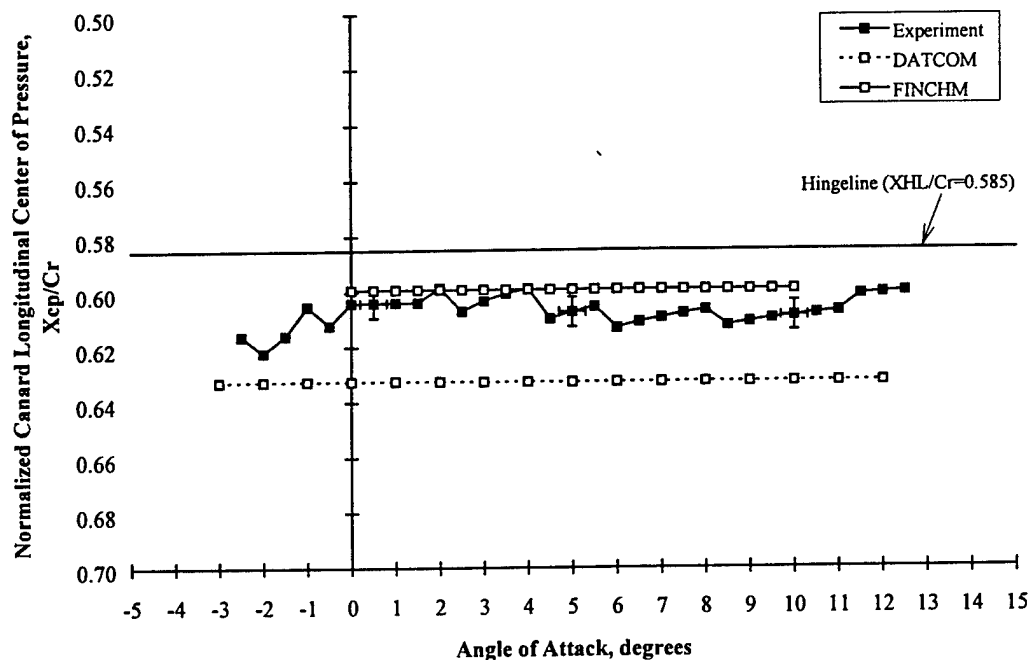
Figure 5.18 Canard Center-of-Pressure Variation with Angle of Attack
(Position 3, Mach 2.00)
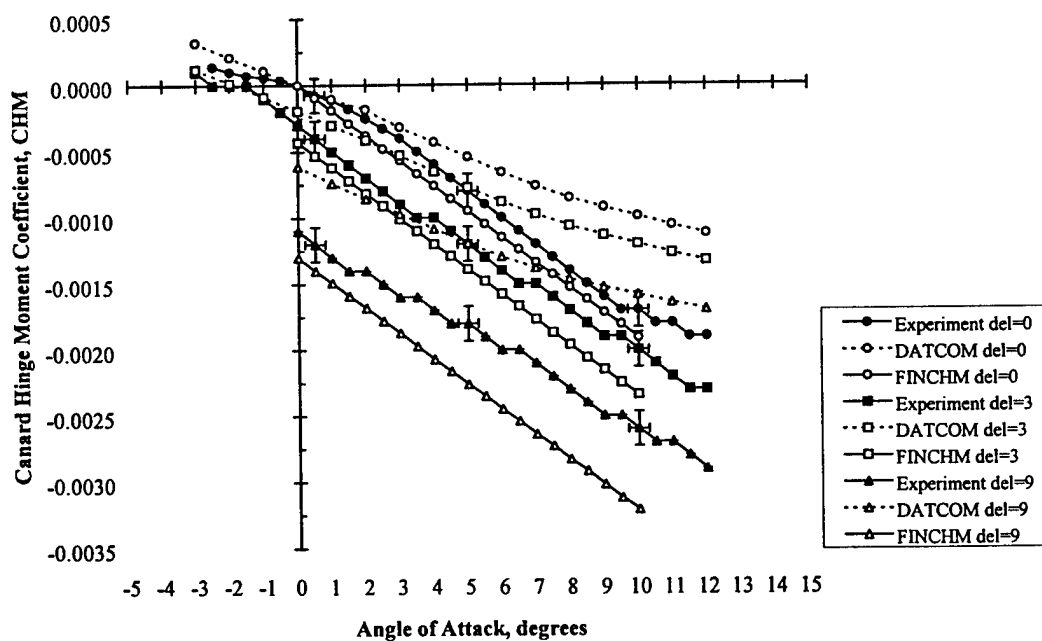
Figure 5.19 Canard Hinge Moment Coefficient Variation with Angle of Attack
(Position 1, Mach 2.00)
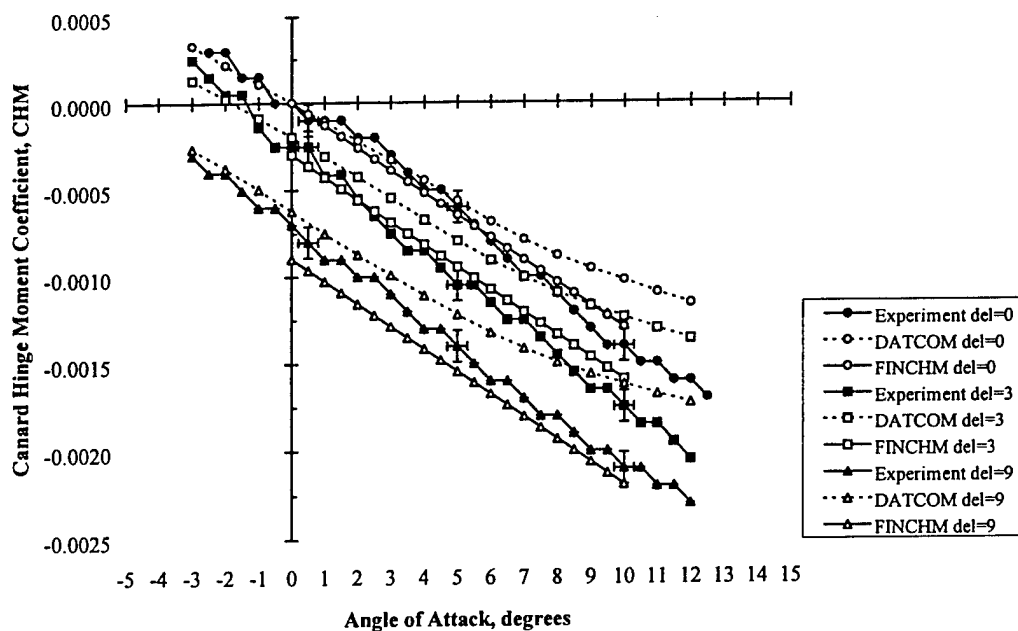
Figure 5.20 Canard Hinge Moment Coefficient Variation with Angle of Attack
(Position 2, Mach 2.00)
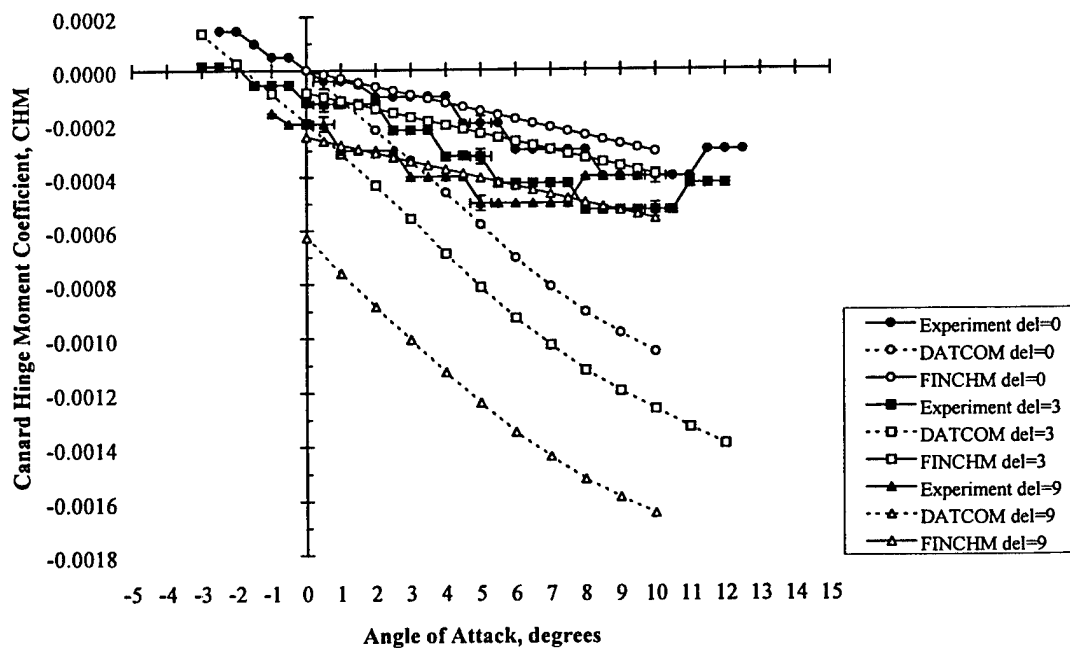
Figure 5.21 Canard Hinge Moment Coefficient Variation with Angle of Attack
(Position 3, Mach 2.00)

Figures 5.22-5.24 show the variation in canard longitudinal center-of-pressure with Mach number for ten degrees angle of attack and zero canard deflection at canard position 1 to 3, respectively. Since canard center-of-pressure has been shown to be invariant with angle of attack and canard deflection for a given Mach number and canard location, these data were chosen as a representative set to observe trends. Both freestream and predicted local Mach numbers are given and the regions of subsonic/supersonic wing leading-edge conditions are defined. A distinct rearward shift in canard center-of-pressure is noted when the local Mach number becomes sufficient to produce a supersonic leading-edge condition. For supersonic leading-edge conditions, an increase in freestream Mach number produces a rearward shift in center-of-pressure at a given canard position. For a constant freestream Mach number, the canard center-of-pressure exhibits a forward shift from position 1 to 3 due to the increasing local Mach number realized by the canard.

The preceding theory and experimental comparison have shown that accurate prediction of canard hinge moment is more sensitive to the accurate prediction of center-of-pressure location than accurate prediction of normal force. Nielsen [8] has concluded that for sufficient predictions of canard normal force, accurate estimations of hinge moment predictions may be obtained if the difference between the experimental data and predictions is within two percent of the root chord. In assessing the accuracy of canard hinge moment predictions, this two percent criteria has been applied to the experimental center-of-pressure data and is shown as bands in Figures 5.22-5.24. Based on this criteria, if the error between the theoretical results and the experimental data is less than two percent of the root chord then the subsequent hinge moment coefficient estimations should be acceptable. It is noted that the two percent root chord criteria is greater than the estimated experimental uncertainty in the center-of-pressure location.

FINCHM estimates the canard center-of-pressure location with a high degree of accuracy, well within the two percent error margin. Therefore it is postulated that acceptable values of hinge moment coefficient may be obtained from this method. This is confirmed by the excellent agreement between *FINCHM* predictions and experimental hinge moment coefficients shown in the preceding analysis. In comparison, DATCOM predictions are shown to lie well outside the two percent error criteria for position 1. For the cases where DATCOM predictions
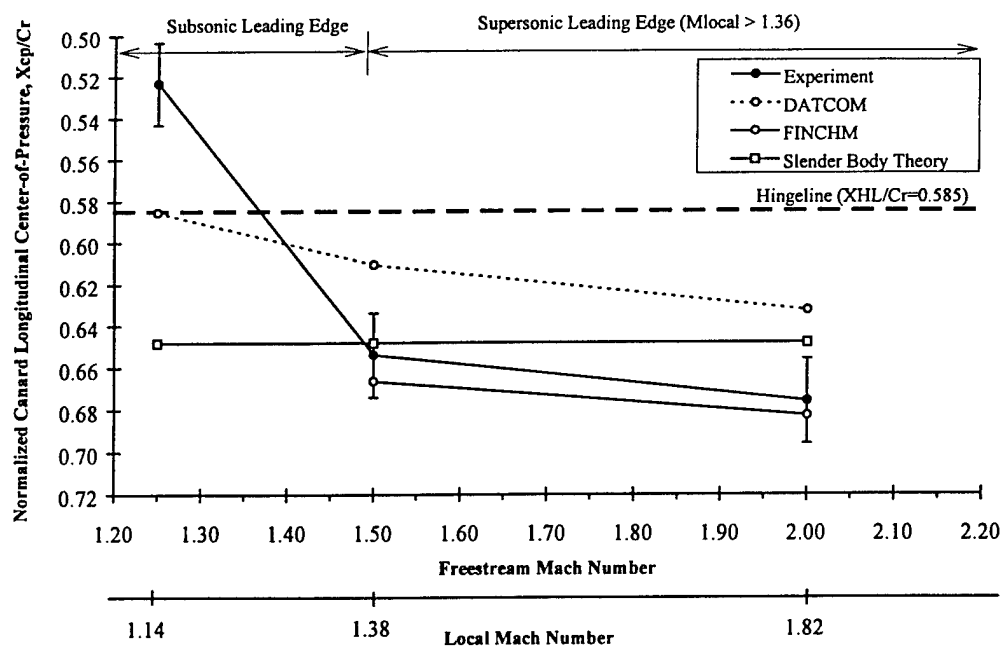
Figure 5.22 Canard Center-of-Pressure Variation with Mach Number
(Position 1 - α=10°, δ=0°)
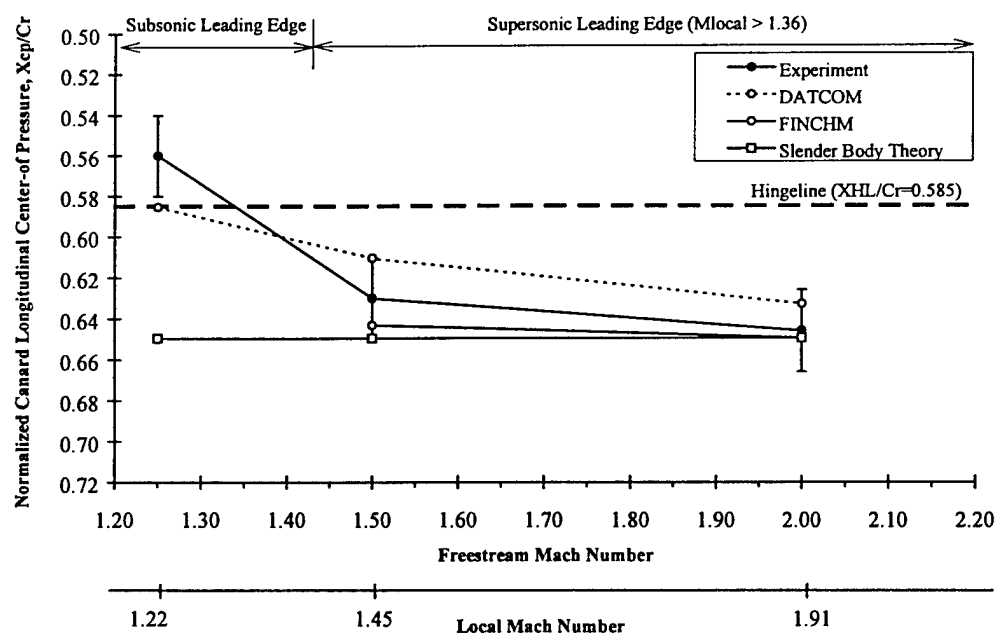
Figure 5.23 Canard Center-of-Pressure Variation with Mach Number
(Position 2 - α=10°, δ=0°)
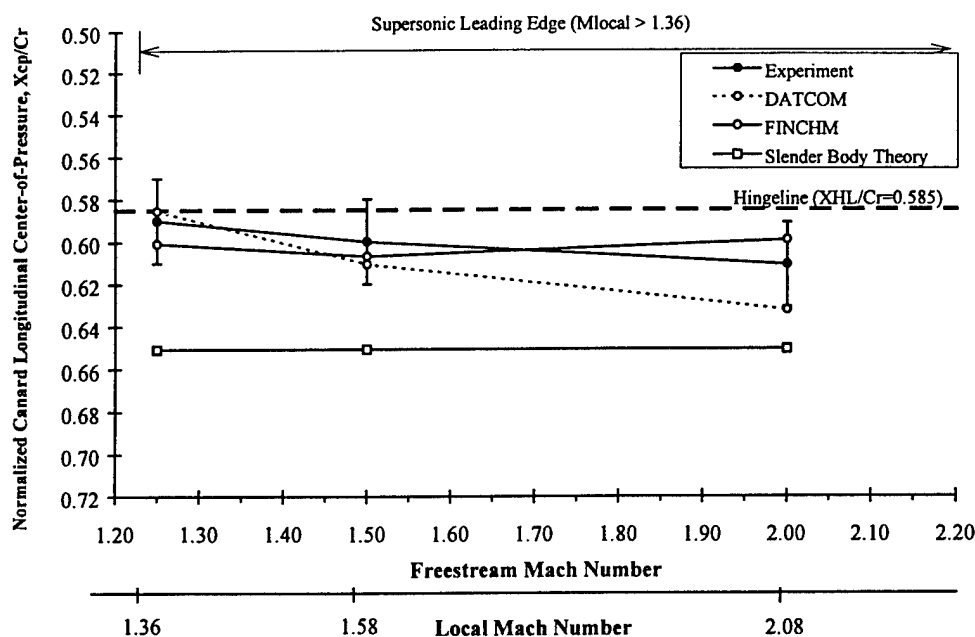
Figure 5.24 Canard Center-of-Pressure Variation with Mach Number
(Position 3 - α=10°, δ=0°)

are maintained within the error bounds (i.e. position 3 at Mach 1.50 and position 2 at Mach 2.00), good agreement for hinge moment coefficient is exhibited as shown in Figures 5.12 and 5.20. An exception occurs for Mach 1.25 at position 3 where the center-of-pressure predicted by DATCOM lies within the two percent error but is located in close proximity to the hingeline, resulting in poor prediction of hinge moments.

For comparison, the center-of-pressure for the canard in the presence of an infinite cylinder, defined by slender-body theory in Equation 4.30, is also shown. The slender-body theory values are based solely on the semispan-radius ratio (s/r) assuming a thin wing and do not include airfoil thickness effects. Therefore, slender-body theory results are invariant with Mach number and canard position and do not offer a consistently accurate estimation of canard center-of-pressure location.

Chapter 6

CONCLUSIONS AND RECOMMENDATIONS

The accurate determination of canard hinge moment coefficient is necessary for design purposes but often difficult to attain due to the inability to predict the canard longitudinal center-of-pressure location with sufficient accuracy. The aerodynamic characteristics of nose-mounted canards are strongly dependent on local flowfield conditions in the vicinity of the rocket nose shock wave. In comparison to canards mounted on a cylindrical section of the body, nose-mounted canards are inclined along the rocket nose which effectively alters the geometric characteristics of the canard in relation to the freestream flow.

Research findings have shown canard hinge moment estimations to be more sensitive to relatively small deviations in the center-of-pressure location in relation to the hingeline than relatively large shifts in canard normal force coefficient. It becomes imperative that canard center-of-pressure be predicted to the greatest degree of accuracy possible to achieve accurate estimates of canard hinge moment coefficient. With an adequate representation of canard normal force coefficient, it has been shown that an accurate prediction of canard hinge moment may be obtained when the difference in experimental data and predictions is less than two percent of the canard root chord.

The Missile DATCOM 6/93 code, based on semi-empirical methods, has been used to predict the aerodynamic characteristics of nose-mounted canard controls at angles of attack and canard deflection for Mach numbers of 1.25, 1.50, and 2.00. While DATCOM may adequately estimate canard normal force coefficient, it has been shown in most instances to be inadequate in predicting canard hinge moment coefficient due to the empirical nature of the code in determining center-of-pressure. These instances occur when the error between DATCOM center-of-pressure predictions and experimental data is greater than two percent of the root chord. Since DATCOM does not account for local Mach number effects, predictions of canard center-of-pressure and normal force coefficient are invariant with position along the nose. Therefore, DATCOM predicts constant canard hinge moment coefficient. From the observations

in the previous section it is concluded that DATCOM cannot consistently predict hinge moment coefficients with sufficient accuracy for a canard mounted at various locations along a rocket nose.

A newly developed theoretical approach, called *FINCHM*, was derived from basic compressible flow theory and accounts for local Mach number. While *FINCHM* does not predict canard normal force coefficient as accurately as DATCOM, it does offer excellent predictions of center-of-pressure, within two percent of root chord, for all cases. This consistent accuracy in center-of-pressure prediction at each canard position results in generally excellent agreement with experimental data for the canard hinge moment coefficient trends with angle of attack and canard deflection for Mach numbers of 1.25, 1.50, and 2.00.

The characterization of body carryover interference effects based on slender-body theory is applicable to a canard located sufficiently aft of the rocket nose on an infinite cylinder of uniform diameter. For the case of nose-mounted canards, the slender-body assumptions are not upheld and the applicability of the carryover interference effects is unknown. The canard-body carryover effects calculated from the modified slender-body theory of DATCOM compared favorably with ZEUS flowfield computations and were utilized to characterize such effects in the *FINCHM* predictions. Based on theoretical results, the application of the body carryover effects calculated by ZEUS and DATCOM proved to be acceptable in the cases investigated.

Based on comparisons with experimental data, it is concluded from the research investigation that the *FINCHM* approach predicts the hinge moment coefficient of a nose-mounted canard at supersonic Mach numbers more accurately than DATCOM. The excellent agreement between the *FINCHM* predictions and experimental data results from the ability of the theoretical method to predict canard longitudinal center-of-pressure with a higher degree of accuracy than DATCOM. The accurate estimation of canard hinge moment coefficient at each of the various positions along the nose of the rocket is a direct result of aerodynamic predictions of canard normal force coefficient and center-of-pressure based on the local Mach number of the flow in the nose region.

Since the *FINCHM* method has been coded in a subroutine which relies on inputs common to DATCOM, it could be easily incorporated in DATCOM to provide more accurate

and consistent estimations of hinge moment coefficient for nose-mounted canards. In particular, this approach could be utilized in developing and sizing the control actuation system to meet packaging requirements for preliminary design purposes. The method may be utilized to provide more accurate pre-test aerodynamic load estimates in developing a wind tunnel test and aid in defining the wind tunnel test matrix for a nose-mounted canard configuration. This could possibly reduce wind tunnel test time by defining pertinent conditions for obtaining test data. The *FINCHM* approach may also be utilized to supply canard aerodynamic predictions where experimental data are lacking.

Further investigations should be performed to validate the theoretical approach for higher canard deflection angles, additional canard geometries, and higher supersonic Mach numbers as such data for nose-mounted canards becomes available. In addition, the applicability of slender-body theory to characterize the body interference effects on nose-mounted canards requires further investigation and validation.

The robustness of the *FINCHM* code allows for modifications to be easily incorporated. Such modifications may include definition of other canard geometries and airfoil sections, calculation of the canard lateral center-of-pressure location and root bending moment, incorporation of techniques for canards positioned out of the horizontal plane, and inclusion of external effects such as mutual canard interference and gap effects which are not presently considered.

APPENDICES

APPENDIX A

UNCERTAINTY ANALYSIS

A detailed uncertainty analysis was performed for the experimental data obtained from the *CANARD* database to assess the quality of the data for validating *FINCHM* and Missile DATCOM predictions. In particular uncertainties associated with canard normal force coefficient, canard hinge moment coefficient, and canard longitudinal center-of-pressure have been determined. The uncertainties associated with the independent measurements of the systems utilized during the wind tunnel tests, presented in Table A.1, were applied in an error propagation method based on a Taylor series approach [26, 27, 29].

Table A.1 Estimated Uncertainties in System Measurements

Canard Balance		Wind Tunnel Model			Wind Tunnel Facility*		
Normal Force (lbf)	Hinge Moment (in-lbf)	Model Geometry (in.)	δcanard (degrees)	Canard Hingeline Location (in.)	Mach	P_T (in. of Hg)	α (degrees)
± 0.40	± 0.25	± 0.005	± 0.20	± 0.01	± 1.0%	± 0.004	± 0.10

* Calspan tunnel uncertainties were assumed to be comparable to quoted NASA Ames 6-by-6 foot wind tunnel

Estimation of measurement errors in the independent variables associated with the wind tunnel model, canard balances, and wind tunnel facilities were determined from available test documentation and supplemented with data from expert sources [31-33]. Due to the limited amount of information available regarding the canard balances and wind tunnel facilities at the time of testing, such expert sources were required to acquire some degree of uncertainty for key independent parameters yielding completeness in the uncertainty analysis.

Consider an experimental result, r, which is a function of i measured variables (X_i) which are independent of one another in both functional relation and uncertainty. The data

reduction equation for determining r from the measured variables X_i is then given as

$$r = r\left(X_1, X_2, \ldots, X_i\right) \quad .$$

<div align="right">(A.1)</div>

Based on a Taylor series expansion approach detailed by Coleman and Steele [27], the uncertainty in the experimental result is given by

$$U_r = \left[\left(\frac{\partial r}{\partial X_1} U_{X_1}\right)^2 + \left(\frac{\partial r}{\partial X_2} U_{X_2}\right)^2 + \cdots + \left(\frac{\partial r}{\partial X_i} U_{X_i}\right)^2\right]^{1/2} \quad .$$

<div align="right">(A.2)</div>

A special case of the uncertainty equation may be obtained when the data reduction equation is of the form

$$r = k\, X_1^a\, X_2^b\, X_3^c \ldots$$

<div align="right">(A.3)</div>

where k is a constant and the exponents a, b, c, etc. are positive or negative constants. The uncertainty in the experimental result is thus given by

$$\left(\frac{U_r}{r}\right)^2 = a^2 \left(\frac{U_{X_1}}{X_1}\right)^2 + b^2 \left(\frac{U_{X_2}}{X_2}\right)^2 + c^2 \left(\frac{U_{X_3}}{X_3}\right)^2 + \ldots \quad .$$

<div align="right">(A.4)</div>

In determining the uncertainty in experimental test data Coleman and Stern [26] have formulated the total uncertainty at a data point (X_i, r_i) as

$$U_D^2 = U_{r_i}^2 + \sum_{j=1}^{N} \left(\frac{\partial r}{\partial X_j}\right)_t^2 \left(U_{X_j}\right)_t^2$$

<div align="right">(A.5)</div>

which includes not only the uncertainty in the experimental result itself, r_i, but also the additional uncertainties in r_i due to measurement uncertainties of the X_i independent variables.

Clark [29] has presented uncertainty formulations for aerodynamic coefficients obtained in high-speed wind tunnel testing. The estimations assume that the measurement variables are independent as in Equation A.1 which allows formulation by the Taylor series method in Equation A.2. Normal force coefficient is defined by

$$CN = \frac{NF}{q_\infty S} \quad .$$

(A.6)

The uncertainty in the normal force coefficient is therefore given by Equation A.7 as

$$\left(\frac{U_{CN}}{CN}\right) = \left[\left(\frac{U_{NF}}{NF}\right)^2 + \left(\frac{U_{q_\infty}}{q_\infty}\right)^2 + \left(\frac{U_S}{S}\right)^2\right]^{1/2}$$

(A.7)

where normal force is directly measured and the uncertainty in normal force is a function of the balance accuracy. The uncertainties in the tunnel freestream dynamic pressure and model geometry are functions of more fundamental quantities. The uncertainty in tunnel dynamic pressure is given as

$$\frac{U_{q_\infty}}{q_\infty} = \left[\left(\frac{M_\infty}{R} \frac{\partial R}{\partial M_\infty} \frac{U_{M_\infty}}{M_\infty}\right)^2 + \left(\frac{U_{P_T}}{P_T}\right)^2\right]^{1/2} \quad .$$

(A.8)

Based on $\dfrac{P_\infty}{P_{t_\infty}} = \left(1 + \dfrac{\gamma-1}{2} M_\infty^2\right)^{\frac{-\gamma}{\gamma-1}}$ and $\dfrac{q_\infty}{P_{t_\infty}} = \dfrac{\gamma}{2} M_\infty^2 \left(\dfrac{P_\infty}{P_{t_\infty}}\right)$ and assuming $\gamma=1.40$, the relative sensitivity coefficient is given by

$$\frac{M_\infty}{R} \frac{\partial R}{\partial M_\infty} = \frac{2 - M_\infty^2}{1 + \dfrac{\gamma-1}{2} M_\infty^2} \quad .$$

(A.9)

Since the reference area is defined as $S=\pi d^2/4$, the uncertainty in the model reference area becomes

$$\frac{U_S}{S} = 2\frac{U_d}{d} \quad . \tag{A.10}$$

Substitution of Equation A.7, A.8, and A.9 into Equation A.5 yields the total uncertainty in canard normal force coefficient as

$$\left(\frac{U_{CN_{total}}}{CN_{total}}\right) = \left[\left(\frac{U_{NF}}{NF}\right)^2 + \left(\frac{U_{q_\infty}}{q_\infty}\right)^2 + \left(\frac{2U_d}{d}\right)^2 + \sum_{j=1}^{n}\left(\frac{\partial CN}{\partial\alpha_j}\right)^2\left(U_{\alpha_j}\right)^2 + \sum_{j=1}^{n}\left(\frac{\partial CN}{\partial\delta_j}\right)^2\left(U_{\delta_j}\right)^2\right]^{1/2} \quad . \tag{A.11}$$

Due to the small uncertainties in angle of attack and canard deflection, the partial derivative summations in Equation A.11 were found to be very small in magnitude in comparison to the other independent variables and were thus neglected. Applying the uncertainties in balance measurements, wind tunnel operating condition measurements, and model geometry tolerances in Equation A.11, the estimation of uncertainty in the experimental canard normal force coefficient was determined for each angle of attack and canard deflection to produce a band of uncertainty about the data. For Mach 1.50 the uncertainty in canard normal force coefficient was calculated as

$$\left(\frac{U_{CN_{total}}}{CN_{total}}\right) = \left[(0.05)^2 + \left\{\left(\frac{2-(1.50(\pm 1.01))^2}{1+\left(\frac{1.4-1}{2}\right)(1.50(\pm 1.01))^2}\left(\frac{0.004}{1.50(\pm 1.01)}\right)\right)^2 + \left(\frac{0.004}{0.5(29.922)}\right)^2\right\} + \left(\frac{2(0.005)}{5.0}\right)^2\right]^{1/2} \tag{A.12}$$

$$\left(\frac{U_{CN_{total}}}{CN_{total}}\right) = \pm 0.0501 \, or \pm 5.01\% \quad .$$

The uncertainty was determined for Mach 1.25 and 2.00 in the same manner. It is apparent that the uncertainty in the balance force measurement was the largest source of measurement error in the propagation to the final uncertainty.

Canard hinge moment coefficient is defined as

$$CHM = \frac{HM}{q_\infty Sd} \quad .$$
(A.13)

The uncertainty in hinge moment coefficient can therefore be estimated by the formulation

$$\left(\frac{U_{CHM}}{CHM}\right) = \left[\left(\frac{U_{HM}}{HM}\right)^2 + \left(\frac{U_{q_\infty}}{q_\infty}\right)^2 + \left(\frac{U_S}{S}\right)^2 + \left(\frac{U_d}{d}\right)^2\right]^{1/2} \quad .$$
(A.14)

Since the reference area is a function of the reference diameter (Equation A.10), the last two terms in Equation A.14 are replaced by the term

$$\left(\frac{3U_d}{d}\right)^2 \quad .$$
(A.15)

Therefore the total uncertainty in canard hinge moment coefficient can be cast in the form of Equation A.5 as

$$\left(\frac{U_{CHM_{total}}}{CHM_{total}}\right) = \left[\left(\frac{U_{HM}}{HM}\right)^2 + \left(\frac{U_{q_\infty}}{q_\infty}\right)^2 + \left(\frac{3U_d}{d}\right)^2 + \sum_{j=1}^{n}\left(\frac{\partial CHM}{\partial \alpha_j}\right)^2 \left(U_{\alpha_j}\right)^2 + \sum_{j=1}^{n}\left(\frac{\partial CHM}{\partial \delta_j}\right)^2 \left(U_{\delta_j}\right)^2\right]^{1/2} \quad .$$
(A.16)

As with normal force coefficient, the partial derivative summations in Equation A.16 were found to be very small in magnitude in comparison to the other independent variables and were thus neglected. Applying the uncertainties in balance measurements, wind tunnel operating condition measurements, and model geometry tolerances in Equation A.16, the estimation of uncertainty in

the experimental canard hinge moment coefficient was determined for each angle of attack and canard deflection to produce a band of uncertainty about the data. For Mach 1.50 the uncertainty in canard hinge moment coefficient was calculated as

$$\left(\frac{U_{CHM_{total}}}{CHM_{total}}\right) = \left[(0.05)^2 + \left\{\left(\frac{2-\left(1.50(\pm 1.01)\right)^2}{1+\left(\frac{1.4-1}{2}\right)\left(1.50(\pm 1.01)\right)^2}\left(\frac{0.004}{1.50(\pm 1.01)}\right)\right)^2 + \left(\frac{0.004}{0.5(29.922)}\right)^2\right\} + \left(\frac{3(0.005)}{5.0}\right)^2\right]^{1/2}$$ (A.17)

$$\left(\frac{U_{CHM_{total}}}{CHM_{total}}\right) = \pm\ 0.0501\ or\ \pm 5.01\%\ .$$

The uncertainty was determined for Mach 1.25 and 2.00 in the same manner. It is apparent that the uncertainty in the balance moment measurement was the largest source of measurement error in the propagation to the final uncertainty. The uncertainty of the canard hinge moment coefficient was estimated as $\pm$ 5.01%.

The nondimensional canard longitudinal center-of-pressure is a calculated value dependent upon the measurement of canard hinge moment and normal force. For the hinge moment measured about the canard hingeline, the canard center-of-pressure is determined from the relation

$$\frac{CHM}{CN} = \frac{XHL - XCP}{d}$$ (A.18)

where

$$XCP = XHL - \left(\frac{\left(\frac{HM}{q_\infty Sd}\right)}{\left(\frac{NF}{q_\infty S}\right)}\right)d = XHL - \frac{HM}{NF}\ .$$ (A.19)

The canard hingeline and resulting longitudinal center-of-pressure are measured aft of the canard leading edge along the root chord. Equation A.19 shows that canard center-of-pressure becomes a function of three independent variables (canard hingeline location, canard normal force, and canard hinge moment) and cannot be cast in the special form of Equation A.3. Therefore Equation A.2 must be utilized to determine the uncertainty in the calculated value of canard center-of-pressure given as

$$U_{XCP} = \left[\left(\frac{\partial XCP}{\partial XHL} U_{XHL} \right)^2 + \left(\frac{\partial XCP}{\partial HM} U_{HM} \right)^2 + \left(\frac{\partial XCP}{\partial NF} U_{NF} \right)^2 \right]^{1/2} . \quad (A.20)$$

Evaluating the partial derivatives with Equation A.19, the uncertainty equation takes the form

$$U_{XCP} = \left[\left((1) U_{XHL} \right)^2 + \left(\left(\frac{-1}{NF} \right) U_{HM} \right)^2 + \left(\left(\frac{HM}{NF^2} \right) U_{NF} \right)^2 \right]^{1/2} . \quad (A.21)$$

The second term in Equation A.21 reveals that the change in canard longitudinal center-of-pressure with the change in hinge moment equates to the inverse of normal force. Thus as the normal force goes to zero, the second term of the equation approaches infinity resulting in an infinite total uncertainty.

Experimental data show that canard center-of-pressure is invariant with angle of attack for a given canard position along the nose for all Mach numbers and canard deflections. Therefore, to address the uncertainty in center-of-pressure a condition with the maximum angle of attack of 10 degrees and zero canard deflection was chosen as a typical case to ensure sufficient balance loading. For the three canard positions at Mach 1.25, 1.50, and 2.00, coefficients of normal force and hinge moment were obtained at the condition stated and normal force and hinge moment were calculated based on the tunnel dynamic pressure and reference quantities. Next the values were substituted into Equation A.21 to determine the resulting uncertainty. This estimated uncertainty was applied to the entire angle of attack range. An

example of the estimated uncertainty for canard center-of-pressure is given for the canard located at position 1 at Mach 1.50, 10 degrees angle of attack, and zero canard deflection. For such test conditions, the canard normal force and hinge moment were determined to be 4.479 lbf and -0.06532 ft-lbf, respectively. Therefore,

$$U_{XCP} = \left[\left((1)\left(\frac{0.01}{12}\right) \right)^2 + \left(\left(\frac{-1}{4.479}\right)(0.05(-0.06532)) \right)^2 + \left(\left(\frac{-0.06532}{(4.479)^2}\right)(0.05(4.479)) \right)^2 \right]^{1/2} \tag{A.22}$$

$$U_{XCP} = 0.00133\,ft = 0.01596\,in$$

$$\frac{U_{XCP}}{C_{root}} = \frac{0.01596\,in}{2.0\,in} = 0.00798 \qquad .$$

The estimated uncertainty in center-of-pressure has been nondimensionalized by dividing by the canard root chord, allowing the presentation of uncertainty bands on calculated values of Xcp/Croot based on experimental normal force coefficient and hinge moment coefficient data.

The estimated uncertainties in canard normal force coefficient, canard hinge moment coefficient, and nondimensional longitudinal center-of-pressure are summarized in Table A.2 for maximum balance loading conditions at ten degrees angle of attack and nine degrees canard deflection. As shown in Table A.2 the estimation in center-of-pressure uncertainty increases due to the decrease in canard normal force with increasing Mach number at a given canard position. Uncertainty bands are presented on plots of experimental data to allow validation of theoretical results and Missile DATCOM predictions.

Table A.2 Estimated Uncertainties in Experimental Data

Mach	U_{CN}/CN	U_{CHM}/CHM	$U_{Xcp}/Croot$		
			Position 1	Position 2	Position 3
1.25	± 5.01%	± 5.01%	± 0.0061	± 0.0054	± 0.0052
1.50	± 5.01%	± 5.01%	± 0.0080	± 0.0071	± 0.0053
2.00	± 5.01%	± 5.01%	± 0.0081	± 0.0075	± 0.0054

APPENDIX B

FINCHM SOURCE CODE

```
C MAIN PROGRAM TO CALL SUBROUTINE FINCHM
C
C Written by: Michael G. Landers
C 9-14-96
C Last Modification:
C 3-17-97
C
C CONDITIONS TO COMPUTE CANARD NORMAL FORCE COEFFICIENT,
C CENTER-OF-PRESSURE WITH AIRFOIL THICKNESS, AND
C CANARD HINGE MOMENT COEFFICIENT
C
C
C ASSUMES: - CANARD ON NOSE IN HORIZONTAL PLANE
C          - POSITIVE AOA AND CANARD DEFLECTION
C          - STRAIGHT TAPER/CLIPPED DELTA CANARD WITH ZERO T.E.SWEEP
C          - HINGELINE SKEW ANGLE DEFINED AS +CCW FROM VERTICAL FOR
C               CANARDS INCLINED ON NOSE WHERE SKEW ANGLE BECOMES
C               LOCAL BODY INCLINATION ANGLE
C          - RLMAXU IS CONSTANT ON EACH SIDE OF RLFLATU
C          - XLE1,XLE2 MEASURED FROM BODY CENTERLINE
C          - AIRFOIL SECTIONS ARE SYMMETRICAL
C          - LINEAR AERODYNAMICS FOR CN-ALPHA
C          - SURFACES CAN BE APPROXIMATED BY A CONNECTED SERIES OF
C               STRAIGHT LINE SEGMENTS
C          - SHOCK WAVE ON AIRFOIL L.E. IS ATTACHED AT ALL TIMES
C               (DELTAC LESS THAN DELTACMAX FOR ATTACHED SHOCK)
C               NOTE: THIS MAY REQUIRE AIRFOIL GEOMETRY MODIFICATION
C                       TO GET DELTAC LESS THAN DELTACMAX!!
C
C SET NUMBER OF ANGLE OF ATTACK (AOA MUST BE POSITIVE AND < = 10 DEG)
C       DIMENSION ALPHA(21)
C       NALPHA=21
C SET ARRAY FOR NUMBER OF ANGLE OF ATTACK AND FIN DEFLECTIONS TO CALCULATE AERO
      DIMENSION DELTA(2)
      DIMENSION XCPCR(21),XCPCROOT(21),CNFIN(21),XCPFIN(21),XCPFINB(21)
C OPEN UNIT 12 TO WRITE OUTPUT TO FILE
      OPEN(UNIT=12,FILE='M2P3.OUT',STATUS='UNKNOWN')
      OPEN(UNIT=28,FILE='M2P3CN.OUT',STATUS='UNKNOWN')
C SET NUMBER OF STRIPS, J, FOR STRIP THEORY - STRIP MUST BE ODD NUMBER!!
C (ODD NUMBER OF J REQUIRED FOR SIMPSON'S RULE OF INTEGRATION)
      J=101
C*******************************************************************
      NALPHA=21
      NDELTA=2
      DELTA(1)=3.0
      DELTA(2)=9.0
      DELTACDEG=0.0
      PI=4.0*ATAN(1.0)
      RADTODEG=180.0/PI
      DEGTORAD=1.0/RADTODEG
      RMACH=2.08
      RMACHFS=2.0
      RLMAXU1=0.3333
      RLMAXU2=0.025
      RLMAXL1=0.3333
      RLMAXL2=0.025
      RLFLATU1=0.3333
      RLFLATU2=0.95
      RLFLATL1=0.3333
      RLFLATL2=0.95
      ZUPPER1=0.025
      ZUPPER2=0.025
      ZLOWER1=0.025
      ZLOWER2=0.025
      CROOT=2.0
      CTIP=0.6
      XLE1=2.5
      XLE2=4.0
      SEMISPAN=XLE2-XLE1
      RLREF=5.0
      BODYRAD=2.5
      R=BODYRAD
      S=R+SEMISPAN
      XHINGELINE=1.17
      XHINGECR=XHINGELINE/CROOT
      SKEWDEG=0.0
      RMRP=0.0
      ARFINS=2.3077
C DETERMINE WING-BODY INTERFERENCE FACTOR, KW(B) AS FUNCTION OF AOA AND kw(b)
C AS FUNCTION OF DELTA FOR R/S RATIO   EQ. 14 AND 19 NACA 1307 - SLENDER BODY THEORY
```

```
          T=S/R
C CALCULATE KW(B) for AOA
          RKWBSBT=(PI/2.*((T**2.-1.)/T)**2.+((T**2.+1.)/T)**2.*ASIN((T**2.
     $-1.)/(T**2.+1.))-2.*(T**2.-1.)/T)/(PI*(T-1.)**2.)
C CALCULATE kw(b) for fin deflection
          RKKWBSBT=(PI**2./4.*((T+1.)/T)**2.+PI*((T**2.+1.)/(T*(T-1.)))**2.*
     $ASIN((T**2.-1.)/(T**2.+1.))-2.*PI*(T+1.)/(T*(T-1.))+(T**2.+1.)**2.
     $/(T**2.*(T-1.)**2.)*(ASIN((T**2.-1.)/(T**2.+1.)))**2.-4.*(T+1.)/
     $(T*(T-1.))*ASIN((T**2.-1.)/(T**2.+1.))+8./(T-1.)**2.*ALOG((T+1./
     $T)/2.))/PI**2.
C ENTER RKWB DETERMINED FROM ZEUS AT HINGELINE LONGITUDINAL POSITION AND MIDCHORD SPAN
C RKWB=(ALPHA LOCAL/ALPHA FREESTREAM)
          RKWB=1.32
C
          WRITE(*,*)'INTERFERENCE FACTORS KW(B), kw(b)'
          WRITE(*,*)'KW(B) SBT= ',RKWBSBT
          WRITE(*,*)'KW(B) ZEUS=',RKWB
          WRITE(*,*)'kw(b) SBT =',RKKWBSBT
C DETERMINE XCP/CROOT WING-IN PRESENCE OF BODY CORRECTION DUE TO FIN-BODY INTERFERENCE
C FOR ANGLE OF ATTACK AND R/S RATIO  EQ.58 NACA 1307 (NIELSEN 1988 TABLE 5-1)
C FOR R AND S
          T1=1./(1.-(R/S))
          T2=2.*((1./3.)+(R/S)**4.)*(ATAN(S/R))
          T3=(2./3.)*((R/S)**3.)*LOG(((S*S+R*R)/(2.*S*S))**2.*(S/R))
          T4=(1./3.)*((R/S)**3.)*((2.*PI)-1.0+(S/R)**2.)
          T5=((1.+(R/S)*(R/S))**2.0)*(ATAN(S/R))
          T6=((R/S)**2.)*(PI+((S/R)-(R/S)))
          T7=(R/S)/(1.-(R/S))
          XCPCRWBAOARS1=T1*((T2+T3-T4)/(T5-T6))-T7
          WRITE(*,*)'XCPCRWBAOARS1=',XCPCRWBAOARS1
C DETERMINE XCP/CROOT WING-IN PRESENCE OF BODY CORRECTION DUE TO FIN-BODY INTERFERENCE
C FOR ANGLE OF ATTACK AND A/SM RATIO  EQ.58 NACA 1307 (NIELSEN 1988 TABLE 5-1)
C FOR R/S=0.0, XCP/CR ACTS AT AREA CENTROID OF FIN
          XCPCRWBAOARS2=(2./3.)
          WRITE(*,*)'XCPCRWBAOARS2=',XCPCRWBAOARS2
C LOOP THROUGH ANGLE OF ATTACK FOR COMPUTATIONS AT DELTA=0.0 AND DETERMINE CN-ALPHA SLOPE
C FOR AOA=1 DEG, ASSUMING LINEAR AERO
          ALPHA=0.5
          DELTALPHA=0.0
          DO 32 M=1,NALPHA
            ALPHA=ALPHA+DELTALPHA
            ALPHARAD=ALPHA*DEGTORAD
            DELTALPHA=0.5
            WRITE(*,*)'ALPHA,DELTA',ALPHA,DELTACDEG
C ***************************************************************
C CALL SUBROUTINE TO COMPUTE DELTA XCP DUE TO AIRFOIL THICKNESS
C ***************************************************************
          IF(ALPHA.GT.1.0) GOTO 33
C         WRITE(*,*)'CALL FINCHM'
          CALL FINCHM(J,M,RMACH,ALPHARAD,RLMAXU1,RLMAXU2,RLFLATU1,RLFLATU2,
     $CROOT,CTIP,ZUPPER1,ZUPPER2,XLE1,XLE2,RLREF,XHINGELINE,SKEWDEG,
     $RMACHFS,ARFINS,RKWB,RKWBSBT,XCPCRWBAOARS1,XCPCRWBAOARS2,
     $DELXCPCRT,RMRP,CNFIN2,CNFB,XCPOCR,XCPOCROOT,CHM,METHODFAIL)

C CALCULATE SLOPE (CN-ALPHA)FIN ALONE (WITH TIP EFFECT AND QLOCAL/QFREESTREAM ADJUST)
C FOR DETERMINING CNF(B) FOR DELTA .GE. 0.0 BASED ON MODIFIED SBT
          IF(ALPHA.EQ.1.0) THEN
            CNFALPHADEG=CNFIN2/ALPHA
          ENDIF
C CALCULATE XCP/CROOT FOR FIN IN PRESENCE OF BODY USING CHM/CNFB ABOUT HINGELINE
          XCPOCRF=-1.0*((CHM/CNFB)*(RLREF)-XHINGELINE)/CROOT
C CALCULATE XCPOCRFIN FOR XCPOCROOT WITH FORWARD SHIFT DUE TO TIP EFFECT (CNFIN2)
          XCPOCRFIN=XCPOCROOT*(0.98)
C CALCULATE FIN ALONE HINGE MOMENT
          CHMF=(CNFIN2*(XHINGECR-XCPOCRFIN))*(CROOT/RLREF)

          IF(M.EQ.1) THEN
          WRITE(12,*)' M DELTA ALPHADEG  CNF       XCP/CRF      CHMF
     $ CNF(B)    XCP/CRF(B)  CHMF(B)  XCP/CR'
          ENDIF

          WRITE(12,80)M,DELTACDEG,ALPHA,CNFIN2,XCPOCRFIN,CHMF,CNFB,XCPOCR,
     $CHM,XCPOCRF
80        FORMAT(1X,I3,2X,F4.1,2X,F4.1,7(1X,F11.8))
          IF(ALPHA.LE.1.0) GOTO 32
C CALCULATE CNF(B) FOR FIN DEFLECTION USING CN-ALPHA SLOPE AND KW(B),kw(b)
C FOR SBT AND ZEUS
33        CNF=CNFALPHADEG*ALPHA
          CNFB=(RKWB*(ALPHA)+RKKWBSBT*(0.0))*CNFALPHADEG
          CHM=(CNFB*(XHINGECR-XCPOCR))*(CROOT/RLREF)
```

```
C CALCULATE XCPOCRFIN FOR XCPOCROOT WITH FORWARD SHIFT DUE TO TIP EFFECT (CNFIN2)
      XCPOCRFIN=XCPOCROOT*(0.98)
      CHMF=(CNF*(XHINGECR-XCPOCRFIN))*(CROOT/RLREF)
C CALCULATE XCP/CROOT FOR FIN IN PRESENCE OF BODY USING CHM/CNFB ABOUT HINGELINE
      XCPOCRF=-1.0*((CHM/CNFB)*(RLREF)-XHINGELINE)/CROOT

      WRITE(12,80)M,DELTACDEG,ALPHA,CNF,XCPOCRFIN,CHMF,CNFB,XCPOCR,
     $CHM,XCPOCRF
32    CONTINUE
      WRITE(*,*)'RETURN FROM SUB FINTHIK... END DELTA=0 PROGRAM'
C LOOP FOR FIN DEFLECTIONS USING SLENDER BODY THEORY
C CN-ALPHA AT +-1 DEG FOR SLOPE (1/DEG) , KW(B) AND kw(b) from SBT
      DO 85 I=1,NDELTA
      ALPHA=0.0
      DELTACDEG=DELTA(I)
      WRITE(*,*)
      WRITE(*,*)'CALCULATING AERO FOR DELTA=',DELTA(I),'DEG'
      DELTALPHA=0.0
      DO 87 M=1,NALPHA
      ALPHA=ALPHA+DELTALPHA
      DELTALPHA=0.5
C CALCULATE CNF(B) FOR FIN DEFLECTION USING CN-ALPHA SLOPE AND KW(B),kw(b)
C FOR SBT AND ZEUS
      CNF=CNFALPHADEG*(ALPHA+DELTA(I))
      CHMF=(CNF*(XHINGECR-XCPOCRFIN))*(CROOT/RLREF)
      CNFB=(RKWB*(ALPHA)+RKKWBSBT*(DELTA(I)))*CNFALPHADEG
      CHM=(CNFALPHADEG*(RKWB*ALPHA*(XHINGECR-XCPOCR)+RKKWBSBT*
     $DELTA(I)*(XHINGECR-XCPOCRFIN)))*(CROOT/RLREF)
C CALCULATE XCP/CROOT FOR FIN IN PRESENCE OF BODY USING CHM/CNFB ABOUT HINGELINE
      XCPOCRF=-1.0*((CHM/CNFB)*(RLREF)-XHINGELINE)/CROOT

      IF(M.EQ.1) THEN
      WRITE(12,*)
      WRITE(12,*)
      ENDIF

      WRITE(12,80)M,DELTACDEG,ALPHA,CNF,XCPOCRFIN,CHMF,CNFB,XCPOCR,
     $CHM,XCPOCRF
87    CONTINUE
85    CONTINUE

      STOP
      END
C *********************************************************************
C *********************************************************************
      SUBROUTINE FINCHM(J,M,RMACH,ALPHARAD,RLMAXU1,RLMAXU2,RLFLATU1,
     $RLFLATU2,CROOT,CTIP,ZUPPER1,ZUPPER2,XLE1,XLE2,RLREF,XHINGELINE,
     $SKEWDEG,RMACHFS,ARFINS,RKWB,RKWBSBT,XCPCRWBAOARS1,
     $XCPCRWBAOARS2,DELXCPCRT,RMRP,
     $CNFIN2,CNFB,XCPOCR,XCPOCROOT,CHM,METHODFAIL)
C  THIS SUBROUTINE COMPUTES THE CANARD LONGITUDINAL
C  CENTER-OF-PRESSURE (XCP) INCLUDING AIRFOIL THICKNESS
C  BY SHOCK EXPANSION THEORY AND STRIP THEORY AS DESCRIBED IN
C  NEAR TR-268, March 1982
C    (EQUATION NUMBERS CORRESPOND TO THOSE IN NEAR TR-268)
C
C  APPLIES TO DOUBLE-WEDGE AND MODIFIED DOUBLE-WEDGE AIRFOILS IN
C  SUPERSONIC FLOW AT POSITIVE AOA, POSITIVE DEFLECTION AND
C  CANARD IN HORIZONTAL PLANE
C
C  Written by: Michael G. Landers
C  9-14-96
C
C
C  INPUTS:
C     J          - NUMBER OF STRIPS FOR AIRFOIL SECTIONS FOR STRIP THEORY
C                    (INCLUDING 2 STRIPS FOR ROOT AND TIP -   J .GE. 2)
C     RMACH      - LOCAL MACN NUMBER AT CANARD LEADING EDGE
C     ALPHARAD   - FIN ANGLE OF ATTACK (RADIANS)
C     RLMAXU1/2  - MAXIMUM THICKNESS OF AIRFOIL UPPER SURFACE AT ROOT(1)
C                    AND TIP (2)   (PERCENT ROOT CHORD)
C     RLFLATU1/2 - LENGTH OF MAXIMUM THICKNESS SECTION UPPER SURFACE AT
C                    ROOT (1) AND TIP (2) (PERCENT ROOT CHORD)
C     CROOT      - ROOT CHORD LENGTH
C     CTIP       - TIP CHORD LENGTH
C     ZUPPER1/2  - THICKNESS OF UPPER HALF OF AIRFOIL AT ROOT (1) AND
C                    TIP (2)   (PERCENT ROOT CHORD)
C     XLE1       - DISTANCE FROM BODY CENTERLINE TO CROOT
C     XLE2       - DISTANCE FROM BODY CENTERLINE TO CTIP
C     XHINGE     - DISTANCE FROM L.E. AT ROOT TO HINGELINE
```

```
C     RLREF       - REFERNECE LENGTH
C     XHINGELINE  - DISTANCE FROM CANARD LEADING EDGE TO HINGELINE
C     SKEWDEG     - SKEW ANGLE OF HINGELINE MEASURED + CCW FROM VERTICAL
C     RMACHFS     - FREESTREAM MACH NUMBER AHEAD OF MISSILE NOSE
C     ARFINS      - ASPECT RATIO OF CANARDS (TWO PANELS JOINED AT ROOT,
C                   EXCLUDING BODY)
C     RKWB        - CANARD-BODY INTERFERENCE FACTOR WITH AOA (DATCOM/ZEUS)
C     RKWBSBT     - CANARD-BODY INTERFERENCE FACTOR WITH AOA
C                   (SLENDER BODY THEORY)
C     XCPCRWBAOARS1 - XCP/CROOT FROM SLENDER BODY THEORY AT AOA FOR R/S
C     XCPCRWBAOARS2 - XCP/CROOT FROM SLENDER BODY THEORY AT AOA FOR R/S=0
C                   =(2/3)
C     RMRP        - MOMENT REFERENCE POINT FOR COMPUTING AIRFOIL COMPONENT
C                   (RMRP=0.0 IS LEADING EDGE, RMRP POSITIVE AFT OF L.E.)
C
C  OUTPUT:
C     DELXCPCRT - TOTAL SHIFT IN AIRFOIL CENTER-OF-PRESSURE DUE TO
C                   AIRFOIL THICKNESS (PERCENT ROOT CHORD)
C     CNFIN2      - NORMAL FORCE COEFFICIENT FOR CANARD-ALONE W/TIP LOSSES
C     CNFB        - NORMAL FORCE COEFFICIENT FOR CANARD IN PRESENCE OF BODY
C     XCPOCR      - CANARD LONGITUDINAL CENTER-OF-PRESSURE CORRECTED FOR CANARD
C                   IN PRESENCE OF BODY  (PERCENT ROOT CHORD)
C     XCPOCROOT - CANARD LONGITUDINAL CENTER-OF-PRESSURE (PERCENT ROOT CHORD)
C     CHM         - CANARD HINGE MOMENT COEFFICIENT CORRECTED FOR CANARD IN
C                   PRESENCE OF BODY
C
C
C DIMENSION PRESSURE, NORMAL FORCE, AND HINGE MOMENT COEFFICIENTS FOR EACH
C AIRFOIL SECITON AT EACH STRIP
C     CPPL(N,J), CPPU(N,J)   Y(J):
C       WHERE N=AIRFOIL REGIONS, J=MAX NUMBER OF STRIPS FOR THEORY
        DIMENSION CN(3,1000),CM(3,1000),CPPL(3,1000),CPPU(3,1000)
        DIMENSION Y(1000),DELXCP(1000),X(4),CBAR(1000)
        DIMENSION CNRT(1000),XCPOCBAR(1000),DELX(1000),XHLOCBAR(1000)
        DIMENSION XHM(1000),XHINGE(1000),DELXHINGE(1000)
C       DELXCPCRT(100)
        REAL L1,L2,L3,LHS,LHS2,LOCALCHORD
C       WRITE(*,*)'ENTERED SUB FINCPTK'
C       WRITE(*,*)'J,RMACH,ALPHARAD,RLMAXU1,RLMAXU2,RLFLATU1,
C     $RLFLATU2,CROOT,CTIP,ZUPPER1,ZUPPER2,XLE1,XLE2',J,RMACH,ALPHARAD,
C     $RLMAXU1,RLMAXU2,RLFLATU1,
C     $RLFLATU2,CROOT,CTIP,ZUPPER1,ZUPPER2,XLE1,XLE2
C ************************************************************************
C  CONSTANTS:
        PI=4.0*ATAN(1.0)
        GAMMA     = 1.4
        GAMMAP1 = GAMMA + 1.0
        GAMMAM1 = GAMMA - 1.0
        SEMISPAN=XLE2-XLE1
        RLAMBDALE=ATAN((CROOT-CTIP)/SEMISPAN)
        TOVERC=ZUPPER1
        SKEWRAD=SKEWDEG*(PI/180.0)
C RATIO OF STATIC FREESTREAM PRESSURE TO TOTAL FREESTREAM PRESSURE - EQ.B-14
        POPT=(1.0+(GAMMAM1/2.0)*(RMACH**2.0))**(-GAMMA/GAMMAM1)
C RATIO OF FREESTREAM DYNAMIC PRESSURE TO TOTAL FREESTREAM PRESS - EQ.B-15
        QOPT=(GAMMA/2.0)*(RMACH**2.0)*POPT
C
C ************************************************************************
C ************************************************************************
C CHECK FOR ATTACHED SHOCK FOR CANARD AT TIP FOR GIVEN MACH NUMBER
C    (MODIFY CANARD GEOMETRY TO PROVIDE ATTACHED SHOCK AT TIP AT MAX AOA=20 DEG,
C     THUS MAINTAIN ATTACHED SHOCK AT ALL POINTS ALONG L.E. FOR ANY GIVEN STRIP)
C COMPUTE LOWER/UPPER AIRFOIL SURFACE ANGLES AT TIP
C
CC SET ALPHARADMAX FOR MAXIMUM AOA
        ALPHARADMAX=10.0*(PI/180.0)
C *****************************
C
        L1=RLMAXU2*CTIP
        THETAL1=ATAN((ZUPPER2*CTIP)/L1)
C DEFLECTION ANGLE OF FREESTREAM FLOW INCLUDING AOA FOR FIN - EQ. B-1
        DELTAC=ALPHARAD+THETAL1
C       WRITE(*,*)'DELTAC', DELTAC
C COMPUTE MAXIMUM SHOCK WAVE ANGLE FOR DELTAC - EQ. B-4
        R1=-(4.0-(GAMMAP1*RMACH**2.))
        R2=SQRT(GAMMAP1**2.*RMACH**4.+8.0*GAMMAP1*GAMMAM1*RMACH**2.+
     %16.0*GAMMAP1)
        R3=4.*GAMMA*RMACH**2.
        THETASMAX=ASIN(SQRT((R1+R2)/R3))
C       WRITE(*,*)'THETASMAX=',THETASMAX
```

```
C DETERMINE MAXIMUM VALUE OF DEFLECTION ANGLE FOR ATTACHED SHOCK ON FIN
      R4=TAN(THETASMAX)
      R5=GAMMAP1*RMACH**2.
      R6=2.0*(RMACH**2.*SIN(THETASMAX)**2.-1.0)
      R7=(R5/R6)-1.0
      DELTACMAX=ATAN(1.0/(R4*R7))
C      WRITE(*,*)'DELTACMAX=',DELTACMAX
C +++ TEMPORARY FIX FOR ATTACHED SHOCK UNTIL METHOD FOR DETACHED SHOCK ARE
C      DETERMINED ++++++++++++++++++++++
      IF(DELTAC.GT.DELTACMAX) THEN
         WRITE(*,*)'DELTAC GREATER THAN DELTACMAX !!'
         WRITE(*,*)'....MODIFYING DELTAC=DELTACMAX-1 FOR CANARD TIP'
         WRITE(*,*)'....MODIFYING CANARD TIP GEOMETRY FOR ATTACHED SHOCK
     %                   FOR MAX AOA=10 DEG !!'
         DELTAC=DELTACMAX-(1.0*(PI/180.0))
         THETAL1=ABS(DELTAC-ALPHARADMAX)
         THETAL3=-THETAL1
         THETAU1=THETAL1
         THETAU3=THETAL3
         RLMAXU2=((ZUPPER2*CTIP)/(TAN(THETAU1)))/(CTIP)
         RLMAXL2=RLMAXU2
         RLFLATU2=1.0-(RLMAXU2*2.0)
         RLFLATL2=RLFLATU2
C         WRITE(*,*)'THETAL1 FOR ATTACHED SHOCK CALC', THETAL1
C         write(*,*)'deltac for attached shock', deltac
C         WRITE(*,*)'RLMAXU2,RLFLATU2',RLMAXU2,RLFLATU2
      ENDIF
C *******************************************************************
C *******************************************************************
CC LOOP THROUGH AIRFOIL SECTIONS FOR GIVEN NUMBER OF STRIPS (J) IN STRIP THEORY
      DO 15 I=1,J
      WRITE(*,*)'I=',I
C
C *******************************************************************
C DETERMINE AIRFOIL TYPE: DOUBLE WEDGE/MODIFIED DOUBLE WEDGE
C BY DETERMINING REGIONS AND WEDGE ANGLES FOR PRESSURE CALCULATIONS
C      DOUBLE WEDGE AIRFOIL
      IF(RLFLATU1.EQ.0.000) THEN
         N=2
      ELSE
         N=3
      ENDIF
      WRITE(*,*)'N=',N
C *** MODIFIED DOUBLE WEDGE AIRFOIL ***
C COMPUTE LOWER/UPPER AIRFOIL SURFACE ANGLES AT ROOT
      IF(I.EQ.1.AND.N.EQ.3) THEN
         L1=RLMAXU1*CROOT
         L2=RLFLATU1*CROOT
         L3=L1
C      WRITE(*,*)'L1,L2,L3',L1,L2,L3
         THETAL1=ATAN((ZUPPER1*CROOT)/L1)
         THETAL2=0.0
         THETAL3=-THETAL1
         THETAU1=THETAL1
         THETAU2=THETAL2
         THETAU3=THETAL3
         LOCALCHORD=CROOT
         CBAR(I)=LOCALCHORD
         DELX(I)=0.0
         DELXHINGE(I)=0.0
         XHINGE(I)=XHINGELINE+DELXHINGE(I)
C      WRITE(*,*)'THETAL1,THETAL2,THETAL3',THETAL1,THETAL2,THETAL3
      ENDIF
C COMPUTE LOWER/UPPER AIRFOIL SURFACE ANGLES AT TIP
      IF(I.EQ.J.AND.N.EQ.3) THEN
         L1=RLMAXU2*CTIP
         L2=RLFLATU2*CTIP
         L3=L1
         THETAL1=ATAN((ZUPPER2*CTIP)/L1)
         THETAL2=0.0
         THETAL3=-THETAL1
         THETAU1=THETAL1
         THETAU2=THETAL2
         THETAU3=THETAL3
         LOCALCHORD=CTIP
         CBAR(I)=LOCALCHORD
         DELX(I)=TAN(RLAMBDALE)*SEMISPAN
         DELXHINGE(I)=SEMISPAN*TAN(SKEWRAD)
         XHINGE(I)=XHINGELINE+DELXHINGE(I)
C         WRITE(*,*)'IN SUB FOR CTIP'
```

```
C           WRITE(*,*)'THETAL1=',THETAL1
C           WRITE(*,*)'L1,L2,L3',L1,L2,L3
        ENDIF
C COMPUTE LOWER/UPPER AIRFOIL SURFACE ANGLES AT STRIP BETWEEN ROOT & TIP
        IF(I.GT.1.AND.I.LT.J.AND.N.EQ.3) THEN
        BETA2=ATAN(SEMISPAN/(((CROOT-CTIP)+(RLMAXU2*CTIP))-
     $(RLMAXU1*CROOT)))
C        WRITE(*,*)'BETA2,SEMISPAN,RLMAXU1,RLMAXU2,CTIP,CROOT',BETA2,
C     %SEMISPAN,RLMAXU1,RLMAXU2,CTIP,CROOT
        BETA3=ATAN(SEMISPAN/((RLMAXU1*CROOT)-(RLMAXU2*CTIP)))
C        WRITE(*,*)'BETA3',BETA3
        Y(1)=0.0
        DELY=SEMISPAN/(J-1)
        Y(I)=Y(I-1)+DELY
        DELX(I)=TAN(RLAMBDALE)*Y(I)
        LOCALCHORD=CROOT-DELX(I)
        CBAR(I)=LOCALCHORD
        X2=Y(I)/TAN(BETA2)
        X3=Y(I)/TAN(BETA3)
        L3=(RLMAXU1*CROOT)-X3
        L2=(((RLMAXU1+RLFLATU1)*CROOT)+X3)-((RLMAXU1*CROOT)+X2)
        L1=LOCALCHORD-L2-L3
        THETAL1=ATAN((TOVERC*LOCALCHORD)/L1)
        THETAL2=0.0
        THETAL3=-ATAN((TOVERC*LOCALCHORD)/L3)
        THETAU1=THETAL1
        THETAU2=THETAL2
        THETAU3=THETAL3
        DELXHINGE(I)=Y(I)*TAN(SKEWRAD)
        XHINGE(I)=XHINGELINE+DELXHINGE(I)
        WRITE(*,*)'DELY,Y(I),DELX(I),LOCALCHORD',DELY,Y(I),DELX(I),
     $LOCALCHORD
        WRITE(*,*)'X2,X3,L3,L2,L1',X2,X3,L3,L2,L1
C        WRITE(*,*)'THETAL1,THETAL3',THETAL1,THETAL3
C        WRITE(*,*)'BETA2,BETA3',BETA2,BETA3
        ENDIF
C *** DOUBLE WEDGE AIRFOIL ***
C COMPUTE LOWER/UPPER AIRFOIL SURFACE ANGLES AT ROOT
        IF(I.EQ.1.AND.N.EQ.2) THEN
           L1=RLMAXU1*CROOT
           L2=CROOT-L1
           THETAL1=ATAN((ZUPPER1*CROOT)/L1)
           THETAL2=-ATAN((ZUPPER1*CROOT)/L2)
           THETAU1=THETAL1
           THETAU2=THETAL2
           LOCALCHORD=CROOT
           CBAR(I)=LOCALCHORD
           DELX(I)=0.0
           DELXHINGE(I)=0.0
           XHINGE(I)=XHINGELINE+DELXHINGE(I)
        ENDIF
C COMPUTE LOWER/UPPER AIRFOIL SURFACE ANGLES AT TIP
        IF(I.EQ.J.AND.N.EQ.2) THEN
           L1=RLMAXU2*CTIP
           L2=CTIP-L1
           THETAL1=ATAN((ZUPPER2*CTIP)/L1)
           THETAL2=-ATAN((ZUPPER2*CTIP)/L2)
           THETAU1=THETAL1
           THETAU2=THETAL2
           LOCALCHORD=CTIP
           CBAR(I)=LOCALCHORD
           DELX(I)=TAN(RLAMBDALE)*SEMISPAN
           DELXHINGE(I)=SEMISPAN*TAN(SKEWRAD)
           XHINGE(I)=XHINGELINE+DELXHINGE(I)
        ENDIF
C COMPUTE LOWER/UPPER AIRFOIL SURFACE ANGLES AT STRIP BETWEEN ROOT & TIP
        IF(I.GT.1.AND.I.LT.J.AND.N.EQ.2) THEN
        DELY=SEMISPAN/(J-1)
        Y(I)=Y(I-1)+DELY
        DELX(I)=TAN(RLAMBDALE)*Y(I)
        LOCALCHORD=CROOT-DELX(I)
        CBAR(I)=LOCALCHORD
        X2=Y(I)/TAN(BETA2)
        L2=(RLMAXU1*CROOT)-X2
        L1=LOCALCHORD-L2
        THETAL1=ATAN((TOVERC*LOCALCHORD)/L1)
        THETAL2=-ATAN((TOVERC*LOCALCHORD)/L2)
        THETAU1=THETAL1
        THETAU2=THETAL2
        DELXHINGE(I)=Y(I)*TAN(SKEWRAD)
```

```
        XHINGE(I)=XHINGELINE+DELXHINGE(I)
        ENDIF
C
C*********************************************************************
C AIRFOIL LOWER SURFACE - REGION 1
C*********************************************************************
C DEFLECTION ANGLE OF FREESTREAM FLOW INCLUDING AOA FOR FIN - EQ. B-1
        DELTAC=ALPHARAD+THETAL1
C       WRITE(*,*)'DELTAC', DELTAC
C COMPUTE MAXIMUM SHOCK WAVE ANGLE FOR DELTAC - EQ. B-4
        R1=-(4.0-(GAMMAP1*RMACH**2.))
        R2=SQRT(GAMMAP1**2.*RMACH**4.+8.0*GAMMAP1*GAMMAM1*RMACH**2.+
     %16.0*GAMMAP1)
        R3=4.*GAMMA*RMACH**2.
        THETASMAX=ASIN(SQRT((R1+R2)/R3))
C       WRITE(*,*)'r1,r2,r3,THETASMAX=',r1,r2,r3,THETASMAX
C DETERMINE MAXIMUM VALUE OF DEFLECTION ANGLE FOR ATTACHED SHOCK ON FIN
        R4=TAN(THETASMAX)
        R5=GAMMAP1*RMACH**2.
        R6=2.0*(RMACH**2.*SIN(THETASMAX)**2.-1.0)
        R7=(R5/R6)-1.0
        DELTACMAX=ATAN(1.0/(R4*R7))
C       WRITE(*,*)'DELTACMAX=',DELTACMAX
C ITERATIVE SOLUTION FOR ATTACHED SHOCK ON FIN - EQ. B-2
C   (WEAK SHOCK SOLUTION DETERMINED FOR DOUBLE-VALUED THETAS)
        THETAS=1.0*(PI/180.0)
        LHS=1.0/(TAN(DELTAC))
c        WRITE(*,*)'deltac, LHS=',deltac, LHS
120     R6=2.0*(RMACH**2.*SIN(THETAS)**2.-1.0)
        R7=(R5/R6)-1.0
        TANTHETAS=TAN(THETAS)
        RHS=TANTHETAS*R7
        IF(RHS.LE.0.000) THEN
        DELTHETA=0.5*(PI/180.0)
        GOTO 122
        ENDIF
C        WRITE(*,*)'R6,R7,TANTHETAS,RHS',R6,R7,TANTHETAS,RHS
        ABSDIFF=ABS(RHS-LHS)
        DIFF=RHS-LHS
c        WRITE(*,*)'LHS,  RHS', LHS, RHS
c        WRITE(*,*)'ABSDIFF=',ABSDIFF
c        WRITE(*,*)'DIFF',DIFF
        IF(DIFF.LE.0.0001) GOTO 130
C TEST FOR CONVERGENCE ON ITERATIVE SOLUTION
        IF(RHS.GT.0.000.AND.DIFF.GT.0.00) GOTO 115
        IF(RHS.GT.0.000.AND.DIFF.LT.0.00) THEN
           DELTHETA=-0.1*(PI/180.0)
           GOTO 122
        ENDIF
C        IF(RHS.GT.0.000) DELTHETA=0.001*(PI/180.0)
115     IF(ABSDIFF.GE.10.0) DELTHETA=0.5*(PI/180.0)
        IF(ABSDIFF.LT.10.0) DELTHETA=0.0005*(PI/180.0)
122     THETAS=THETAS+DELTHETA
c        WRITE(*,*)'DELTHETA',DELTHETA
c        WRITE(*,*)'THETAS',THETAS
        GOTO 120
C PRESSURE COEFFICIENT - EQ. B-5
130     CPL1=(4.0*(RMACH**2.*(SIN(THETAS)**2.)-1.))/
     $(GAMMAP1*(RMACH)**2.)
C MACH NUMBER - EQ. B-6
        RM2SIN2=(RMACH**2.)*(SIN(THETAS)**2.)
        T1=(GAMMAP1)**2.*RM2SIN2*RMACH**2.
        T2=4.0*(RM2SIN2-1.0)*(GAMMA*RM2SIN2+1.0)
        T3=2.0*GAMMA*RM2SIN2-GAMMAM1
        T4=GAMMAM1*RM2SIN2+2.0
C            WRITE(*,*)'THETAS',THETAS
        RMACHL1=SQRT((T1-T2)/(T3*T4))
        WRITE(*,*)'RMACHL1',RMACHL1
        IF(RMACHL1.LT.1.00) THEN
        WRITE(*,*)'RMACHL1 LESS THAN 1.0, SUBSONIC FLOW !!'
        WRITE(*,*)'MACH ON LOWER AIRFOIL SURFACE LESS THAN 1.0'
        WRITE(*,*)'...SUBSONIC FLOW, METHOD FAILS'
        WRITE(*,*)'CALCULATING AERO WITH CN-ALPHA SLOPE'
        WRITE(12,*)'MACH ON LOWER AIRFOIL SURFACE LESS THAN 1.0'
        WRITE(12,*)'...SUBSONIC FLOW, METHOD FAILS'
        WRITE(12,*)'CALCULATING AERO WITH CN-ALPHA SLOPE'
        METHODFAIL=1
        GOTO 48
        ENDIF
C PRANDTL-MEYER ANGLE FOR ML1 - EQ. B-7
```

```
          T5=SQRT(GAMMAP1/GAMMAM1)
          T6=SQRT((GAMMAM1/GAMMAP1)*(RMACHL1**2.-1.0))
C          WRITE(*,*)'T6',T6
          T7=SQRT(RMACHL1**2.-1.)
          RNUL1=T5*ATAN(T6)-ATAN(T7)
C RATIO OF TOTAL PRESSURE TO FREESTREAM TOTAL PRESSURE - EQ. B-8
          T8=((GAMMAP1*RM2SIN2)/(GAMMAM1*RM2SIN2+2.0))**(GAMMA/GAMMAM1)
          T9=((GAMMAP1)/(2.0*GAMMA*RM2SIN2-GAMMAM1))**(1.0/GAMMAM1)
          PTL1OPT=T8*T9
C
C*********************************************************************
C AIRFOIL LOWER SURFACE - REGION 2
C*********************************************************************
C COMPUTE LOWER SURFACE EXPANSION ANGLE
          EXPANG2=THETAL1-THETAL2
          RNUL2=RNUL1+EXPANG2
          RNUMAX=(PI/2.)*(SQRT(GAMMAP1/GAMMAM1)-1.0)
          RNUBAR=(RNUL2/RNUMAX)**(2./3.)
C MACH NUMBER  - EQ. B-10
          RMACHL2=(1.0+1.3604*(RNUBAR)+0.0962*(RNUBAR**2.0)-
     $0.5127*(RNUBAR**3.0))/(1.0-0.6722*(RNUBAR)-0.3278*(RNUBAR**2.0))
C RATIO OF STATIC PRESSURE TO FREESTREAM TOTAL PRESSURE - EQ. B-12
          PL2OPTL2=(1.0+(GAMMAM1/2.0)*(RMACHL2**2.0))**(-GAMMA/GAMMAM1)
C PRESSURE COEFFICIENT -  EQ B-13
          CPL2=(PL2OPTL2*PTL1OPT-POPT)/(QOPT)
C          REGION 3 IF MODIFIED DOUBLE WEDGE
          IF(N.EQ.2) GOTO 300
C
C*********************************************************************
C AIRFOIL LOWER SURFACE - REGION 3
C*********************************************************************
C COMPUTE LOWER SURFACE EXPANSION SURFACE ANGLE
          EXPANG3=THETAL2-THETAL3
          RNUL3=RNUL2+EXPANG3
C          WRITE(*,*)'THETAL2,THETAL3,RNUL2,EXPANG3,RNUL3',THETAL2,THETAL3,
C     $RNUL2,EXPANG3,RNUL3
          RNUMAX=(PI/2.0)*(SQRT(GAMMAP1/GAMMAM1)-1.0)
          RNUBAR=(RNUL3/RNUMAX)**(2./3.)
C          WRITE(*,*)'RNUMAX,RNUBAR',RNUMAX,RNUBAR
C MACH NUMBER  - EQ. B-10
          RMACHL3=(1.0+1.3604*(RNUBAR)+0.0962*(RNUBAR**2.0)-
     $0.5127*(RNUBAR**3.0))/(1.0-0.6722*(RNUBAR)-0.3278*(RNUBAR**2.0))
C RATIO OF STATIC PRESSURE TO FREESTREAM TOTAL PRESSURE - EQ. B-12
          PL3OPTL3=(1.0+GAMMAM1/2.0*(RMACHL3**2.0))**(-GAMMA/GAMMAM1)
C PRESSURE COEFFICIENT -  EQ B-13
          CPL3=(PL3OPTL3*PTL1OPT-POPT)/(QOPT)
C          WRITE(*,*)'RMACHL3,PL3OPTL3,CPL3',RMACHL3,PL3OPTL3,CPL3
300   CONTINUE
C
C
C*********************************************************************
C   AIRFOIL UPPER SURFACE - REGION 1
C   METHOD 1 - COMPRESSION (ALPHA .LE. THETAU1)
C*********************************************************************
C DEFLECTION ANGLE OF FREESTREAM FLOW INCLUDING AOA FOR FIN - EQ. B-16
          WRITE(*,*)'START UPPER SURFACE CALCS'
          IF(ALPHARAD.LE.THETAU1) THEN
             DELTAC=-(ALPHARAD-THETAU1)
C             write(*,*)
C             write(*,*)'alpharad,thetau1,deltac',alpharad,thetau1,deltac
C             write(*,*)
          ELSE
          GOTO 160
          ENDIF
C COMPUTE MAXIMUM SHOCK WAVE ANGLE FOR DELTAC - EQ. B-4
          R1=-(4.0-(GAMMAP1*RMACH**2.))
          R2=SQRT(GAMMAP1**2.*RMACH**4.+8.0*GAMMAP1*GAMMAM1*RMACH**2.+
     %16.0*GAMMAP1)
          R3=4.*GAMMA*RMACH**2.
          THETASMAX=ASIN(SQRT((R1+R2)/R3))
C          WRITE(*,*)'THETASMAX',THETASMAX
C DETERMINE MAXIMUM VALUE OF DEFLECTION ANGLE FOR ATTACHED SHOCK ON FIN
          R4=TAN(THETASMAX)
          R5=GAMMAP1*RMACH**2.
          R6=2.0*(RMACH**2.*SIN(THETASMAX)**2.-1.0)
          R7=(R5/R6)-1.0
          DELTACMAX=ATAN(1.0/(R4*R7))
C          WRITE(*,*)'R5,R6,R7,DELTACMAX',R5,R6,R7,DELTACMAX
C ITERATIVE SOLUTION FOR ATTACHED SHOCK ON FIN - EQ. B-2
C   (WEAK SHOCK SOLUTION DETERMINED FOR DOUBLE-VALUED THETAS)
```

```
        THETAS=1.0*(PI/180.0)
          LHS2=1.0/(TAN(DELTAC))
145     R6=2.0*(RMACH**2.*SIN(THETAS)**2.-1.0)
        R7=(R5/R6)-1.0
        TANTHETAS=TAN(THETAS)
        RHS2=TANTHETAS*R7
C        WRITE(*,*)'LHS2,R6,R7,TANTHETAS,RHS2',LHS2,R6,R7,TANTHETAS,RHS2
        IF(RHS2.LE.0.000) THEN
          DELTHETA=0.5*(PI/180.0)
          GOTO 123
        ENDIF
          ABSDIFF=ABS(RHS2-LHS2)
          DIFF=RHS2-LHS2
C        WRITE(*,*)'LHS2, RHS2', LHS2, RHS2
C        WRITE(*,*)'ABSDIFF=',   ABSDIFF
C        WRITE(*,*)'DIFF', DIFF
        IF(DIFF.LE.0.0001) GOTO 161
C TEST FOR CONVERGENCE ON ITERATIVE SOLUTION
        IF(RHS2.GT.0.000.AND.DIFF.GT.0.00) GOTO 119
        IF(RHS2.GT.0.000.AND.DIFF.LT.0.00) THEN
            DELTHETA=-0.1*(PI/180.0)
            GOTO 123
        ENDIF
C         IF(RHS2.GT.0.000) DELTHETA=0.0001*(PI/180.0)
119     IF(ABSDIFF.GE.10.0) DELTHETA=0.5*(PI/180.0)
        IF(ABSDIFF.LT.10.0) DELTHETA=0.0005*(PI/180.0)
123     THETAS=THETAS+DELTHETA
c        write(*,*)'thetas for upper surface=',thetas
        GOTO 145
C PRESSURE COEFFICIENT - EQ. B-17
161     CPU1=(4.0*(RMACH**2.*(SIN(THETAS)**2.)-1.))/
        $(GAMMAP1*(RMACH)**2.)
C MACH NUMBER - EQ. B-18
        RM2SIN2=(RMACH**2.)*(SIN(THETAS)**2.)
        T1=(GAMMAP1)**2.*RM2SIN2*RMACH**2.
        T2=4.0*(RM2SIN2-1.0)*(GAMMA*RM2SIN2+1.0)
        T3=2.0*GAMMA*RM2SIN2-GAMMAM1
        T4=GAMMAM1*RM2SIN2+2.0
        RMACHU1=SQRT((T1-T2)/(T3*T4))
C         write(*,*)'thetas,t1,t2,t3,t4',thetas,t1,t2,t3,t4
        write(*,*)'rmachu1',rmachu1
C PRANDTL-MEYER ANGLE FOR MU1 - EQ. B-19
        T5=SQRT(GAMMAP1/GAMMAM1)
        T6=SQRT((GAMMAM1/GAMMAP1)*(RMACHU1**2.-1.0))
        T7=SQRT(RMACHU1**2.-1.)
        RNUU1=T5*ATAN(T6)-ATAN(T7)
C RATIO OF TOTAL PRESSURE TO FREESTREAM TOTAL PRESSURE - EQ. B-20
        T8=((GAMMAP1*RM2SIN2)/(GAMMAM1*RM2SIN2+2.0))**(GAMMA/GAMMAM1)
        T9=((GAMMAP1)/(2.0*GAMMA*RM2SIN2-GAMMAM1))**(1.0/GAMMAM1)
        PTU1OPT=T8*T9
C
C**********************************************************************
C AIRFOIL UPPER SURFACE - REGION 2
C**********************************************************************
C COMPUTE UPPER SURFACE EXPANSION ANGLE
        EXPANG2=THETAU1-THETAU2
        RNUU2=RNUU1+EXPANG2
        RNUMAX=(PI/2.)*(SQRT(GAMMAP1/GAMMAM1)-1.0)
        RNUBAR=(RNUU2/RNUMAX)**(2./3.)
C MACH NUMBER  - EQ. B-29
        RMACHU2=(1.0+1.3604*(RNUBAR)+0.0962*(RNUBAR**2.0)-
        $0.5127*(RNUBAR**3.0))/(1.0-0.6722*(RNUBAR)-0.3278*(RNUBAR**2.0))
C RATIO OF STATIC PRESSURE TO FREESTREAM TOTAL PRESSURE - EQ. B-31
        PU2OPTU2=(1.0+(GAMMAM1/2.0)*(RMACHU2**2.0))**(-GAMMA/GAMMAM1)
C PRESSURE COEFFICIENT -  EQ B-32
        CPU2=(PU2OPTU2*PTU1OPT-POPT)/(QOPT)
C        REGION 3 IF MODIFIED DOUBLE WEDGE
        IF(N.EQ.2) GOTO 160
C
C**********************************************************************
C AIRFOIL UPPER SURFACE - REGION 3
C**********************************************************************
C COMPUTE UPPER SURFACE EXPANSION SURFACE ANGLE
        EXPANG3=THETAU2-THETAU3
        RNUU3=RNUU2+EXPANG3
        RNUMAX=(PI/2.)*(SQRT(GAMMAP1/GAMMAM1)-1.0)
        RNUBAR=(RNUU3/RNUMAX)**(2./3.)
C MACH NUMBER  - EQ. B-29
        RMACHU3=(1.0+1.3604*(RNUBAR)+0.0962*(RNUBAR**2.0)-
        $0.5127*(RNUBAR**3.0))/(1.0-0.6722*(RNUBAR)-0.3278*(RNUBAR**2.0))
```

```
C RATIO OF STATIC PRESSURE TO FREESTREAM TOTAL PRESSURE - EQ. B-31
      PU3OPTU3=(1.0+GAMMAM1/2.0*(RMACHU3**2.0))**(-GAMMA/GAMMAM1)
C PRESSURE COEFFICIENT -   EQ B-32
      CPU3=(PU3OPTU3*PTU1OPT-POPT)/(QOPT)
C      WRITE(*,*)'cpu3 method1=',cpu3
      GOTO 400
C
C*************************************************************************
C   AIRFOIL UPPER SURFACE - REGION 1
C   METHOD 2 - EXPANSION (ALPHA .GT. THETAU1)
C*************************************************************************
C
160   IF(ALPHARAD.GT.THETAU1) THEN
C COMPUTE UPPER SURFACE EXPANSION ANGLE
      EXPANG1=ALPHARAD-THETAU1
C PRANDTL-MEYER ANGLE FOR FREESTREAM MACH - EQ. B-21
      T5=SQRT(GAMMAP1/GAMMAM1)
      T6=SQRT((GAMMAM1/GAMMAP1)*(RMACH**2.-1.0))
      T7=SQRT(RMACH**2.-1.)
      RNU=T5*ATAN(T6)-ATAN(T7)
      RNUU1=RNU+EXPANG1
      RNUMAX=(PI/2.)*(SQRT(GAMMAP1/GAMMAM1)-1.0)
      RNUBAR=(RNUU1/RNUMAX)**(2./3.)
C MACH NUMBER  - EQ. B-23
      RMACHU1=(1.0+1.3604*(RNUBAR)+0.0962*(RNUBAR**2.0)-
     $0.5127*(RNUBAR**3.0))/(1.0-0.6722*(RNUBAR)-0.3278*(RNUBAR**2.0))
C RATIO OF STATIC PRESSURE TO FREESTREAM TOTAL PRESSURE - EQ. B-25
      PU1OPTU1=(1.0+GAMMAM1/2.0*(RMACHU1**2.0))**(-GAMMA/GAMMAM1)
C RATIO OF LOCAL TOTAL PRESSURE TO FREESTREAM TOTAL PRESSURE
C   SINCE NO SHOCK WAVE, PTU1/PT=1.0
      PTU1OPT=1.0
C PRESSURE COEFFICIENT -   EQ B-27
      CPU1=(PU1OPTU1*PTU1OPT-POPT)/(QOPT)
      ENDIF
C
C*************************************************************************
C AIRFOIL UPPER SURFACE - REGION 2
C*************************************************************************
C COMPUTE UPPER SURFACE EXPANSION ANGLE
      EXPANG2=THETAU1-THETAU2
      RNUU2=RNUU1+EXPANG2
      RNUMAX=(PI/2.)*(SQRT(GAMMAP1/GAMMAM1)-1.0)
      RNUBAR=(RNUU2/RNUMAX)**(2./3.)
C MACH NUMBER  - EQ. B-29
      RMACHU2=(1.0+1.3604*(RNUBAR)+0.0962*(RNUBAR**2.0)-
     $0.5127*(RNUBAR**3.0))/(1.0-0.6722*(RNUBAR)-0.3278*(RNUBAR**2.0))
C RATIO OF STATIC PRESSURE TO FREESTREAM TOTAL PRESSURE - EQ. B-31
      PU2OPTU2=(1.0+(GAMMAM1/2.0)*RMACHU2**2.0)**(-GAMMA/GAMMAM1)
C PRESSURE COEFFICIENT -   EQ B-32
      CPU2=(PU2OPTU2*PTU1OPT-POPT)/(QOPT)
C      REGION 3 IF MODIFIED DOUBLE WEDGE
      IF(N.EQ.2) GOTO 400
C
C*************************************************************************
C AIRFOIL UPPER SURFACE - REGION 3
C*************************************************************************
C COMPUTE LOWER SURFACE EXPANSION SURFACE ANGLE
      EXPANG3=THETAU2-THETAU3
      RNUU3=RNUU2+EXPANG3
      RNUMAX=(PI/2.)*(SQRT(GAMMAP1/GAMMAM1)-1.0)
      RNUBAR=(RNUU3/RNUMAX)**(2./3.)
C MACH NUMBER  - EQ. B-29
      RMACHU3=(1.0+1.3604*(RNUBAR)+0.0962*(RNUBAR**2.0)-
     $0.5127*(RNUBAR**3.0))/(1.0-0.6722*(RNUBAR)-0.3278*(RNUBAR**2.0))
C RATIO OF STATIC PRESSURE TO FREESTREAM TOTAL PRESSURE - EQ. B-31
      PU3OPTU3=(1.0+GAMMAM1/2.0*(RMACHU3**2.0))**(-GAMMA/GAMMAM1)
C PRESSURE COEFFICIENT -   EQ B-32
      CPU3=(PU3OPTU3*PTU1OPT-POPT)/(QOPT)
C      WRITE(*,*)'CPU3 method2=',CPU3
400   CONTINUE
C
C*************************************************************************
C END AIRFOIL SHOCK EXPANSION CALCULATIONS
C*************************************************************************
C PLACE PRESSURE COEFFICIENTS FOR AIRFOIL SEGMENTS/STRIP IN MATRIX FORMAT
      CPPL(1,I)=CPL1
      CPPU(1,I)=CPU1
      CPPL(2,I)=CPL2
      CPPU(2,I)=CPU2
      IF (N.EQ.3) THEN
```

```
              CPPL(3,I)=CPL3
              CPPU(3,I)=CPU3
              ENDIF
              WRITE(*,*)'CPPL1,CPPL2,CPPL3',CPPL(1,I),CPPL(2,I),CPPL(3,I)
              WRITE(*,*)'CPPU1,CPPU2,CPPU3',CPPU(1,I),CPPU(2,I),CPPU(3,I)
C
C*********************************************************************
C CALCULATE CENTER-OF-PRESSURE SHIFT FOR SECTION DUE TO THICKNESS
C*********************************************************************
C  NORMAL FORCE COEFFICIENT/PITCHING MOMENT COEFFICIENT INCREMENTS
C  FOR EACH SECTION SURFACE
              X(1)=0.0
              X(2)=L1
              X(3)=LOCALCHORD
              IF (N.EQ.3) THEN
                 X(3)=L1+L2
                 X(4)=LOCALCHORD
              ENDIF
              WRITE(*,*)'X1,X2,X3,X4',X(1),X(2),X(3),X(4)
              CNRT(I)=0.0
              DO 28 K=1,N
                 CN(K,I)=((CPPL(K,I)-CPPU(K,I))*(X(K+1)-X(K)))/(RLREF)
                 CNRT(I)=CNRT(I)+CN(K,I)
                 WRITE(*,*) 'I, K, CN(K,I)', I, K, CN(K,I)
                 WRITE(*,*) 'I,CNRT(I)', I, CNRT(I)
                 WRITE(*,*) 'LOCALCHORD',LOCALCHORD
                  CM(K,I)=CN(K,I)*(RMRP-((X(K+1)+X(K))/(2.0*LOCALCHORD)))
c                 CM(K,I)=CN(K,I)*(xhlocbar(i)-((X(K+1)+X(K))/(2.0*LOCALCHORD)))
                 WRITE(*,*) 'I, K, CM(K,I)', I, K, CM(K,I)
28            CONTINUE
              WRITE(*,*) 'I=',I,      'N=',N
              WRITE(*,*) CN(1,I),CN(2,I),CN(3,I)
              WRITE(*,*) CM(1,I),CM(2,I),CM(3,I)
              WRITE(*,*)'CM SUMM',CM(1,I)+CM(2,I)+CM(3,I)
              WRITE(*,*)'CN SUMM',CN(1,I)+CN(2,I)+CN(3,I)
C  AIRFOIL XCP SHIFT DUE TO THICKNESS/CBAR (PERCENT LOCAL CHORD)
C  DELXCP=(RMRP-XCP)/CBAR
              DELXCP(I)=(CM(1,I)+CM(2,I)+CM(3,I))/(CN(1,I)+CN(2,I)+CN(3,I))
C  SUBTRACT XCP SHIFT DUE TO THICKNESS ABOUT RMRP FROM RMPR/CBAR
C  AT EACH STRIP TO GET NEW XCP/CBAR FOR EACH STRIP MEASURED FROM RMRP
              XCPOCBAR(I)=RMRP-DELXCP(I)
c             xcpocbar(i)=xhlocbar(i)-delxcp(i)
C  COMPUTE XHLOCBAR (PERCENT LOCAL CHORD) MEASURED FROM LOCAL L.E. FOR EACH STRIP
C  - USED TO COMPUTE DELTA HINGE MOMENT ABOUT HINGE LINE FOR DELTA XCP DUE TO THICKNESS
              XHLOCBAR(I)=(XHINGE(I)-DELX(I))/CBAR(I)
C  SUBTRACT XHLOCBAR-XCPOCBAR TO GET DISTANCE FROM HL TO SHIFTED XCP FROM RMRP
C  FOR CHM CALCULATION (PERCENT LOCAL CHORD)
              XHM(I)=XHLOCBAR(I)-XCPOCBAR(I)
c             xhm(i)=delxcp(i)
              WRITE(*,*)'M=', M,      'I=',I,      'N=',N
              WRITE(*,*)'DELXCP=',DELXCP(I)
              WRITE(*,*)'XCPOCBAR=',XCPOCBAR(I)
              WRITE(*,*)'XHLOCBAR=',XHLOCBAR(I)
              write(*,*)'xhinge(I),delx(i)',xhinge(I),delx(i)
              WRITE(*,*)'XHM=',XHM(I)
              write(*,*)'cbar', CBAR(I)
C WRITE CN FIN TO OUTPUT FOR CN DISTRIBUTION WITH STRIP
              IF(I.EQ.1) THEN
              WRITE(28,*)'I    SPAN    CNFIN'
              ENDIF
              IF(ALPHARAD.LT.0.0174) THEN
              WRITE(28,99)I,Y(I),CNRT(I)
 99           FORMAT (I4,1X,F6.3,1X,F9.6)
              ENDIF
15            CONTINUE
C  *********************************************************************
C  SIMPSON'S RULE OF INTEGRATION
C  COMPUTE UPPER INTEGRAL (CHM) AND LOWER INTEGRAL (CN) FOR DELXCP/CROOT
C  DUE TO AIRFOIL THICKNESS USING STRIP THEORY
C  *********************************************************************
              S0U=(((CBAR(1)*CBAR(1))/CROOT)*CNRT(1)*XHM(1))+
       $           (((CBAR(J)*CBAR(J))/CROOT)*CNRT(J)*XHM(J))
              S0L=(CBAR(1)*CNRT(1))+(CBAR(J)*CNRT(J))
              S1U=0.0
              S1L=0.0
              DO 101 I=2,J-1,2
              S1U=S1U+(((CBAR(I)*CBAR(I))/CROOT)*CNRT(I)*XHM(I))
              S1L=S1L+(CBAR(I)*CNRT(I))
101           CONTINUE
              S2U=0.0
```

```
            S2L=0.0
        DO 102 I=3,J-2,2
            S2U=S2U+(((CBAR(I)*CBAR(I))/CROOT)*CNRT(I)*XHM(I))
            S2L=S2L+(CBAR(I)*CNRT(I))
102     CONTINUE
        H=DELY
        RINTEGU=(H/3.0)*(S0U+4.0*S1U+2.0*S2U)
        RINTEGL=(H/3.0)*(S0L+4.0*S1L+2.0*S2L)
        DELXCPCRT=(RINTEGU/RINTEGL)*(RLREF/CROOT)
C ***************************************************************
        XCPOCROOT=(XHINGE(1)/CROOT)-DELXCPCRT
C CORRECT XCPOCROOT FOR WING IN PRESENC OF BODY AT AOA
        XCPOCR=XCPOCROOT-(XCPCRWBAOARS2-XCPCRWBAOARS1)
C CALCULATE CNFIN ANOTHER WAY WITH INTEGRATION
C       CNFINTOT=RINTEGCN/RLREF
        CNFINTOT=(RINTEGL/RLREF)
C       CNFINTOT=RINTEGL/CROOT
C ACCOUNT FOR TIP EFFECTS AND TIP LOSSES (CHIN P.
        BETAMACH=SQRT(RMACHFS*RMACHFS-1.0)
        EFFARFIN=BETAMACH*ARFINS
        RTIPEFF=1.0-(1.0/(2.0*EFFARFIN))
        CNFIN1=CNFINTOT*RTIPEFF
C MULTIPLY CNTOTAL BY (MLOCAL^2/MFREESREAM^2) TO REFERENCE TO FREESTREAM
C DYNAMIC PRESSURE TO MATCH CONVENTION OF FREESTREAM REFERENCE
C ...THUS FAR ALL QUANTITIES ARE REFERENCED TO LOCAL VALUES
C SINCE q/M^2=constant for given altitude...
C THEN   (qL/ML) / (q FS/M FS) = M L^2 /M FS^2
        CNFIN2=CNFIN1*((RMACH*RMACH)/(RMACHFS*RMACHFS))
C
C MULTIPLY CNFIN ALONE BY INTERFERENCE FACTOR FROM ZUES, K TO
C DETERMINE CN FIN IN PRESENCE OF BODY...
C DETERMINED BY TAN(AOA local)zeus/ TAN(AOA freestream)body OR
C K FROM DATCOM OR NACA 1307.
        CNFB=CNFIN2*RKWB
C
C CALCULATE HINGE MOMENT ABOUT HINGELINE AT ROOT CHORD REFERENCE TO REF LENGTH
        CHM=CNFB*(((XHINGELINE/CROOT)-XCPOCR))*(CROOT/RLREF)

            WRITE(*,*)
            write(*,*)'h', h
            WRITE(*,*)'S0U,S0L,S1U,S1L,S2U,S2L',S0U,S0L,S1U,S1L,S2U,S2L
            WRITE(*,*)'RINTEGU,RINTEGL',RINTEGU,RINTEGL
            WRITE(*,*)'DELXCPI',DELXCPI
            WRITE(*,*)'DELXCPCRT=', DELXCPCRT
            WRITE(*,*)'XCPOCROOT=', XCPOCROOT
            WRITE(*,*)'XCPOCR=', XCPOCR
            WRITE(*,*)'ORIGINAL METHOD...CNTOTAL=',CNFINTOT
            WRITE(*,*)
            WRITE(*,*)'FIN ALONE WITH TIP/MACH CORR. =', CNFIN2
            WRITE(*,*)
            WRITE(*,*)'FIN IN PRES. OF BODY  CNFB=',CNFB
            WRITE(*,*)
            WRITE(*,*)'FIN HINGE MOMENT=', CHM


48      RETURN
        END
```

APPENDIX C

FINCHM CODE OUTPUT

Table C.1 *FINCHM* Code Output (Mach=1.25, Position 3)

M	DELTA	ALPHA	CNF	XCP/CRF	CHMF	CNF(B)	XCP/CRF(B)	CHMF(B)	XCP/CR
1	.0	.5	.00361731	.60446580	-.00002817	.00477485	.60087590	-.00003032	.60087590
2	.0	1.0	.00722098	.60290600	-.00005172	.00953169	.59928420	-.00005446	.59928420
3	.0	1.5	.01083147	.60290600	-.00007758	.01429753	.59928420	-.00008169	.59928420
4	.0	2.0	.01444195	.60290600	-.00010344	.01906338	.59928420	-.00010892	.59928420
5	.0	2.5	.01805244	.60290600	-.00012930	.02382922	.59928420	-.00013615	.59928420
6	.0	3.0	.02166293	.60290600	-.00015516	.02859507	.59928420	-.00016338	.59928420
7	.0	3.5	.02527342	.60290600	-.00018102	.03336091	.59928420	-.00019061	.59928420
8	.0	4.0	.02888391	.60290600	-.00020688	.03812676	.59928420	-.00021784	.59928420
9	.0	4.5	.03249440	.60290600	-.00023274	.04289260	.59928420	-.00024508	.59928420
10	.0	5.0	.03610488	.60290600	-.00025860	.04765845	.59928420	-.00027231	.59928420
11	.0	5.5	.03971537	.60290600	-.00028446	.05242429	.59928420	-.00029954	.59928420
12	.0	6.0	.04332586	.60290600	-.00031032	.05719014	.59928420	-.00032677	.59928420
13	.0	6.5	.04693635	.60290600	-.00033618	.06195598	.59928420	-.00035400	.59928420
14	.0	7.0	.05054684	.60290600	-.00036204	.06672183	.59928420	-.00038123	.59928420
15	.0	7.5	.05415732	.60290600	-.00038790	.07148767	.59928420	-.00040846	.59928420
16	.0	8.0	.05776781	.60290600	-.00041376	.07625352	.59928420	-.00043569	.59928420
17	.0	8.5	.06137830	.60290600	-.00043962	.08101936	.59928420	-.00046292	.59928420
18	.0	9.0	.06498879	.60290600	-.00046548	.08578520	.59928420	-.00049015	.59928420
19	.0	9.5	.06859928	.60290600	-.00049134	.09055105	.59928420	-.00051738	.59928420
20	.0	10.0	.07220977	.60290600	-.00051720	.09531689	.59928420	-.00054461	.59928420
21	.0	10.5	.07582025	.60290600	-.00054306	.10008270	.59928420	-.00057184	.59928420
1	3.0	.0	.02166293	.60290600	-.00015516	.02058735	.59928420	-.00014745	.60290600
2	3.0	.5	.02527342	.60290600	-.00018102	.02535319	.59928420	-.00017469	.60222520
3	3.0	1.0	.02888391	.60290600	-.00020688	.03011904	.59928420	-.00020192	.60175990
4	3.0	1.5	.03249440	.60290600	-.00023274	.03488488	.59928420	-.00022915	.60142160
5	3.0	2.0	.03610488	.60290600	-.00025860	.03965073	.59928420	-.00025638	.60116470
6	3.0	2.5	.03971537	.60290600	-.00028446	.04441657	.59928420	-.00028361	.60096290
7	3.0	3.0	.04332586	.60290600	-.00031032	.04918242	.59928420	-.00031084	.60080030
8	3.0	3.5	.04693635	.60290600	-.00033618	.05394826	.59928420	-.00033807	.60066630
9	3.0	4.0	.05054684	.60290600	-.00036204	.05871410	.59928420	-.00036530	.60055420
10	3.0	4.5	.05415732	.60290600	-.00038790	.06347995	.59928420	-.00039253	.60045880
11	3.0	5.0	.05776781	.60290600	-.00041376	.06824579	.59928420	-.00041976	.60037680
12	3.0	5.5	.06137830	.60290600	-.00043962	.07301164	.59928420	-.00044699	.60030550
13	3.0	6.0	.06498879	.60290600	-.00046548	.07777748	.59928420	-.00047422	.60024290
14	3.0	6.5	.06859928	.60290600	-.00049134	.08254333	.59928420	-.00050145	.60018750
15	3.0	7.0	.07220977	.60290600	-.00051720	.08730917	.59928420	-.00052868	.60013820
16	3.0	7.5	.07582025	.60290600	-.00054306	.09207502	.59928420	-.00055591	.60009400
17	3.0	8.0	.07943074	.60290600	-.00056892	.09684086	.59928420	-.00058314	.60005420
18	3.0	8.5	.08304123	.60290600	-.00059477	.10160670	.59928420	-.00061038	.60001810
19	3.0	9.0	.08665172	.60290600	-.00062063	.10637260	.59928420	-.00063761	.59998520
20	3.0	9.5	.09026220	.60290600	-.00064649	.11113840	.59928420	-.00066484	.59995510
21	3.0	10.0	.09387270	.60290600	-.00067235	.11590420	.59928420	-.00069207	.59992750
1	9.0	.0	.06498879	.60290600	-.00046548	.06176204	.59928420	-.00044236	.60290600
2	9.0	.5	.06859928	.60290600	-.00049134	.06652789	.59928420	-.00046960	.60264650
3	9.0	1.0	.07220977	.60290600	-.00051720	.07129373	.59928420	-.00049683	.60242180
4	9.0	1.5	.07582025	.60290600	-.00054306	.07605957	.59928420	-.00052406	.60222520
5	9.0	2.0	.07943074	.60290600	-.00056892	.08082542	.59928420	-.00055129	.60205180
6	9.0	2.5	.08304123	.60290600	-.00059477	.08559126	.59928420	-.00057852	.60189770
7	9.0	3.0	.08665172	.60290600	-.00062063	.09035711	.59928420	-.00060575	.60175980
8	9.0	3.5	.09026220	.60290600	-.00064649	.09512296	.59928420	-.00063298	.60163580
9	9.0	4.0	.09387270	.60290600	-.00067235	.09988879	.59928420	-.00066021	.60152360
10	9.0	4.5	.09748318	.60290600	-.00069821	.10465460	.59928420	-.00068744	.60142160
11	9.0	5.0	.10109370	.60290600	-.00072407	.10942050	.59928420	-.00071467	.60132850
12	9.0	5.5	.10470420	.60290600	-.00074993	.11418630	.59928420	-.00074190	.60124320
13	9.0	6.0	.10831460	.60290600	-.00077579	.11895220	.59928420	-.00076913	.60116470
14	9.0	6.5	.11192510	.60290600	-.00080165	.12371800	.59928420	-.00079636	.60109230
15	9.0	7.0	.11553560	.60290600	-.00082751	.12848390	.59928420	-.00082359	.60102520
16	9.0	7.5	.11914610	.60290600	-.00085337	.13324970	.59928420	-.00085082	.60096290
17	9.0	8.0	.12275660	.60290600	-.00087923	.13801560	.59928420	-.00087805	.60090490
18	9.0	8.5	.12636710	.60290600	-.00090509	.14278140	.59928420	-.00090529	.60085090
19	9.0	9.0	.12997760	.60290600	-.00093095	.14754720	.59928420	-.00093252	.60080030
20	9.0	9.5	.13358810	.60290600	-.00095681	.15231310	.59928420	-.00095975	.60075280
21	9.0	10.0	.13719860	.60290600	-.00098267	.15707890	.59928420	-.00098698	.60070820

Table C.2 *FINCHM* Code Output (Mach=1.50, Position 1)

M	DELTA	ALPHA	CNF	XCP/CRF	CHMF	CNF(B)	XCP/CRF(B)	CHMF(B)	XCP/CR
1	.0	.5	.00289251	.67122070	-.00009976	.00376026	.66651540	-.00012261	.66651540
2	.0	1.0	.00579204	.67055450	-.00019821	.00752965	.66583560	-.00024347	.66583560
3	.0	1.5	.00868806	.67055450	-.00029732	.01129448	.66583560	-.00036520	.66583560
4	.0	2.0	.01158408	.67055450	-.00039643	.01505931	.66583560	-.00048693	.66583560
5	.0	2.5	.01448010	.67055450	-.00049553	.01882413	.66583560	-.00060866	.66583560
6	.0	3.0	.01737612	.67055450	-.00059464	.02258896	.66583560	-.00073040	.66583560
7	.0	3.5	.02027214	.67055450	-.00069375	.02635379	.66583560	-.00085213	.66583560
8	.0	4.0	.02316816	.67055450	-.00079286	.03011861	.66583560	-.00097386	.66583560
9	.0	4.5	.02606418	.67055450	-.00089196	.03388344	.66583560	-.00109559	.66583560
10	.0	5.0	.02896020	.67055450	-.00099107	.03764826	.66583560	-.00121733	.66583560
11	.0	5.5	.03185622	.67055450	-.00109018	.04141309	.66583560	-.00133906	.66583560
12	.0	6.0	.03475225	.67055450	-.00118928	.04517792	.66583560	-.00146079	.66583560
13	.0	6.5	.03764826	.67055450	-.00128839	.04894274	.66583560	-.00158253	.66583560
14	.0	7.0	.04054429	.67055450	-.00138750	.05270757	.66583560	-.00170426	.66583560
15	.0	7.5	.04344030	.67055450	-.00148660	.05647239	.66583560	-.00182599	.66583560
16	.0	8.0	.04633633	.67055450	-.00158571	.06023722	.66583560	-.00194772	.66583560
17	.0	8.5	.04923235	.67055450	-.00168482	.06400205	.66583560	-.00206946	.66583560
18	.0	9.0	.05212837	.67055450	-.00178393	.06776688	.66583560	-.00219119	.66583560
19	.0	9.5	.05502439	.67055450	-.00188303	.07153170	.66583560	-.00231292	.66583560
20	.0	10.0	.05792041	.67055450	-.00198214	.07529653	.66583560	-.00243466	.66583560
21	.0	10.5	.06081643	.67055450	-.00208125	.07906135	.66583560	-.00255639	.66583560
1	3.0	.0	.01737612	.67055450	-.00059464	.01637620	.66583560	-.00056042	.67055450
2	3.0	.5	.02027214	.67055450	-.00069375	.02014102	.66583560	-.00068216	.66967240
3	3.0	1.0	.02316816	.67055450	-.00079286	.02390585	.66583560	-.00080389	.66906820
4	3.0	1.5	.02606418	.67055450	-.00089196	.02767068	.66583560	-.00092562	.66862830
5	3.0	2.0	.02896020	.67055450	-.00099107	.03143550	.66583560	-.00104735	.66829380
6	3.0	2.5	.03185622	.67055450	-.00109018	.03520033	.66583560	-.00116909	.66803090
7	3.0	3.0	.03475225	.67055450	-.00118928	.03896515	.66583560	-.00129082	.66781880
8	3.0	3.5	.03764826	.67055450	-.00128839	.04272998	.66583560	-.00141255	.66764410
9	3.0	4.0	.04054429	.67055450	-.00138750	.04649481	.66583560	-.00153428	.66749760
10	3.0	4.5	.04344030	.67055450	-.00148661	.05025963	.66583560	-.00165602	.66737310
11	3.0	5.0	.04633633	.67055450	-.00158571	.05402446	.66583560	-.00177775	.66726600
12	3.0	5.5	.04923235	.67055450	-.00168482	.05778928	.66583560	-.00189948	.66717280
13	3.0	6.0	.05212837	.67055450	-.00178393	.06155411	.66583560	-.00202122	.66709100
14	3.0	6.5	.05502439	.67055450	-.00188303	.06531894	.66583560	-.00214295	.66701870
15	3.0	7.0	.05792041	.67055450	-.00198214	.06908377	.66583560	-.00226468	.66695420
16	3.0	7.5	.06081643	.67055450	-.00208125	.07284860	.66583560	-.00238641	.66689630
17	3.0	8.0	.06371245	.67055450	-.00218035	.07661342	.66583560	-.00250815	.66684420
18	3.0	8.5	.06660847	.67055450	-.00227946	.08037824	.66583560	-.00262988	.66679700
19	3.0	9.0	.06950449	.67055450	-.00237857	.08414307	.66583560	-.00275161	.66675390
20	3.0	9.5	.07240051	.67055450	-.00247768	.08790790	.66583560	-.00287335	.66671460
21	3.0	10.0	.07529653	.67055450	-.00257678	.09167273	.66583560	-.00299508	.66667850
1	9.0	.0	.05212837	.67055450	-.00178393	.04912859	.66583560	-.00168127	.67055450
2	9.0	.5	.05502439	.67055450	-.00188303	.05289342	.66583560	-.00180300	.67021860
3	9.0	1.0	.05792041	.67055450	-.00198214	.05665824	.66583560	-.00192473	.66992740
4	9.0	1.5	.06081643	.67055450	-.00208125	.06042306	.66583560	-.00204647	.66967240
5	9.0	2.0	.06371245	.67055450	-.00218035	.06418789	.66583560	-.00216820	.66944740
6	9.0	2.5	.06660847	.67055450	-.00227946	.06795272	.66583560	-.00228993	.66924720
7	9.0	3.0	.06950449	.67055450	-.00237857	.07171755	.66583560	-.00241166	.66906820
8	9.0	3.5	.07240051	.67055450	-.00247768	.07548238	.66583560	-.00253340	.66890690
9	9.0	4.0	.07529653	.67055450	-.00257678	.07924720	.66583560	-.00265513	.66876100
10	9.0	4.5	.07819255	.67055450	-.00267589	.08301202	.66583560	-.00277686	.66862830
11	9.0	5.0	.08108857	.67055450	-.00277500	.08677685	.66583560	-.00289860	.66850720
12	9.0	5.5	.08398459	.67055450	-.00287410	.09054168	.66583560	-.00302033	.66839610
13	9.0	6.0	.08688061	.67055450	-.00297321	.09430651	.66583560	-.00314206	.66829380
14	9.0	6.5	.08977664	.67055450	-.00307232	.09807133	.66583560	-.00326379	.66819950
15	9.0	7.0	.09267265	.67055450	-.00317142	.10183620	.66583560	-.00338553	.66811210
16	9.0	7.5	.09556867	.67055450	-.00327053	.10560100	.66583560	-.00350726	.66803090
17	9.0	8.0	.09846470	.67055450	-.00336964	.10936580	.66583560	-.00362899	.66795530
18	9.0	8.5	.10136070	.67055450	-.00346875	.11313060	.66583560	-.00375073	.66788480
19	9.0	9.0	.10425670	.67055450	-.00356785	.11689550	.66583560	-.00387246	.66781880
20	9.0	9.5	.10715280	.67055450	-.00366696	.12066030	.66583560	-.00399419	.66775690
21	9.0	10.0	.11004880	.67055450	-.00376607	.12442510	.66583560	-.00411592	.66769880

Table C.3 *FINCHM* Code Output (Mach=1.50, Position 2)

M	DELTA	ALPHA	CNF	XCP/CRF	CHMF	CNF(B)	XCP/CRF(B)	CHMF(B)	XCP/CR
1	.0	.5	.00286674	.64705900	-.00007116	.00372677	.64313720	-.00008667	.64313720
2	.0	1.0	.00572875	.64543710	-.00013849	.00744737	.64148210	-.00016826	.64148210
3	.0	1.5	.00859312	.64543710	-.00020774	.01117106	.64148210	-.00025239	.64148210
4	.0	2.0	.01145750	.64543710	-.00027698	.01489475	.64148210	-.00033651	.64148210
5	.0	2.5	.01432187	.64543710	-.00034623	.01861843	.64148210	-.00042064	.64148210
6	.0	3.0	.01718625	.64543710	-.00041547	.02234212	.64148210	-.00050477	.64148210
7	.0	3.5	.02005062	.64543710	-.00048472	.02606581	.64148210	-.00058890	.64148210
8	.0	4.0	.02291499	.64543710	-.00055397	.02978949	.64148210	-.00067303	.64148210
9	.0	4.5	.02577937	.64543710	-.00062321	.03351318	.64148210	-.00075716	.64148210
10	.0	5.0	.02864374	.64543710	-.00069246	.03723687	.64148210	-.00084129	.64148210
11	.0	5.5	.03150812	.64543710	-.00076170	.04096055	.64148210	-.00092542	.64148210
12	.0	6.0	.03437249	.64543710	-.00083095	.04468424	.64148210	-.00100954	.64148210
13	.0	6.5	.03723687	.64543710	-.00090019	.04840792	.64148210	-.00109367	.64148210
14	.0	7.0	.04010124	.64543710	-.00096944	.05213161	.64148210	-.00117780	.64148210
15	.0	7.5	.04296561	.64543710	-.00103869	.05585530	.64148210	-.00126193	.64148210
16	.0	8.0	.04582999	.64543710	-.00110793	.05957898	.64148210	-.00134606	.64148210
17	.0	8.5	.04869436	.64543710	-.00117718	.06330267	.64148210	-.00143019	.64148210
18	.0	9.0	.05155874	.64543710	-.00124642	.06702635	.64148210	-.00151432	.64148210
19	.0	9.5	.05442311	.64543710	-.00131567	.07075004	.64148210	-.00159845	.64148210
20	.0	10.0	.05728748	.64543710	-.00138491	.07447373	.64148210	-.00168257	.64148210
21	.0	10.5	.06015186	.64543710	-.00145416	.07819741	.64148210	-.00176670	.64148210
1	3.0	.0	.01718625	.64543710	-.00041547	.01626774	.64148210	-.00039327	.64543710
2	3.0	.5	.02005062	.64543710	-.00048472	.01999143	.64148210	-.00047740	.64470040
3	3.0	1.0	.02291499	.64543710	-.00055397	.02371511	.64148210	-.00056153	.64419510
4	3.0	1.5	.02577937	.64543710	-.00062321	.02743880	.64148210	-.00064566	.64382690
5	3.0	2.0	.02864374	.64543710	-.00069246	.03116249	.64148210	-.00072978	.64354670
6	3.0	2.5	.03150812	.64543710	-.00076170	.03488617	.64148210	-.00081391	.64332630
7	3.0	3.0	.03437249	.64543710	-.00083095	.03860986	.64148210	-.00089804	.64314850
8	3.0	3.5	.03723687	.64543710	-.00090020	.04233355	.64148210	-.00098217	.64300190
9	3.0	4.0	.04010124	.64543710	-.00096944	.04605723	.64148210	-.00106630	.64287900
10	3.0	4.5	.04296561	.64543710	-.00103869	.04978092	.64148210	-.00115043	.64277450
11	3.0	5.0	.04582999	.64543710	-.00110793	.05350460	.64148210	-.00123456	.64268460
12	3.0	5.5	.04869436	.64543710	-.00117718	.05722829	.64148210	-.00131869	.64260640
13	3.0	6.0	.05155874	.64543710	-.00124642	.06095198	.64148210	-.00140281	.64253770
14	3.0	6.5	.05442311	.64543710	-.00131567	.06467567	.64148210	-.00148694	.64247690
15	3.0	7.0	.05728748	.64543710	-.00138492	.06839935	.64148210	-.00157107	.64242270
16	3.0	7.5	.06015186	.64543710	-.00145416	.07212304	.64148210	-.00165520	.64237420
17	3.0	8.0	.06301624	.64543710	-.00152341	.07584672	.64148210	-.00173933	.64233040
18	3.0	8.5	.06588061	.64543710	-.00159265	.07957041	.64148210	-.00182346	.64229070
19	3.0	9.0	.06874499	.64543710	-.00166190	.08329409	.64148210	-.00190759	.64225450
20	3.0	9.5	.07160936	.64543710	-.00173114	.08701778	.64148210	-.00199172	.64222150
21	3.0	10.0	.07447373	.64543710	-.00180039	.09074147	.64148210	-.00207584	.64219110
1	9.0	.0	.05155874	.64543710	-.00124642	.04880322	.64148210	-.00117981	.64543710
2	9.0	.5	.05442311	.64543710	-.00131567	.05252691	.64148210	-.00126394	.64515670
3	9.0	1.0	.05728748	.64543710	-.00138492	.05625059	.64148210	-.00134807	.64491340
4	9.0	1.5	.06015186	.64543710	-.00145416	.05997428	.64148210	-.00143220	.64470040
5	9.0	2.0	.06301624	.64543710	-.00152341	.06369797	.64148210	-.00151632	.64451220
6	9.0	2.5	.06588061	.64543710	-.00159265	.06742165	.64148210	-.00160045	.64434490
7	9.0	3.0	.06874499	.64543710	-.00166190	.07114534	.64148210	-.00168458	.64419510
8	9.0	3.5	.07160936	.64543710	-.00173114	.07486903	.64148210	-.00176871	.64406010
9	9.0	4.0	.07447373	.64543710	-.00180039	.07859271	.64148210	-.00185284	.64393800
10	9.0	4.5	.07733811	.64543710	-.00186964	.08231640	.64148210	-.00193697	.64382690
11	9.0	5.0	.08020248	.64543710	-.00193888	.08604009	.64148210	-.00202110	.64372540
12	9.0	5.5	.08306686	.64543710	-.00200813	.08976378	.64148210	-.00210523	.64363240
13	9.0	6.0	.08593123	.64543710	-.00207737	.09348746	.64148210	-.00218935	.64354670
14	9.0	6.5	.08879560	.64543710	-.00214662	.09721114	.64148210	-.00227348	.64346760
15	9.0	7.0	.09165998	.64543710	-.00221586	.10093480	.64148210	-.00235761	.64339440
16	9.0	7.5	.09452435	.64543710	-.00228511	.10465850	.64148210	-.00244174	.64332630
17	9.0	8.0	.09738873	.64543710	-.00235436	.10838220	.64148210	-.00252587	.64326300
18	9.0	8.5	.10025310	.64543710	-.00242360	.11210590	.64148210	-.00261000	.64320390
19	9.0	9.0	.10311750	.64543710	-.00249285	.11582960	.64148210	-.00269413	.64314850
20	9.0	9.5	.10598180	.64543710	-.00256209	.11955330	.64148210	-.00277826	.64309660
21	9.0	10.0	.10884620	.64543710	-.00263134	.12327690	.64148210	-.00286238	.64304780

Table C.4 *FINCHM* Code Output (Mach=1.50, Position 3)

M	DELTA	ALPHA	CNF	XCP/CRF	CHMF	CNF(B)	XCP/CRF(B)	CHMF(B)	XCP/CR
1	.0	.5	.00288718	.61041480	-.00002935	.00375333	.60694630	-.00003295	.60694630
2	.0	1.0	.00577648	.61034300	-.00005856	.00750943	.60687300	-.00006570	.60687300
3	.0	1.5	.00866472	.61034300	-.00008784	.01126414	.60687300	-.00009855	.60687300
4	.0	2.0	.01155297	.61034300	-.00011711	.01501885	.60687300	-.00013140	.60687300
5	.0	2.5	.01444121	.61034300	-.00014639	.01877357	.60687300	-.00016425	.60687300
6	.0	3.0	.01732945	.61034300	-.00017567	.02252828	.60687300	-.00019710	.60687300
7	.0	3.5	.02021769	.61034300	-.00020495	.02628300	.60687300	-.00022996	.60687300
8	.0	4.0	.02310593	.61034300	-.00023423	.03003771	.60687300	-.00026281	.60687300
9	.0	4.5	.02599417	.61034300	-.00026351	.03379242	.60687300	-.00029566	.60687300
10	.0	5.0	.02888241	.61034300	-.00029279	.03754714	.60687300	-.00032851	.60687300
11	.0	5.5	.03177065	.61034300	-.00032207	.04130185	.60687300	-.00036136	.60687300
12	.0	6.0	.03465889	.61034300	-.00035134	.04505656	.60687300	-.00039421	.60687300
13	.0	6.5	.03754714	.61034300	-.00038062	.04881128	.60687300	-.00042706	.60687300
14	.0	7.0	.04043538	.61034300	-.00040990	.05256599	.60687300	-.00045991	.60687300
15	.0	7.5	.04332362	.61034300	-.00043918	.05632070	.60687300	-.00049276	.60687300
16	.0	8.0	.04621186	.61034300	-.00046846	.06007542	.60687300	-.00052561	.60687300
17	.0	8.5	.04910010	.61034300	-.00049774	.06383013	.60687300	-.00055846	.60687300
18	.0	9.0	.05198834	.61034300	-.00052702	.06758484	.60687300	-.00059131	.60687300
19	.0	9.5	.05487658	.61034300	-.00055629	.07133956	.60687300	-.00062416	.60687300
20	.0	10.0	.05776483	.61034300	-.00058557	.07509428	.60687300	-.00065701	.60687300
21	.0	10.5	.06065307	.61034300	-.00061485	.07884899	.60687300	-.00068987	.60687300
1	3.0	.0	.01732945	.61034300	-.00017567	.01646903	.60687300	-.00016695	.61034300
2	3.0	.5	.02021769	.61034300	-.00020495	.02022374	.60687300	-.00019980	.60969870
3	3.0	1.0	.02310593	.61034300	-.00023423	.02397845	.60687300	-.00023265	.60925630
4	3.0	1.5	.02599417	.61034300	-.00026351	.02773317	.60687300	-.00026550	.60893360
5	3.0	2.0	.02888241	.61034300	-.00029279	.03148788	.60687300	-.00029835	.60868790
6	3.0	2.5	.03177065	.61034300	-.00032207	.03524259	.60687300	-.00033120	.60849450
7	3.0	3.0	.03465889	.61034300	-.00035134	.03899731	.60687300	-.00036405	.60833840
8	3.0	3.5	.03754714	.61034300	-.00038062	.04275202	.60687300	-.00039690	.60820970
9	3.0	4.0	.04043538	.61034300	-.00040990	.04650674	.60687300	-.00042976	.60810180
10	3.0	4.5	.04332362	.61034300	-.00043918	.05026145	.60687300	-.00046261	.60801000
11	3.0	5.0	.04621186	.61034300	-.00046846	.05401616	.60687300	-.00049546	.60793100
12	3.0	5.5	.04910010	.61034300	-.00049774	.05777087	.60687300	-.00052831	.60786220
13	3.0	6.0	.05198834	.61034300	-.00052702	.06152559	.60687300	-.00056116	.60780180
14	3.0	6.5	.05487658	.61034300	-.00055629	.06528030	.60687300	-.00059401	.60774840
15	3.0	7.0	.05776483	.61034300	-.00058557	.06903502	.60687300	-.00062686	.60770080
16	3.0	7.5	.06065307	.61034300	-.00061485	.07278973	.60687300	-.00065971	.60765810
17	3.0	8.0	.06354131	.61034300	-.00064413	.07654444	.60687300	-.00069256	.60761960
18	3.0	8.5	.06642955	.61034300	-.00067341	.08029915	.60687300	-.00072541	.60758470
19	3.0	9.0	.06931779	.61034300	-.00070269	.08405387	.60687300	-.00075826	.60755290
20	3.0	9.5	.07220604	.61034300	-.00073197	.08780859	.60687300	-.00079111	.60752380
21	3.0	10.0	.07509428	.61034300	-.00076125	.09156330	.60687300	-.00082396	.60749710
1	9.0	.0	.05198834	.61034300	-.00052702	.04940708	.60687300	-.00050085	.61034300
2	9.0	.5	.05487658	.61034300	-.00055629	.05316179	.60687300	-.00053370	.61009790
3	9.0	1.0	.05776483	.61034300	-.00058557	.05691651	.60687300	-.00056655	.60988520
4	9.0	1.5	.06065307	.61034300	-.00061485	.06067122	.60687300	-.00059940	.60969880
5	9.0	2.0	.06354131	.61034300	-.00064413	.06442593	.60687300	-.00063225	.60953410
6	9.0	2.5	.06642955	.61034300	-.00067341	.06818064	.60687300	-.00066510	.60938750
7	9.0	3.0	.06931779	.61034300	-.00070269	.07193536	.60687300	-.00069795	.60925630
8	9.0	3.5	.07220604	.61034300	-.00073197	.07569008	.60687300	-.00073080	.60913800
9	9.0	4.0	.07509428	.61034300	-.00076125	.07944479	.60687300	-.00076366	.60903100
10	9.0	4.5	.07798252	.61034300	-.00079052	.08319950	.60687300	-.00079651	.60893360
11	9.0	5.0	.08087076	.61034300	-.00081980	.08695421	.60687300	-.00082936	.60884460
12	9.0	5.5	.08375899	.61034300	-.00084908	.09070893	.60687300	-.00086221	.60876300
13	9.0	6.0	.08664724	.61034300	-.00087836	.09446364	.60687300	-.00089506	.60868790
14	9.0	6.5	.08953548	.61034300	-.00090764	.09821835	.60687300	-.00092791	.60861850
15	9.0	7.0	.09242372	.61034300	-.00093692	.10197310	.60687300	-.00096076	.60855420
16	9.0	7.5	.09531196	.61034300	-.00096620	.10572780	.60687300	-.00099361	.60849450
17	9.0	8.0	.09820020	.61034300	-.00099548	.10948250	.60687300	-.00102646	.60843890
18	9.0	8.5	.10108840	.61034300	-.00102475	.11323720	.60687300	-.00105931	.60838700
19	9.0	9.0	.10397670	.61034300	-.00105403	.11699190	.60687300	-.00109216	.60833840
20	9.0	9.5	.10686490	.61034300	-.00108331	.12074660	.60687300	-.00112501	.60829280
21	9.0	10.0	.10975320	.61034300	-.00111259	.12450130	.60687300	-.00115786	.60825000

Table C.5 *FINCHM* Code Output (Mach=2.00, Position 1)

M	DELTA	ALPHA	CNF	XCP/CRF	CHMF	CNF(B)	XCP/CRF(B)	CHMF(B)	XCP/CR
1	.0	.5	.00187495	.68727100	-.00007670	.00243744	.68289330	-.00009544	.68289330
2	.0	1.0	.00375083	.68726700	-.00015343	.00487609	.68288920	-.00019093	.68288920
3	.0	1.5	.00562625	.68726700	-.00023015	.00731413	.68288920	-.00028639	.68288920
4	.0	2.0	.00750167	.68726700	-.00030687	.00975217	.68288920	-.00038185	.68288920
5	.0	2.5	.00937709	.68726700	-.00038359	.01219021	.68288920	-.00047732	.68288920
6	.0	3.0	.01125250	.68726700	-.00046030	.01462826	.68288920	-.00057278	.68288920
7	.0	3.5	.01312792	.68726700	-.00053702	.01706630	.68288920	-.00066824	.68288920
8	.0	4.0	.01500334	.68726700	-.00061374	.01950434	.68288920	-.00076371	.68288920
9	.0	4.5	.01687876	.68726700	-.00069046	.02194238	.68288920	-.00085917	.68288920
10	.0	5.0	.01875417	.68726700	-.00076717	.02438042	.68288920	-.00095463	.68288920
11	.0	5.5	.02062959	.68726700	-.00084389	.02681847	.68288920	-.00105010	.68288920
12	.0	6.0	.02250501	.68726700	-.00092061	.02925651	.68288920	-.00114556	.68288920
13	.0	6.5	.02438043	.68726700	-.00099733	.03169455	.68288920	-.00124102	.68288920
14	.0	7.0	.02625584	.68726700	-.00107404	.03413260	.68288920	-.00133649	.68288920
15	.0	7.5	.02813126	.68726700	-.00115076	.03657064	.68288920	-.00143195	.68288920
16	.0	8.0	.03000668	.68726700	-.00122748	.03900868	.68288920	-.00152741	.68288920
17	.0	8.5	.03188210	.68726700	-.00130420	.04144672	.68288920	-.00162288	.68288920
18	.0	9.0	.03375752	.68726700	-.00138091	.04388477	.68288920	-.00171834	.68288920
19	.0	9.5	.03563293	.68726700	-.00145763	.04632281	.68288920	-.00181380	.68288920
20	.0	10.0	.03750835	.68726700	-.00153435	.04876085	.68288920	-.00190927	.68288920
21	.0	10.5	.03938377	.68726700	-.00161106	.05119889	.68288920	-.00200473	.68288920
1	3.0	.0	.01125250	.68726700	-.00046030	.01060497	.68288920	-.00043382	.68726700
2	3.0	.5	.01312792	.68726700	-.00053702	.01304301	.68288920	-.00052928	.68644870
3	3.0	1.0	.01500334	.68726700	-.00061374	.01548105	.68288920	-.00062474	.68588810
4	3.0	1.5	.01687876	.68726700	-.00069046	.01791910	.68288920	-.00072021	.68548010
5	3.0	2.0	.01875417	.68726700	-.00076717	.02035714	.68288920	-.00081567	.68516980
6	3.0	2.5	.02062959	.68726700	-.00084389	.02279518	.68288920	-.00091113	.68492590
7	3.0	3.0	.02250501	.68726700	-.00092061	.02523322	.68288920	-.00100659	.68472910
8	3.0	3.5	.02438043	.68726700	-.00099733	.02767127	.68288920	-.00110206	.68456700
9	3.0	4.0	.02625584	.68726700	-.00107404	.03010931	.68288920	-.00119752	.68443110
10	3.0	4.5	.02813126	.68726700	-.00115076	.03254735	.68288920	-.00129298	.68431560
11	3.0	5.0	.03000668	.68726700	-.00122748	.03498539	.68288920	-.00138845	.68421630
12	3.0	5.5	.03188210	.68726700	-.00130419	.03742344	.68288920	-.00148391	.68412980
13	3.0	6.0	.03375752	.68726700	-.00138091	.03986148	.68288920	-.00157937	.68405390
14	3.0	6.5	.03563293	.68726700	-.00145763	.04229952	.68288920	-.00167484	.68398680
15	3.0	7.0	.03750835	.68726700	-.00153435	.04473756	.68288920	-.00177030	.68392700
16	3.0	7.5	.03938377	.68726700	-.00161106	.04717560	.68288920	-.00186576	.68387340
17	3.0	8.0	.04125918	.68726700	-.00168778	.04961365	.68288920	-.00196123	.68382500
18	3.0	8.5	.04313460	.68726700	-.00176450	.05205169	.68288920	-.00205669	.68378110
19	3.0	9.0	.04501002	.68726700	-.00184122	.05448974	.68288920	-.00215215	.68374120
20	3.0	9.5	.04688543	.68726700	-.00191793	.05692778	.68288920	-.00224762	.68370470
21	3.0	10.0	.04876085	.68726700	-.00199465	.05936582	.68288920	-.00234308	.68367120
1	9.0	.0	.03375752	.68726700	-.00138091	.03181490	.68288920	-.00130145	.68726700
2	9.0	.5	.03563293	.68726700	-.00145763	.03425295	.68288920	-.00139691	.68695540
3	9.0	1.0	.03750835	.68726700	-.00153435	.03669099	.68288920	-.00149237	.68668520
4	9.0	1.5	.03938377	.68726700	-.00161106	.03912903	.68288920	-.00158784	.68644870
5	9.0	2.0	.04125918	.68726700	-.00168778	.04156707	.68288920	-.00168330	.68623990
6	9.0	2.5	.04313460	.68726700	-.00176450	.04400511	.68288920	-.00177876	.68605430
7	9.0	3.0	.04501002	.68726700	-.00184122	.04644316	.68288920	-.00187423	.68588810
8	9.0	3.5	.04688543	.68726700	-.00191793	.04888120	.68288920	-.00196969	.68573860
9	9.0	4.0	.04876085	.68726700	-.00199465	.05131925	.68288920	-.00206515	.68560320
10	9.0	4.5	.05063627	.68726700	-.00207137	.05375729	.68288920	-.00216062	.68548010
11	9.0	5.0	.05251169	.68726700	-.00214809	.05619533	.68288920	-.00225608	.68536770
12	9.0	5.5	.05438710	.68726700	-.00222480	.05863337	.68288920	-.00235154	.68526460
13	9.0	6.0	.05626252	.68726700	-.00230152	.06107141	.68288920	-.00244701	.68516980
14	9.0	6.5	.05813794	.68726700	-.00237824	.06350946	.68288920	-.00254247	.68508230
15	9.0	7.0	.06001336	.68726700	-.00245496	.06594750	.68288920	-.00263793	.68500120
16	9.0	7.5	.06188878	.68726700	-.00253167	.06838554	.68288920	-.00273340	.68492590
17	9.0	8.0	.06376419	.68726700	-.00260839	.07082359	.68288920	-.00282886	.68485580
18	9.0	8.5	.06563961	.68726700	-.00268511	.07326163	.68288920	-.00292432	.68479030
19	9.0	9.0	.06751503	.68726700	-.00276182	.07569967	.68288920	-.00301978	.68472910
20	9.0	9.5	.06939045	.68726700	-.00283854	.07813771	.68288920	-.00311525	.68467170
21	9.0	10.0	.07126586	.68726700	-.00291526	.08057576	.68288920	-.00321071	.68461780

Table C.6 *FINCHM* Code Output (Mach=2.00, Position 2)

M	DELTA	ALPHA	CNF	XCP/CRF	CHMF	CNF(B)	XCP/CRF(B)	CHMF(B)	XCP/CR
1	.0	.5	.00192888	.65327120	-.00005267	.00250755	.64947620	-.00006467	.64947620
2	.0	1.0	.00385874	.65326180	-.00010536	.00501636	.64946660	-.00012936	.64946660
3	.0	1.5	.00578811	.65326180	-.00015804	.00752455	.64946660	-.00019403	.64946660
4	.0	2.0	.00771748	.65326180	-.00021072	.01003273	.64946660	-.00025871	.64946660
5	.0	2.5	.00964685	.65326180	-.00026340	.01254091	.64946660	-.00032339	.64946660
6	.0	3.0	.01157622	.65326180	-.00031609	.01504909	.64946660	-.00038807	.64946660
7	.0	3.5	.01350559	.65326180	-.00036877	.01755727	.64946660	-.00045274	.64946660
8	.0	4.0	.01543497	.65326180	-.00042145	.02006545	.64946660	-.00051742	.64946660
9	.0	4.5	.01736434	.65326180	-.00047413	.02257364	.64946660	-.00058210	.64946660
10	.0	5.0	.01929371	.65326180	-.00052681	.02508182	.64946660	-.00064678	.64946660
11	.0	5.5	.02122308	.65326180	-.00057949	.02759000	.64946660	-.00071145	.64946660
12	.0	6.0	.02315245	.65326180	-.00063217	.03009818	.64946660	-.00077613	.64946660
13	.0	6.5	.02508182	.65326180	-.00068485	.03260636	.64946660	-.00084081	.64946660
14	.0	7.0	.02701119	.65326180	-.00073753	.03511455	.64946660	-.00090549	.64946660
15	.0	7.5	.02894056	.65326180	-.00079021	.03762273	.64946660	-.00097016	.64946660
16	.0	8.0	.03086993	.65326180	-.00084290	.04013091	.64946660	-.00103484	.64946660
17	.0	8.5	.03279930	.65326180	-.00089558	.04263909	.64946660	-.00109952	.64946660
18	.0	9.0	.03472867	.65326180	-.00094826	.04514727	.64946660	-.00116420	.64946660
19	.0	9.5	.03665804	.65326180	-.00100094	.04765546	.64946660	-.00122887	.64946660
20	.0	10.0	.03858741	.65326180	-.00105362	.05016364	.64946660	-.00129355	.64946660
21	.0	10.5	.04051679	.65326180	-.00110630	.05267182	.64946660	-.00135823	.64946660
1	3.0	.0	.01157622	.65326180	-.00031609	.01095754	.64946660	-.00029919	.65326180
2	3.0	.5	.01350559	.65326180	-.00036877	.01346572	.64946660	-.00036387	.65255490
3	3.0	1.0	.01543497	.65326180	-.00042145	.01597391	.64946660	-.00042855	.65206990
4	3.0	1.5	.01736434	.65326180	-.00047413	.01848209	.64946660	-.00049323	.65171660
5	3.0	2.0	.01929371	.65326180	-.00052681	.02099027	.64946660	-.00055790	.65144780
6	3.0	2.5	.02122308	.65326180	-.00057949	.02349845	.64946660	-.00062258	.65123630
7	3.0	3.0	.02315245	.65326180	-.00063217	.02600663	.64946660	-.00068726	.65106560
8	3.0	3.5	.02508182	.65326180	-.00068485	.02851482	.64946660	-.00075194	.65092500
9	3.0	4.0	.02701119	.65326180	-.00073753	.03102300	.64946660	-.00081661	.65080710
10	3.0	4.5	.02894056	.65326180	-.00079021	.03353118	.64946660	-.00088129	.65070680
11	3.0	5.0	.03086993	.65326180	-.00084289	.03603936	.64946660	-.00094597	.65062050
12	3.0	5.5	.03279930	.65326180	-.00089558	.03854754	.64946660	-.00101065	.65054540
13	3.0	6.0	.03472867	.65326180	-.00094826	.04105572	.64946660	-.00107532	.65047950
14	3.0	6.5	.03665804	.65326180	-.00100094	.04356391	.64946660	-.00114000	.65042120
15	3.0	7.0	.03858741	.65326180	-.00105362	.04607209	.64946660	-.00120468	.65036920
16	3.0	7.5	.04051679	.65326180	-.00110630	.04858027	.64946660	-.00126936	.65032260
17	3.0	8.0	.04244616	.65326180	-.00115898	.05108845	.64946660	-.00133403	.65028060
18	3.0	8.5	.04437552	.65326180	-.00121166	.05359663	.64946660	-.00139871	.65024250
19	3.0	9.0	.04630490	.65326180	-.00126434	.05610481	.64946660	-.00146339	.65020780
20	3.0	9.5	.04823427	.65326180	-.00131702	.05861299	.64946660	-.00152807	.65017610
21	3.0	10.0	.05016364	.65326180	-.00136970	.06112118	.64946660	-.00159274	.65014700
1	9.0	.0	.03472867	.65326180	-.00094826	.03287262	.64946660	-.00089758	.65326180
2	9.0	.5	.03665804	.65326180	-.00100094	.03538081	.64946660	-.00096226	.65299270
3	9.0	1.0	.03858741	.65326180	-.00105362	.03788899	.64946660	-.00102693	.65275930
4	9.0	1.5	.04051679	.65326180	-.00110630	.04039717	.64946660	-.00109161	.65255490
5	9.0	2.0	.04244616	.65326180	-.00115898	.04290535	.64946660	-.00115629	.65237430
6	9.0	2.5	.04437552	.65326180	-.00121166	.04541354	.64946660	-.00122097	.65221380
7	9.0	3.0	.04630490	.65326180	-.00126434	.04792172	.64946660	-.00128564	.65206990
8	9.0	3.5	.04823427	.65326180	-.00131702	.05042990	.64946660	-.00135032	.65194050
9	9.0	4.0	.05016364	.65326180	-.00136970	.05293808	.64946660	-.00141500	.65182330
10	9.0	4.5	.05209301	.65326180	-.00142238	.05544626	.64946660	-.00147968	.65171660
11	9.0	5.0	.05402238	.65326180	-.00147507	.05795445	.64946660	-.00154435	.65161930
12	9.0	5.5	.05595175	.65326180	-.00152775	.06046263	.64946660	-.00160903	.65153000
13	9.0	6.0	.05788112	.65326180	-.00158043	.06297081	.64946660	-.00167371	.65144780
14	9.0	6.5	.05981049	.65326180	-.00163311	.06547899	.64946660	-.00173839	.65137190
15	9.0	7.0	.06173986	.65326180	-.00168579	.06798717	.64946660	-.00180306	.65130160
16	9.0	7.5	.06366923	.65326180	-.00173847	.07049535	.64946660	-.00186774	.65123630
17	9.0	8.0	.06559861	.65326180	-.00179115	.07300354	.64946660	-.00193242	.65117550
18	9.0	8.5	.06752797	.65326180	-.00184383	.07551172	.64946660	-.00199710	.65111880
19	9.0	9.0	.06945734	.65326180	-.00189651	.07801990	.64946660	-.00206177	.65106560
20	9.0	9.5	.07138672	.65326180	-.00194919	.08052808	.64946660	-.00212645	.65101580
21	9.0	10.0	.07331608	.65326180	-.00200188	.08303626	.64946660	-.00219113	.65096900

Table C.7 *FINCHM* Code Output (Mach=2.00, Position 3)

M	DELTA	ALPHA	CNF	XCP/CRF	CHMF	CNF(B)	XCP/CRF(B)	CHMF(B)	XCP/CR
1	.0	.5	.00204116	.60296800	-.00001467	.00265351	.59934750	-.00001523	.59934750
2	.0	1.0	.00408323	.60299600	-.00002939	.00530820	.59937610	-.00003052	.59937610
3	.0	1.5	.00612484	.60299600	-.00004409	.00796230	.59937610	-.00004579	.59937610
4	.0	2.0	.00816646	.60299600	-.00005879	.01061640	.59937610	-.00006105	.59937610
5	.0	2.5	.01020807	.60299600	-.00007348	.01327049	.59937610	-.00007631	.59937610
6	.0	3.0	.01224969	.60299600	-.00008818	.01592459	.59937610	-.00009157	.59937610
7	.0	3.5	.01429130	.60299600	-.00010287	.01857869	.59937610	-.00010684	.59937610
8	.0	4.0	.01633292	.60299600	-.00011757	.02123279	.59937610	-.00012210	.59937610
9	.0	4.5	.01837453	.60299600	-.00013227	.02388689	.59937610	-.00013736	.59937610
10	.0	5.0	.02041615	.60299600	-.00014696	.02654099	.59937610	-.00015262	.59937610
11	.0	5.5	.02245776	.60299600	-.00016166	.02919509	.59937610	-.00016788	.59937610
12	.0	6.0	.02449938	.60299600	-.00017636	.03184919	.59937610	-.00018315	.59937610
13	.0	6.5	.02654099	.60299600	-.00019105	.03450328	.59937610	-.00019841	.59937610
14	.0	7.0	.02858260	.60299600	-.00020575	.03715738	.59937610	-.00021367	.59937610
15	.0	7.5	.03062422	.60299600	-.00022045	.03981148	.59937610	-.00022893	.59937610
16	.0	8.0	.03266583	.60299600	-.00023514	.04246558	.59937610	-.00024420	.59937610
17	.0	8.5	.03470745	.60299600	-.00024984	.04511968	.59937610	-.00025946	.59937610
18	.0	9.0	.03674906	.60299600	-.00026453	.04777378	.59937610	-.00027472	.59937610
19	.0	9.5	.03879068	.60299600	-.00027923	.05042788	.59937610	-.00028998	.59937610
20	.0	10.0	.04083229	.60299600	-.00029393	.05308198	.59937610	-.00030524	.59937610
21	.0	10.5	.04287391	.60299600	-.00030862	.05573608	.59937610	-.00032051	.59937610
1	3.0	.0	.01224969	.60299600	-.00008818	.01164148	.59937610	-.00008380	.60299600
2	3.0	.5	.01429130	.60299600	-.00010287	.01429558	.59937610	-.00009906	.60232390
3	3.0	1.0	.01633292	.60299600	-.00011757	.01694968	.59937610	-.00011432	.60186230
4	3.0	1.5	.01837453	.60299600	-.00013227	.01960378	.59937610	-.00012959	.60152570
5	3.0	2.0	.02041615	.60299600	-.00014696	.02225788	.59937610	-.00014485	.60126940
6	3.0	2.5	.02245776	.60299600	-.00016166	.02491198	.59937610	-.00016011	.60106770
7	3.0	3.0	.02449938	.60299600	-.00017636	.02756607	.59937610	-.00017537	.60090480
8	3.0	3.5	.02654099	.60299600	-.00019105	.03022017	.59937610	-.00019064	.60077050
9	3.0	4.0	.02858260	.60299600	-.00020575	.03287427	.59937610	-.00020590	.60065790
10	3.0	4.5	.03062422	.60299600	-.00022045	.03552837	.59937610	-.00022116	.60056220
11	3.0	5.0	.03266583	.60299600	-.00023514	.03818247	.59937610	-.00023642	.60047980
12	3.0	5.5	.03470745	.60299600	-.00024984	.04083657	.59937610	-.00025168	.60040800
13	3.0	6.0	.03674906	.60299600	-.00026453	.04349067	.59937610	-.00026695	.60034510
14	3.0	6.5	.03879068	.60299600	-.00027923	.04614476	.59937610	-.00028221	.60028930
15	3.0	7.0	.04083229	.60299600	-.00029393	.04879887	.59937610	-.00029747	.60023960
16	3.0	7.5	.04287391	.60299600	-.00030862	.05145296	.59937610	-.00031273	.60019510
17	3.0	8.0	.04491552	.60299600	-.00032332	.05410706	.59937610	-.00032800	.60015490
18	3.0	8.5	.04695714	.60299600	-.00033802	.05676116	.59937610	-.00034326	.60011850
19	3.0	9.0	.04899875	.60299600	-.00035271	.05941526	.59937610	-.00035852	.60008530
20	3.0	9.5	.05104037	.60299600	-.00036741	.06206936	.59937610	-.00037378	.60005500
21	3.0	10.0	.05308198	.60299600	-.00038211	.06472346	.59937610	-.00038904	.60002720
1	9.0	.0	.03674906	.60299600	-.00026453	.03492444	.59937610	-.00025140	.60299600
2	9.0	.5	.03879068	.60299600	-.00027923	.03757854	.59937610	-.00026666	.60274030
3	9.0	1.0	.04083229	.60299600	-.00029393	.04023264	.59937610	-.00028192	.60251840
4	9.0	1.5	.04287391	.60299600	-.00030862	.04288674	.59937610	-.00029719	.60232390
5	9.0	2.0	.04491552	.60299600	-.00032332	.04554084	.59937610	-.00031245	.60215210
6	9.0	2.5	.04695714	.60299600	-.00033802	.04819493	.59937610	-.00032771	.60199920
7	9.0	3.0	.04899875	.60299600	-.00035271	.05084904	.59937610	-.00034297	.60186230
8	9.0	3.5	.05104037	.60299600	-.00036741	.05350313	.59937610	-.00035824	.60173900
9	9.0	4.0	.05308198	.60299600	-.00038211	.05615723	.59937610	-.00037350	.60162730
10	9.0	4.5	.05512359	.60299600	-.00039680	.05881133	.59937610	-.00038876	.60152570
11	9.0	5.0	.05716521	.60299600	-.00041150	.06146543	.59937610	-.00040402	.60143290
12	9.0	5.5	.05920682	.60299600	-.00042619	.06411953	.59937610	-.00041928	.60134770
13	9.0	6.0	.06124844	.60299600	-.00044089	.06677363	.59937610	-.00043455	.60126940
14	9.0	6.5	.06329005	.60299600	-.00045559	.06942773	.59937610	-.00044981	.60119700
15	9.0	7.0	.06533167	.60299600	-.00047028	.07208183	.59937610	-.00046507	.60112990
16	9.0	7.5	.06737328	.60299600	-.00048498	.07473592	.59937610	-.00048033	.60106770
17	9.0	8.0	.06941490	.60299600	-.00049968	.07739002	.59937610	-.00049560	.60100970
18	9.0	8.5	.07145651	.60299600	-.00051437	.08004412	.59937610	-.00051086	.60095550
19	9.0	9.0	.07349813	.60299600	-.00052907	.08269822	.59937610	-.00052612	.60090480
20	9.0	9.5	.07553974	.60299600	-.00054377	.08535232	.59937610	-.00054138	.60085730
21	9.0	10.0	.07758135	.60299600	-.00055846	.08800642	.59937610	-.00055665	.60081260

APPENDIX D

AGENCY CONSENT FORM

AMSMI-RD-TI (70)   Dr. Smith/epp/6-5449

MEMORANDUM FOR AMSMI-IN, ATTN: D. Harris/G. Snyder

SUBJECT: Initial, Patent Applicability, OPSEC Review and MCTL Determination # _608_
             For Material Being Released to the Public

1. IDENTIFICATION OF MATERIAL
   Title of Material _PREDICTION OF HINGE MOMENT COEFFICIENTS FOR NOSE-MOUNTED CANARD CONTROLS_
   AT SUPERSONIC SPEEDS
   Author(s) _MICHAEL G. LANDERS_   AMSMI-RD-_____

   ( ) Technical Report – give report number _____
   (X) Open Literature – give title of journal _Master's Thesis_ ②_AIAA paper # 97-2248 co-author Dr. D. Brian Land_
   - UAH
   (X) Presentation – give date and place to be presented ___③ AIAA Journal of SPACECRAFT & Rockets_ _to be sent_
   for acceptan
   ( ) ___↳ 15th Applied Aerodynamics Conference AIAA – Atlanta June 24, 1997_

2. INITIAL REVIEW/PATENT APPLICABILITY REVIEW (By a person other than the author)
   The subject material has been reviewed and determined to be factual and unclassified. The subject material
   has been reviewed for patent applicability and the information:

   (X) contains no patentable material.

   ( ) contains patentable material and it has been (   ) / should be (   ) submitted.

   ( ) does not require a patent review since it is not a report or publication.
   Signature _____ Date _6 / 6 / 97_ AV 746- _5716_ AMSMI-RD- _SS-AT_
   Name _GEORGE H. CANDINEHAM_ Title _CH, AERO. TECH._ RD&E Ctr. USAMICOM

3. OPSEC REVIEW (By a designated directorate/office OPSEC reviewer)
   "I, the undersigned, am aware of the hostile intelligence interest in open source publications and in the subject
   matter of the information I have reviewed for OPSEC purposes. I certify that I have sufficient technical expertise
   in the subject matter and that, to the best of my knowledge, the net benefit of this public release outweighs the
   potential damage to the secrecy of all MICOM, AMC, Army, or other DOD programs of which I am aware."
   Signature _____ Date _9 Jun 97_ AV 746- _8108_ AMSMI-RD- _SS-HW_
   Name _Alexander C. Jolly_ Title _Ch, HWIL Sims, SS&DD_ RD&E Ctr. USAMICOM

4. MILITARY CRITICAL TECHNOLOGIES LIST (MCTL) DETERMINATION (By AMSMI-RD-TI)
   (✓) The subject material does not concern the technology items of the MCTL.

   ( ) The subject material does not concern the technology items of the MCTL since it relates to
   _____ and does not relate to technologies
   of _____ as covered in MCTL paragraph _____.

   (✓) Recommend local approval for public release.
   Date _6 / 13 / 97_ _____ Steven P.D. Smith AV 746-5449 AMSMI-RD-TI

5. CLEARANCE ACTION
   Subject material has been (✓) APPROVED / ( ) DISAPPROVED for public release

   _____   _13 June 97_
        Information Office, USAMICOM   Date
   Encl

REFERENCES

[1]   Rigby, Maj. Gen. Randall L., "Extended-Range, Guided Rockets Could Counter Long-Range Threats," *ARMY*, Sept., 1996, p. 64.

[2]   Gamble, Allan, Jenkins, Phil, Tauchen, Brian, and Auman, Lamar, "Design of a Low-Cost Guidance Package for an Existing Free-Flight Rocket," Paper presented at the 14th AIAA Missile Sciences Conference, Monterey, California, November 1994.

[3]   "Aerodynamic Analysis for Missiles - Evaluation of Aerodynamic Prediction Methods," AFWAL-TR-82-3038, U.S. Air Force Wright Laboratory, Wright Patterson Air Force Base, Ohio, 1982.

[4]   "High Speed Prediction Methods Used by Missile DATCOM and AP93," excerpts from unknown source.

[5]   Pitts, William C., Nielsen, Jack N., and Kaattari, George E., "Lift and Center of Pressure of Wing-Body-Tail Combinations at Subsonic, Transonic, and Supersonic Speeds," NACA Report 1307, 1959.

[6]   Burns, Keith A., Deters, Kenneth J., Stoy, Stan L., Vukelich, Steven R., and Blake, William B., "Missile DATCOM User's Manual - Revision 6/93," WL-TR-93-3043, U.S. Air Force Wright Laboratory, Wright Patterson Air Force Base, Ohio, June, 1993.

[7]   Blake, William B., U.S. Air Force Wright Laboratory, Wright Patterson Air Force Base, Ohio, personal communication, 1997.

[8]   Nielsen, Jack N. and Goodwin, Frederick K., "Preliminary Method for Estimating Hinge Moments of All-Movable Controls," NEAR TR 268, Nielsen Engineering and Research, Inc., Mountain View, California, March 1982.

[9]   Nielsen, Jack N., *Missile Aerodynamics*, McGraw-Hill, New York, 1960; republished by Nielsen Engineering and Research, Inc., Mountain View, California, 1988.

[10]   Chin, S. S., *Missile Configuration Design*, McGraw-Hill, New York, 1961.

[11]   Bonney, E. Arthur, *Engineering Supersonic Aerodynamics*, McGraw-Hill, New York, 1950.

[12]   *Tactical Missile Aerodynamics: Prediction Methodology*, Volume 142, American Institute of Aeronautics and Astronautics, Washington, D.C., 1992.

[13]   Jones, Robert T., "Properties of Low-Aspect-Ratio Pointed Wings at Speeds Below and Above the Speed of Sound," NACA Report 835, 1946.

[14]   DeYoung, John and Harper, Charles W., "Theoretical Symmetric Span Loading at Subsonic Speeds for Wings Having Arbitrary Plan Form," NACA Report 921, 1948.

[15]   Goin, Kennith L., "Equations and Charts for the Rapid Estimation of Hinge Moment and Effectiveness Parameters for Trailing-Edge Controls Having Leading and Trailing Edges Swept Ahead of the Mach Lines," NACA Report 1041, 1951.

[16]   Burt, James R., Jr., "An Experimental Investigation of the Aerodynamic Characteristics of Several Nose-Mounted Canard Configurations at Transonic Mach Numbers," Technical Report RD-75-2, U.S. Army Missile Command, Redstone Arsenal, Alabama, August 1974.

[17]   Burt, James R., Jr., "An Experimental Investigation of the Aerodynamic Characteristics of Several Nose-Mounted Canard Configurations at Supersonic Mach Numbers," Technical Report RD-75-17, U.S. Army Missile Command, Redstone Arsenal, Alabama, January 1975.

[18]   Hemsch, Michael J. and Nielsen, Jack N., "Test Report for Canard Missile Tests in Ames 6- by 6-Foot Supersonic Wind Tunnel," NEAR TR 72, Nielsen Engineering and Research, Inc., Mountain View, California, August 1974.

[19]   Burt, James R., Jr., "An Experimental Investigation of the Aerodynamic Characteristics of Nose-Mounted Canard Configurations at Supersonic Mach Numbers (1.5 Through 4.5)" Technical Report RD-77-5, U.S. Army Missile Command, Redstone Arsenal, Alabama, October 1976.

[20]   Burt, James R., Jr., "Pre-Test Information for a Supersonic Investigation of a Model with Nose Mounted Canard Wings (AEDC)," Internal Technical Note RD-76-1, U.S. Army Missile Command, Redstone Arsenal, Alabama, September 1975.

[21]   Chafin, J. M., "User's Guide for Canard Control (CANARD) Aerodynamic Data Base," Interim Technical Report TR 1014, New Technology, Inc., Huntsville, Alabama, June 1979.

[22]   Goodwin, Frederick K. and Nielsen, Jack N., "Determination of Optimum Fin Planform and Airfoil Section for Minimizing Fin Hinge Moment," NEAR TR 286, Nielsen Engineering and Research, Inc., Mountain View, California, February 1983.

[23]   Nielsen, Jack N., "Aerodynamic Characteristics of Missile Controls," *AGARD Special Course on Aerodynamic Characteristics of Controls*, AGARD Report No. 711, March 1983.

[24]   Wardlaw, A. B., Jr., and Davis, S. F., "A Second Order Godunov Method for Supersonic Tactical Missiles," NSWC TR 86-506, Naval Surface Warfare Center, Dahlgren, Virginia, December 1986.

[25]   Wardlaw, A. B., Jr., and Priolo, F. J., "Applying the ZEUS Code," NSWC TR 86-508, Naval Surface Warfare Center, Dahlgren, Virginia, December 1986.

[26]   Coleman, Hugh W. and Stern, Fred, "Uncertainties and CFD Code Validation," to appear in *Journal of Fluids Engineering*, December, 1997.

[27]   Coleman, Hugh W. and Steele, W. Glenn, Jr., *Experimentation and Uncertainty Analysis for Engineers*, John Wiley and Sons, 1989.

[28]   Fluid Dynamics Panel Working Group 15, "Quality Assessment for Wind Tunnel Testing," AGARD-AR-304, July 1994.

[29]   Clark, E. L., "Error Propagation Equations for Estimating the Uncertainty in High-Speed Wind Tunnel Test Results," AIAA Paper No. 94-2588, AIAA 18th Aerospace Ground Testing Conference, Colorado Springs, Colorado, June 20-23, 1994.

[30]   Cahill, D. M., "Experiences with Uncertainty Analysis Application in Wind Tunnel Testing," AIAA Paper No. 94-2586, AIAA 18th Aerospace Ground Testing Conference, Colorado Springs, Colorado, June 20-23, 1994.

[31]   Killough, Tom L., retired U.S. Army Missile Command, Redstone Arsenal, Alabama, personal communication, 1997.

[32]   Cahill, David M., Arnold Engineering Development Center, Arnold Air Force Base, Tennessee, personal communication, 1997.

[33]   Steinle, Frank, retired Chief of Aerodynamic Facilities Branch, NASA-Ames, Mountain View, California, personal communication, 1997.

[34]   Ames Research Staff, "Equations, Tables and Charts for Compressible Flow," NACA Report 1135, 1953.

[35]   Anderson, John D., Jr., *Modern Compressible Flow*, Second Edition, McGraw-Hill, New York, 1990.

[36]   Ferri, Antonio, *Elements of Aerodynamics of Supersonic Flows*, MacMillan, New York, 1949.

[37]   Keuthe, Arnold M., and Chow, Chuen-Yen, *Foundations of Aerodynamics*, Fourth Edition, John Wiley & Sons, 1986.

[38]   Hall, I. M., "Inversions of the Prandtl-Meyer Relation," Aeronautical Journal, Royal Aeronautical Society, U.K., September 1975, pp. 416-418.

INITIAL DISTRIBUTION LIST

COPIES:

IIT Research Institute   1
ATTN: GACIAC
10 W. 35th Street
Chicago, IL 60616

AMSAM-RD-SS,	Dr. K. Grider	1
AMSAM-RD-SS-AT	Mr. G. Landingham	1
AMSAM-RD-SS-AT	Mr. Lamar M. Auman	2

AMSAM-L-G-I,   Mr. Fred Bush   1

AMSMI-RD,   Dr. Rhoades   1

AMSAM-RD-OB-R   5

AMSAM-RD-OB-RT   1

AMSAM-RD-CD-T   1

Administrator   1
Defense Technical Information Center
Cameron Station
ATTN: DTIC-DDA
Alexandria, VA 22314

Director   1
Missiles and Space Intelligence Center
ATTN: MSC-4E2, Mr. Gary Winn
Redstone Arsenal, AL 35898-5500

NASA-Ames Research Center   1
ATTN: Library
Moffett Field, CA 94035

NASA-Langley Research Center   1
ATTN: Technical Library
Hampton, VA 23665

INITIAL DISTRIBUTION LIST (Continued)

COPIES:

Air Force Wright Laboratory   1
WL/FIGC/Bldg 146, Suite 21
ATTN: William Blake
2210 8th Street
Wright-Patterson Air Force Base, OH 45433

Dynetics, Inc.
1000 Explorer Blvd.
ATTN: Mr. Mark Miller   2
       Mr. Michael G. Landers   2
Huntsville, AL 35806